地質調査研究報告

BULLETIN OF THE GEOLOGICAL SURVEY OF JAPAN

表紙の写真

足摺岬花崗岩体の西縁, 臼碆海岸にみられる花崗岩露頭

　足摺岬には中新世の深成岩類が露出し, 四万十層群の最も若い中新世の砂岩・頁岩に貫入する. 深成岩類は花崗岩類との混交現象が顕著な斑れい岩類 (30 %), これと密接な閃長岩類 (35 %) が南部地域に分布し, 四万十層群に接して北部に花崗岩 (35 %) が分布する. 閃長岩類はアルバイトを多く含むカリ長石に富み, 化学的には K_2O-SiO_2 図上でショショナイト―高カリウム域にプロットされる. また Ga, Rb などが多く含まれ A タイプ的な性格を有する. 肉眼的でも識別できるジルコンを多く含み, その含有量は 600―1,200 ppm に達する. REE 成分に富み, それらはチタン石, 褐廉石, フェルグソン石などの微量 REE 鉱物に含まれる. マグマの起源としてアルカリ岩に対しては地殻下部の小規模な部分溶融, 花崗岩については付加体物質同化の可能性が指摘された.

（写真・文：石原舜三）

Cover page

Well-exposed Miocene granite at the Usubae coast of the Cape Ashizuri plutonic complex

　The Ashizuri Peninsula is composed of Miocene plutonic rocks intruding into the early Miocene accretional complex of the Shimanto Surpergroup. The rocks are composed of gabbroids mingled with granitoids (30 %), alkaline granitoids (35 %), and biotite granites (35 %). The alkaline granitoids, occurring in the southern half associated with the gabbroids, are dominant in albite-bearing orthoclase, hence syenitic, and rich in zirconium (600-1,200 ppm), containing visible zircon with naked eyes. Titanite, allanite and REE accessory minerals are common, and therefore the REE contents are the highest among the Japanese granitoids. The granitoids belong to shoshonite-high-K series originated in small amount of melting of mafic igneous source rocks. Mixing of the magmas with sedimentary wall rocks is important to form the biotite granite.

(Photograph and Caption by Shunso Ishihara)

Article

Zircon and REE-rich alkaline plutonic rocks intruded into the accretionary prism at the Cape Ashizuri, Shikoku Island, Japan

Shunso Ishihara[1, *] and Mihoko Hoshino[2]

Abstract: The Cape Ashizuri body is a small, 12 km^2, Miocene plutonic complex having gabbroids, syenite, quartz syenite to syenogranite in its southern half and biotite monzogranite in its northern half, right next to the Shimanto accretionary sediments. Chemical analyses indicate that the granitoids have mostly meta-aluminous value of A/CNK<1.0, except for three monzogranite. The granitoids are rich in K_2O, plotted in the shoshonite-high K fields. The granitoids are also rich in Na_2O and Rb. Ga content is higher than 18 ppm, indicating characteristics of the A-type granitoids. A distinct characteristic of the Cape Ashizuri granitoids is predominance of HFSE (high-field- strength-element), such as Zr (<1,220 ppm), Hf (25.6 ppm), Nb (<202 ppm), Ta (<14 ppm), LREE (<1002 ppm), HREE (<50.5 ppm), Y (<74 ppm), Th (74.2 ppm). Fluorine is also enriched up to 0.43 wt.%.

These HFSE are contained in such common accessory minerals as zircon, ilmenite, allanite and titanite, and rare minerals of fergusonite, chevkinite and others. Zircon is the most common and visible rarely by naked eyes. Zircon in the highest Zr rock, 58A142 sample, contains the maximum values of 2.4 wt.% HfO_2 and 1.0 wt.% Y_2O_3. Ilmenite in the 58A142 sample shows 4.3-5.7 wt.% MnO, but that in other quartz syenite shows lower values as 1.7-1.8 wt.% MnO, while its niobium content, up to 3.8 wt.% Nb_2O_5, is seen along the rim, indicating the niobium concentrated at the latest magmatic stage. Allanite shows Mn-poor character of the magnetite series (0.44 wt.% MnO), and contains 24.6-25.8 wt.% LREE.

The most mafic phase of the gabbroids is 47.0 wt.% SiO_2 and 12.5 wt.% MgO, indicating its origin of the upper mantle. Quartz syenitic rocks have 55-60 wt.% SiO_2 and low Sr_0 ratio of 0.7035, implying a small degree of the partial melting of mafic igneous source rocks in the lower crust for the alkaline rocks. The high contents of HFSE and F were caused by this small degree of the partial melting. The biotite monzogranite in the northern part is considered as a mixed magma generated from the lower igneous crust and overlying accreted sediments of the Shimanto Supergroup. It is interesting to explore hydrothermal REE concentration related to these plutonic and subvolcanic activities.

Keywords: Cape Ashizuri, Miocene, alkaline granite, zircon, REE

1. Introduction

There are many small Miocene granitic stocks intruded into accreted clastic sediments of the late Paleozoic to Tertiary age in the western Shikoku and eastern Kyushu districts in Japan (Fig. 1). These stocks belong generally to calc-alkaline I-type ilmenite-series and are not particularly high in the rare earth elements (REE: Cullers and Graf, 1984), except for one locality at the Cape Ashizuri, southwestern edge of the Shikoku Island. This body contains both alkaline and calc-alkaline plutonic rocks, the alkaline rocks of which were considered to be formed by alkaline metasomatism of the

late magmatic stage (Murakami and Matsuo, 1963), but later re-interpreted that they are intrinsically alkaline magma (Murakami and Masuda, 1984; Murakami and Imaoka, 1985) rich in fluorine with relatively low water and low to moderate oxygen fugacities (Murakami *et al.*, 1983).

The Cape Ashizuri granitoids are considered to belong to A-type for the high Ga contents (Imaoka *et al.*, 1991). Besides the alkalinity, this pluton is different from the others in the Outer Zone of Southwest Japan (e.g., Okueyama pluton) having a moderate contents of rock-forming magnetite (Ishihara, 1979) and a low initial $^{87}Sr/^{86}Sr$ ratio (Sr_0) of 0.7035 (Shibata and Ishi-

[1] AIST, Geological Survey of Japan

[2] AIST, Geological Survey of Japan, Institute for Geo-Resources and Environment

*Corresponding author: S. ISHIHARA, Central 7, 1-1-1 Higashi, Tsukuba, Ibaraki 305-8567, Japan. Email: s-ishihara@aist.go.jp
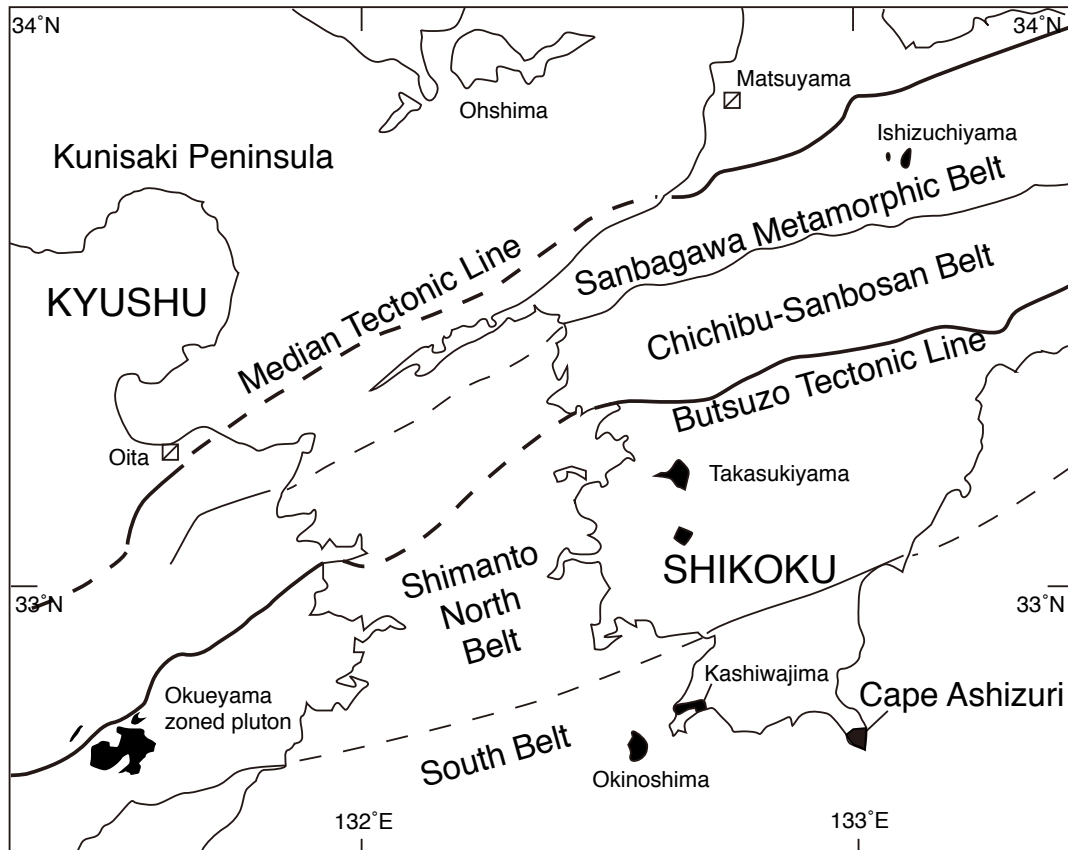
Fig. 1 Accretionary terranes and major faults in the Outer Zone of Shikoku and Kyushu islands from Teraoka *et al.* (1999). Solid mark implying Miocene granitic plutons.

hara, 1979). Zircon can be visible by naked eyes in this pluton, and the zirconium content is the highest at 66 wt.% SiO_2; thus belonging to the high temperature-type granite of Chappell *et al.* (2004). The Cape Ashizuri pluton is, therefore, unique anorogenic granite, occurring in an orogenic environment.

Magnetite and ilmenite were collected from the weathered soil of gabbroic rocks in flat area of the pluton at the north of the community Isa (Fig. 2), and tried to use for coin production in the 18th century by the old Tosa local government. According to re-examination of soil from the gabbroic area after the Second World War, the oxide contents in the soil were measured to vary from 1.33 to 4.12 wt.% (Shibano, 1958), and the oxides sands were considered as Ti-resource. High radioactivity was discovered during uranium exploration stage of 1960s from the abandoned oxides sand. This radioactive sand was composed of ilmenite 67 wt.%, magnetite 15 wt.%, quartz 14 wt.%, zircon 1.7 wt.%, and uranothorite and other heavy minerals 2.3 wt.% (Hayashi *et al.*, 1969).

Ilmenite and magnetite should be contained abundantly in mafic gabbroic rocks remaining as xenolithic bodies, but uranothorite may well be derived from granitic matrix. In order to identify the mode of occurrence of these U-bearing heavy minerals, a shal-

low drilling was performed in quartz syenite hosting gabbroids near the site of the old mining site in the early 1969 under the then-current uranium project. No gabbroids but only quartz syenitic rocks, together with several sheared zones, were discovered for the depth of 250 meters of the drill hole. The syenitic rocks were high in the radioactivity but no anomalous values were observed on the sheared zone. No evidence of hydrothermal alteration was observed through the drill hole. Potentiality of the rare earth elements was also tested in the weathered crust of the Ashizuri plutonic body, and the results were reported in a separate paper (Murakami and Ishihara, 2006).

Including all the chemical data we have, this paper describes chemical characteristics of the unique granitoids of the Cape Ashizuri pluton intruding into the Shimanto accretionary complex, which was formed under a typical orogenic environment. The data are compared with the I-type ilmenite-series chemistry of the Okueyama pluton (Ishihara and Chappell, 2010), which is vertically zoned calc-alkaline pluton (Takahashi, 1986), occurring in the same Outer Zone of Southwest Japan.

2. Geologic background

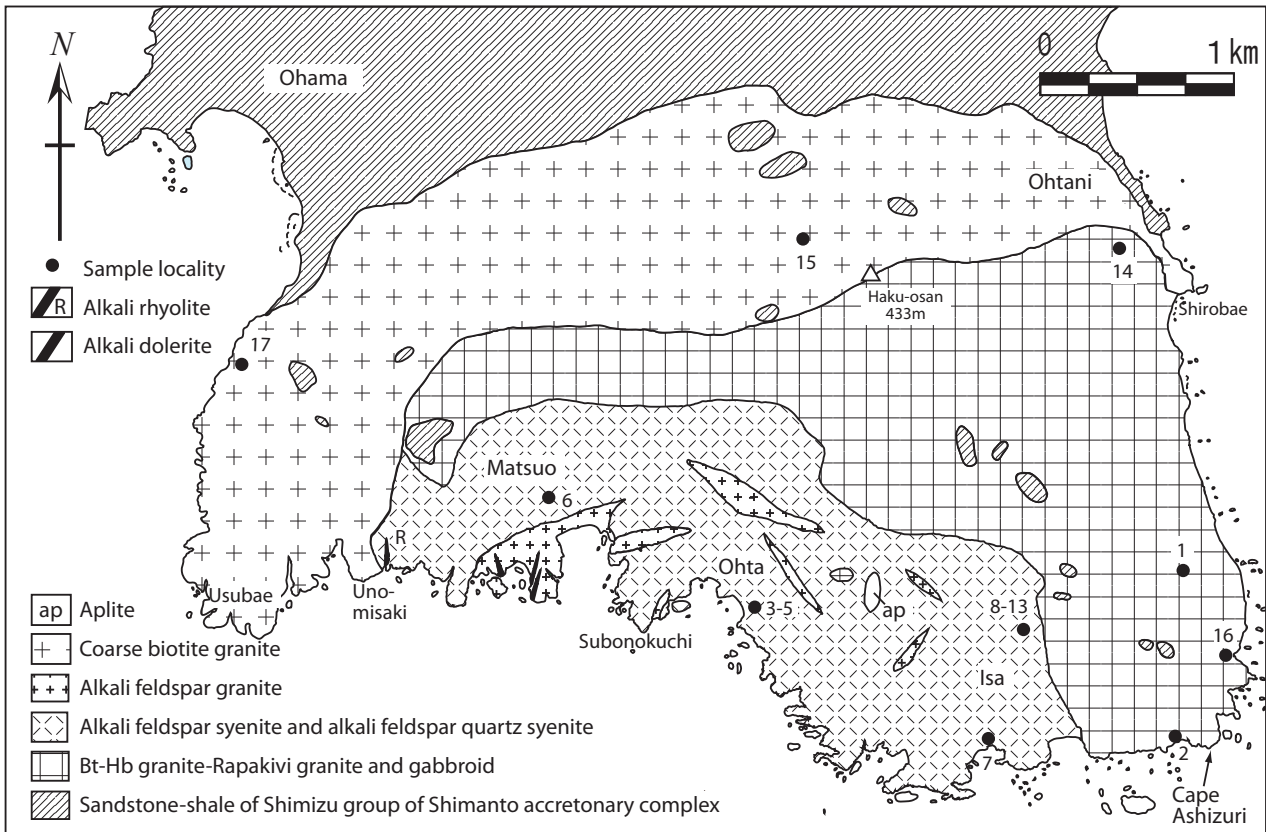Several accreted sedimentary and metamorphic zones

Fig. 2 Rock unit map (modified from T. Imaoka, 1993 unpublished) and location of the analyzed samples. Solid circle with the filing numbers listed in Table 1.

from late Paleozoic to Miocene in age being generally younger toward the southeastern coast with the Pacific Ocean, have been recognized in the western Shikoku Island (Fig. 1). These zones are, from north to south, Sanbagawa metamorphic belt, Chichibu-Sanbosan sedimentary belt and Shimanto sedimentary belt (Fig.1). Accreted sediments of the Shimanto belt are subdivided into the Cretaceous North Belt and Paleogene (-Miocene) South Belt (Fig. 1). The southernmost unit where the Cape Ashizuri intruded is mostly composed of shale having around N75°E strike and steep dip (60-80°) to north (Suzuki, 1938).

The Cape Ashizuri pluton, which is the best observable along the southern coast of the peninsula region (Plate IA), intrudes into the youngest Paleocene-Miocene Shimizu Formation of the Shimanto Supergroup, consisting of the clastics brought from the north (Teraoka, 1979). These clastic rocks were studied chemically, and found that the shales are extremely higher in SiO_2 and lower in Al_2O_3 than older shales occurring to the north, indicating a high maturity of the Paleocene-Miocene shale relative to Cretaceous one (Ishihara *et al.*, 1985). Some of these rocks occur as roof-pendant and xenolithic fragments in the biotite monzogranite phase of the Cape Ashizuri pluton (Fig. 2).

The pluton has an exposed area of 12 km² on land,

and is composed of three intrusive units as, (1) syenite-alkaline granites along the south coast, (2) gabbro and syenite/granites mingled phase, occurring the middle part (gabbro less than 25 vol.%) and (3) biotite monzogranite. The intrusive sequence appears to be the gabbroids, syenites, and then monzogranite. The second unit gabbroids are essentially pyroxene gabbro, but are often converted to dioritic rocks by the mingling and interaction with syenitic rocks. Thus, they are closely associated genetically each other. The monzogranite is a normal monzogranite occurring everywhere in the Japanese orogenic belts. Several alkaline (4.53 wt.% K_2O) dolerite dikes and a few peralkaline rhyolite dikes, very rich in rare earth elements (Ishihara *et al.*, 1990), cut in N-S direction of the western part of the unit 2.

About the radiometric age of the Cape Ashizuri body, Shibata and Nozawa (1982) summarized K-Ar ages on one hornblende and two biotites to be 13 Ma. Iizumi and Murakami (1980) obtained Sr isochron age of 15.6±2.1 Ma for the stage II syenite and alkali granite, and 11.5±0.5 Ma for the Stage IV granites. Murakami *et al.* (1989) added K-Ar ages of two whole rocks of 12.0±0.6 and 14.0±0.7 Ma and one biotite age of 12.9±0.6 Ma, and five fission track ages varying widely from 10.0±1.8 to 16.1±0.7 Ma.
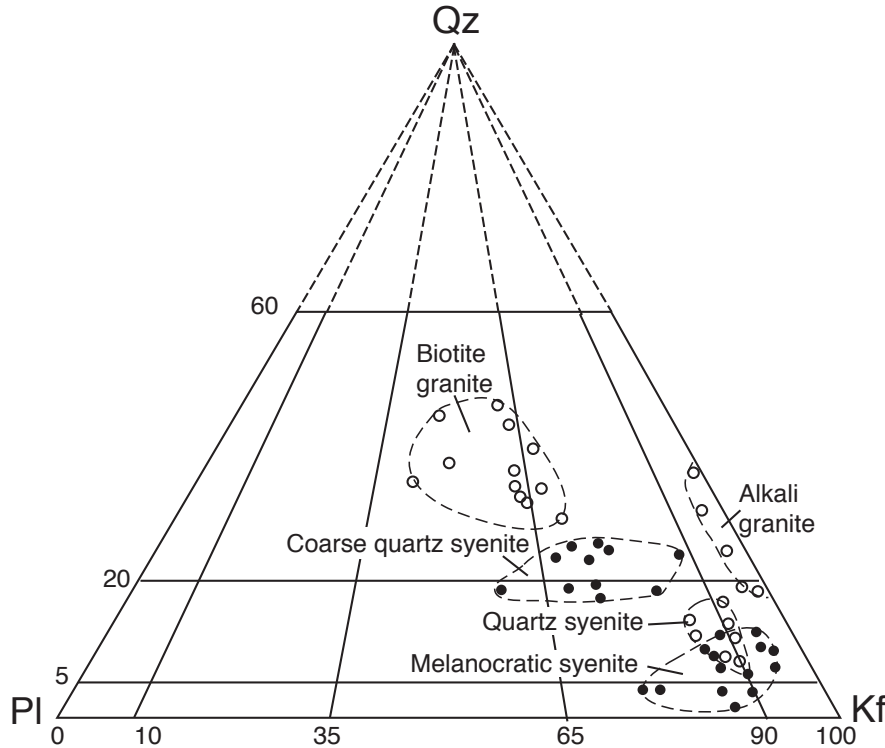
Fig. 3 Modal composition of various granitic rocks of the Cape Ashizuri pluton.

Recent U-Pb ages on zircons must be more reliable than the K-Ar ages, They are 13.12±0.09 Ma for syenite along south coast and 12.95±0.06 Ma for monzogranite at north (Shinjoe *et al.*, 2010). Gabbroids are mingled with these syenite and granite. Thus, all the plutonic rocks intruded in a short period around 13 Ma, but alkali dolerite and alkali rhyolite dike may be younger, because they intruded after solidification of the plutonic body. This Miocene intrusion age is very close to the youngest age of sedimentary rocks of the southernmost Shimanto Supergroup.

Modally speaking, the granitoids are plotted from K-feldspar corner to syenogranite and monzogranite areas (Fig. 3; Murakami and Matsuo, 1963; Hayashi *et al.*, 1969). Mapping this pluton in 1993, Imaoka and his student (personal communication, 2011) recognized three plutonic units:(1) Gabbroids mingled with Rapakivi granite and biotite-hornblende granite, which are typically shown at the Cape Ashizuri (see Plate 1B), (2) Alkaline granite unit occurring along the south coast, which is composed of various grain size of syenite and quartz syenite, and locally alkali feldspar granite, (3) Coarse-grained monzogranite intruded into the above two units (Fig. 2). As mentioned previously, the units 2 and 3 are intruded at 13.12 and 12.95 Ma, respectively, on U-Pb zircon age.

Murakami *et al.* (1989) proposed a ring complex model for the formation of these rocks, having different source rocks with low initial $^{87}Sr/^{86}Sr$ ratio of 0.7038 for the inner gabbroic and syenitic rocks (Unit 1), and higher 0.7059 value for the outer granite (Unit 3).

Therefore, the quartz-free plutonic rocks have a deeper, more primitive source rocks than the quartz-bearing rocks of continental crust, which is supposed to be the youngest members of the Shimanto Supergroup.

3. Chemical characteristics

Chemical analyses of the gabbroic and granitic rocks were newly performed on 17 samples by the Code 4E-research set of the Actlabs, which is done by the total digestion – ICP/MS and lithium metaborate fusion – ICP/MS for 50 major and trace elements, but S by infrared and F by ISE (see the Actlabs webpage for the details: http://www.actlabs.com/). The detection limits and analytical results are listed in Table 1.

In the syenitic rocks, well digested mafic enclaves are sometimes observed. Two examples (Nos. 3 and 4, Fig. 2) of the 58A124 site are high in mafic components such as TiO_2 (1.4-1.6 wt.%), total Fe_2O_3 (8.9-9.1 wt.%), MgO (2.5-2.8 wt.%) and Zn (235-258 ppm) for the SiO_2 55.2-55.5 wt.% rocks. These granitoids may contain zincian ilmenites described by Nakashima and Imaoka (1998) for the high bulk Zn contents (Table 1). Another feature is general high contents of fluorine in the Cape Ashizuri granitoids, especially in the 58A124 rocks of 0.43-0.26 wt.% F. Zirconium contents are also high in the Cape Ashizuri granitoids, in which the highest of 1,220 ppm is seen in the 58A142 quartz syenite.

A drilling for uranium exploration was performed in winter of 1969 at the northern-off part of the community Isa (Fig. 2), southwest of the old placer mining site.

Table 1 Chemical composition of the Cape Ashizuri plutonic rocks.

Filing No.		1	2	3	4	5	6	7	8	9	10	11	12	13	14	15	16	17
Anal. Sym.	Det.Lmt.	58A102	58A101	58A124	58A124M	58A124F	58A126	58A142	DH38.0	DH66.9	DH96.3	DH145.2	DH180.1	DH210.6	58A118	69AZ01	58A152	58A130
SiO2	0.01	51.39	63.62	55.23	55.51	70.59	55.6	66.26	67.1	65.69	64.99	66.09	67.85	66.49	70.08	72.77	73.1	76.08
TiO2	0.001	1.374	0.912	1.382	1.613	0.22	1.915	0.317	0.32	0.357	0.31	0.394	0.351	0.367	0.383	0.371	0.165	0.204
Al2O3	0.01	14.51	14.6	15.25	15.95	13.95	15.39	15.43	15.62	15.95	15.6	16.06	15.31	16.04	13.97	13.46	13.13	12.18
Fe2O3(T)	0.01	8.79	5.6	9.06	8.9	2.16	9.79	3.74	3.93	4.15	3.12	3.77	3.22	3.33	2.55	2.6	2.26	1.7
MnO	0.001	0.146	0.102	0.186	0.184	0.062	0.2	0.103	0.095	0.129	0.073	0.076	0.065	0.074	0.042	0.044	0.024	0.025
MgO	0.01	6.91	2.42	2.45	2.84	0.07	3.25	0.12	0.14	0.18	0.2	0.32	0.29	0.34	0.56	0.44	0.08	0.21
CaO	0.01	11.4	4.69	3.88	4.65	0.83	6.48	0.93	1.04	1.39	1.1	1.16	0.91	1.14	1.16	1.21	0.32	0.65
Na2O	0.01	2.46	3.87	5.73	5.89	4.74	4.22	5.1	5.1	5.26	4.97	5	4.55	4.78	3.25	3.53	3.58	3.28
K2O	0.01	1.56	3.79	3.34	3.02	5.11	2.51	5.49	6.26	5.77	6.34	6.28	6.17	6.3	5.98	4.82	6.76	4.52
P2O5	0.01	0.28	0.21	0.47	0.56	0.03	0.52	0.03	0.04	0.05	0.04	0.07	0.06	0.07	0.09	0.09	0.04	0.04
LOI		1.15	0.57	1.17	0.78	0.6	0.65	0.48	0.3	0.46	0.38	0.34	0.41	0.39	0.55	0.46	0.2	0.36
F	0.01	0.07	0.14	0.34	0.43	0.26	0.17	0.1	0.11	0.17	0.12	0.13	0.13	0.12	0.1	0.13	0.02	0.1
S	0.001	0.107	0.044	0.01	0.02	0.02	0.017	0.02	0.006	0.006	0.004	0.004	0.003	0.002	0.005	0.011	0.002	0.008
Total	0.01	99.98	100.4	98.16	99.89	98.36	100.5	98	99.95	99.38	97.13	99.56	99.19	99.33	98.61	99.81	99.65	99.24
Rb	1	48	133	311	284	281	126	251	239	257	229	250	214	228	239	229	346	284
Cs	0.1	0.9	2.1	7.3	5.4	4.4	2.5	2.6	5.5	3.6	6.8	4.8	6	4.9	6.3	34.4	2.8	9.4
Sr	2	405	203	247	346	19	298	12	13	17	30	47	49	68	84	71	24	31
Ba	1	1189	586	1607	1755	199	623	101	126	158	223	354	393	575	679	411	169	171
Ga	1	15	20	20	21	26	22	26	24	24	23	25	22	24	19	20	24	19
Ge	0.5	1.8	2.2	1.8	2	2	2.1	2.3	2.5	2	2.1	2.6	2.2	1.7	1.9	2	2.1	2
Zr	1	131	186	216	241	487	203	1220	684	799	739	706	606	581	275	275	386	235
Hf	0.1	3.1	4.7	5.5	5.9	12.1	5.3	25.6	13.7	16.8	17.2	16.2	13.8	13.3	7.1	7.7	9.9	7.4
Nb	0.2	38.3	80.5	91.2	110	162	79.7	202	141	173	144	151	118	118	47.4	59.4	122	40.4
Ta	0.01	2.68	6.13	8.04	7.57	11.1	6.87	14	9.45	11.3	10.6	9.2	7.85	7.37	3.62	6.01	10.9	5.98
Be	1	1	3	5	5	4	4	5	4	6	4	4	3	3	3	4	6	5
Sn	1	1	13	15	12	5	7	5	6	5	4	6	5	4	4	5	4	4
W	1	20	50	21	15	31	24	49	13	20	21	15	19	21	87	84	54	78
Mo	2	< 2	< 2	< 2	< 2	< 2	< 2	< 2	< 2	2	11	< 2	< 2	< 2	< 2	5	< 2	< 2
Th	0.05	9.04	25.4	23.6	14.9	51.5	14.5	74.2	36.5	66.3	63.3	50.8	56.2	37.4	24.2	43.5	53.2	69.1
U	0.01	1.63	4.1	5.56	3.65	9.86	3.33	8.6	6.91	12	7.03	5.7	8.27	6.59	3.47	8.27	11.4	11.3
Cr	0.5	32.3	17	17.6	14.4	< 0.5	< 0.5	3.6	< 0.5	< 0.5	< 0.5	< 0.5	< 0.5	< 0.5	8.4	5	< 0.5	3.8
V	5	285	130	115	120	< 5	249	< 5	< 5	< 5	9	12	10	9	32	21	6	10
Co	0.1	39.9	26	15.5	17.4	5	29	9.7	2.4	4.4	4.9	4.2	5	5.3	16.4	15.7	10.9	13.9
Ni	1	52	23	16	17	2	12	2	2	1	2	2	1	2	4	5	2	3
Cu	1	116	36	3	4	3	19	4	3	4	1	5	< 1	2	3	< 1	1	2
Zn	1	55	60	235	258	68	126	75	78	78	59	64	55	56	40	42	28	30
Pb	5	< 5	< 5	5	15	12	8	< 5	10	7	6	< 5	9	6	10	7	< 5	< 5
As	1	2	1	5	2	3	2	2	3	3	4	< 1	1	2	3	6	< 1	2
La	0.05	31.8	49.3	65.8	77.2	130	59.8	263	147	118	232	304	98.7	93.4	69.6	75.7	89.8	72.6
Ce	0.05	56.8	103	123	143	224	117	442	257	212	384	498	175	170	125	140	160	132
Pr	0.01	6.33	11.2	13.3	15.4	21.4	12.8	42	24.3	21.7	35.5	44.7	17.2	17.4	12.5	14.2	15.6	12.9
Nd	0.05	24.1	40.3	48.6	56.6	67.5	46.5	132	79	74.7	109	136	57.1	60	42.6	48	49.9	40.7
Sm	0.01	4.8	7.72	9.39	10.7	11.5	8.84	18.6	12.5	13.7	14.8	18.7	10.1	11	7.77	8.96	9.37	6.49
Eu	0.005	1.43	1.17	2.64	3.07	0.543	1.8	0.507	0.641	0.662	0.68	0.914	0.852	1.11	0.875	0.767	0.439	0.355
LREE		125.26	212.69	262.73	305.97	454.943	246.74	898.107	520.441	440.762	775.98	1002.31	358.952	352.91	258.345	287.627	325.109	265.045
Gd	0.01	4.41	6.66	8.33	9.52	9.13	7.39	12.3	9.58	11.2	9.84	13.1	8.44	9.13	6.15	7.44	7.92	4.82
Tb	0.01	0.73	1.13	1.48	1.63	1.64	1.26	2.06	1.56	1.98	1.41	2.03	1.45	1.58	1.08	1.36	1.58	0.88
Dy	0.01	4.22	6.73	8.71	9.64	9.91	7.3	12.2	9.15	11.6	7.94	11.2	8.82	9.3	6.29	8.04	10.1	5.41
Ho	0.01	0.86	1.43	1.88	2.02	2.17	1.52	2.64	1.93	2.42	1.65	2.27	1.89	1.94	1.28	1.67	2.17	1.19
Er	0.01	2.35	4.13	5.38	5.74	6.23	4.29	8.17	5.69	6.99	5	6.46	5.55	5.57	3.53	4.81	6.44	3.64
Tm	0.005	0.361	0.698	0.91	0.935	1.09	0.707	1.47	0.99	1.25	0.894	1.07	0.947	0.954	0.564	0.831	1.16	0.668
Yb	0.01	2.28	4.45	5.53	5.79	6.41	4.34	10	6.41	7.87	5.89	6.66	5.92	5.87	3.45	5.01	6.92	4.32
Lu	0.002	0.318	0.624	0.777	0.818	0.91	0.636	1.65	0.989	1.18	0.934	1.01	0.875	0.858	0.477	0.728	0.95	0.646
HREE		15.529	25.852	32.997	36.093	37.49	27.443	50.49	36.299	44.49	33.558	43.8	33.892	35.202	22.821	29.889	37.24	21.574
Y	1	23	39	61	60	65	41	74	55	67	47	61	52	52	34	45	62	33
Sc	0.01	38.8	15.7	13.5	15.6	1.67	20.8	4	3.94	4.24	3.28	4.74	3.63	4.45	6.34	5.94	1.14	3.17
NK/A		0.40	0.72	0.86	0.81	0.96	0.63	0.93	0.97	0.93	0.96	0.94	0.93	0.92	0.85	0.82	1.01	0.84
Ga10000/Al		1.95	2.59	2.48	2.49	3.52	2.70	3.19	2.90	2.84	2.79	2.94	2.72	2.83	2.57	2.81	3.46	2.95
ASI		0.55	0.77	0.76	0.74	0.94	0.72	0.96	0.92	0.92	0.92	0.94	0.97	0.96	1.00	1.02	0.95	1.06
ZrT°C		636	748	746	748	877	730	975	900	914	906	905	898	888	830	835	859	829

It cuts through fine to medium grained quartz syenitic rocks, which had been sheared in some places. The fresh quartz syenites are relatively high in F, 1,100-1,700 ppm; Zr, 581-799 ppm, and LREE, 353-1,002 ppm, and radioactive components of Th, 37-66 ppm and U, 6-12 ppm. The highest Zr (1,220 ppm) and thorium (74
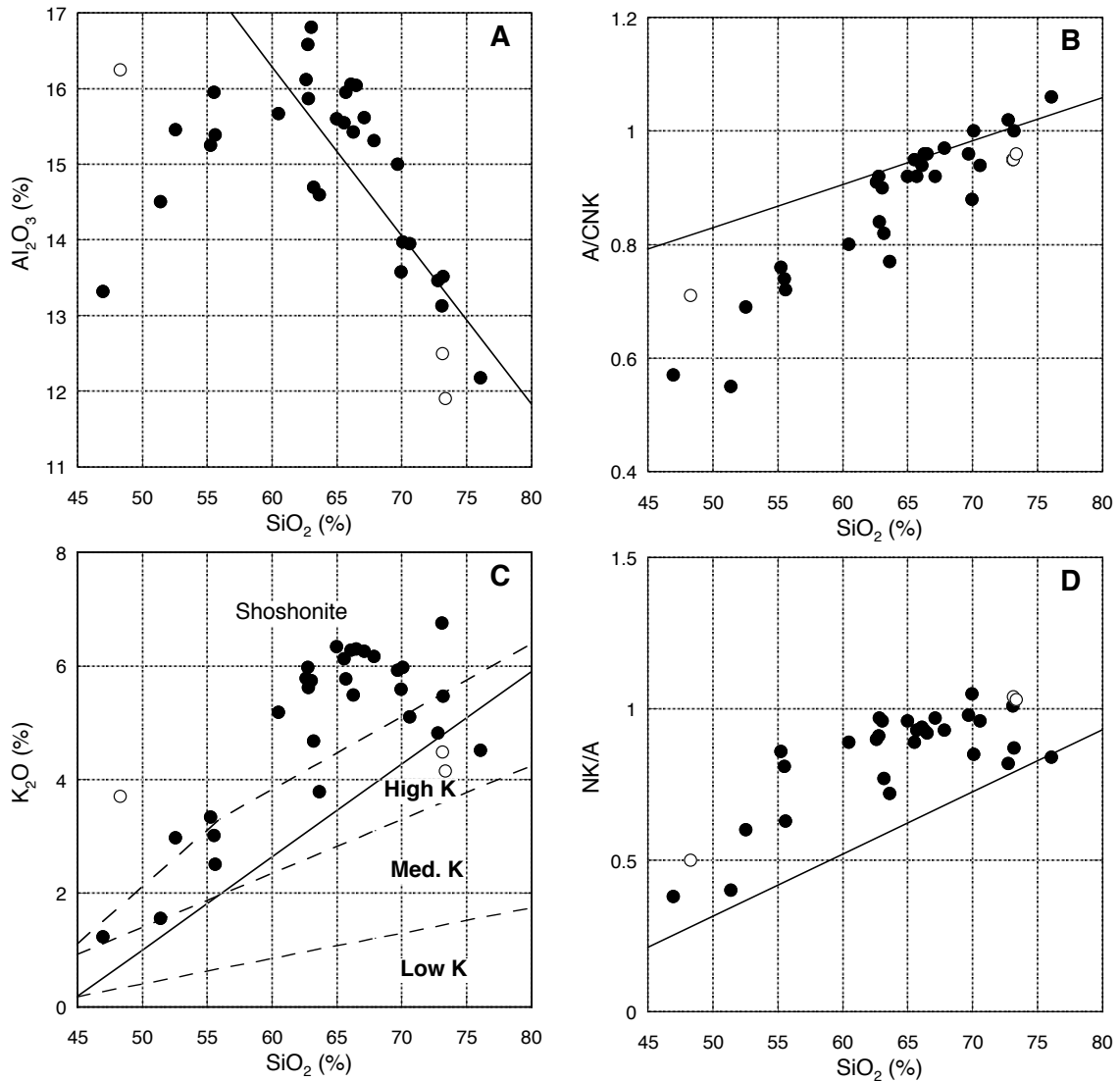
Fig. 4 Harker diagrams for Al_2O_3, A/CNK, K_2O and NK/A. Straight line is an averaged trend of the Okueyama granitoids of Ishihara and Chappell (2010). Open circle, post-plutonic dikes of dolerite (AZ04) and rhyolite (AZ02, 03) from Ishihara *et al*. (1990) for Figs. 4 through 12.

ppm) contents were found at the 58A142 site (No. 6 in Fig. 2).

Chemical data reported in the previous paper (Ishihara and Murakami, 2006) and newly analyzed data in Table 1 are plotted by solid circle in the Harker diagrams from Figures 3 to 7, together with post-plutonic dikes (open circle) of dolerite and rhyolite of Ishihara *et al*. (1990). The straight line in the figures is an average trend of the vertically zoned, Okueyama pluton (Ishihara and Chappell, 2010), which belongs to typical I-type calc-alkaline ilmenite series.

3.1 Harker diagrams

Distribution of Al_2O_3 contents is parallel to that of the Okueyama pluton in the granitic composition (e.g., SiO_2 higher than 65 wt.%), but some gabbroids including diorites, i.e., silica lower than 56 wt.% (e.g., 58A102, 58A124 and 58A126 in Table 1 of this paper;

AZR1 and 58A153 in Table 1 of Ishihara and Muraka-mi, 2006), are low in the content of Al_2O_3 (Fig. 4A). Thus, the Cape Ashizuri pluton is clearly separated into gabbroids and granitoids in the alumina-silica diagram. Both dolerite and rhyolite dikes are lower in the Al_2O_3 contents than the plutonic rocks.

In the A/CNK-SiO_2 diagram (Fig. 4B), however, the Cape Ashizuri rocks, both plutonic and dike rocks, are plotted in similar distribution trend decreasing the Al_2O_3 contents sharply to the low SiO_2 side. This would indicate that feldspars of the Cape Ashizuri pluton belong to the same fractionation trend from the gabbroids to the biotite monzogranite. Also peraluminousness increases sharply toward the high silica rocks but never exceeds 1.2. Compared with the Okueyama granitoids, the Cape Ashizuri rocks are lower in the A/CNK ratio; thus less aluminous.

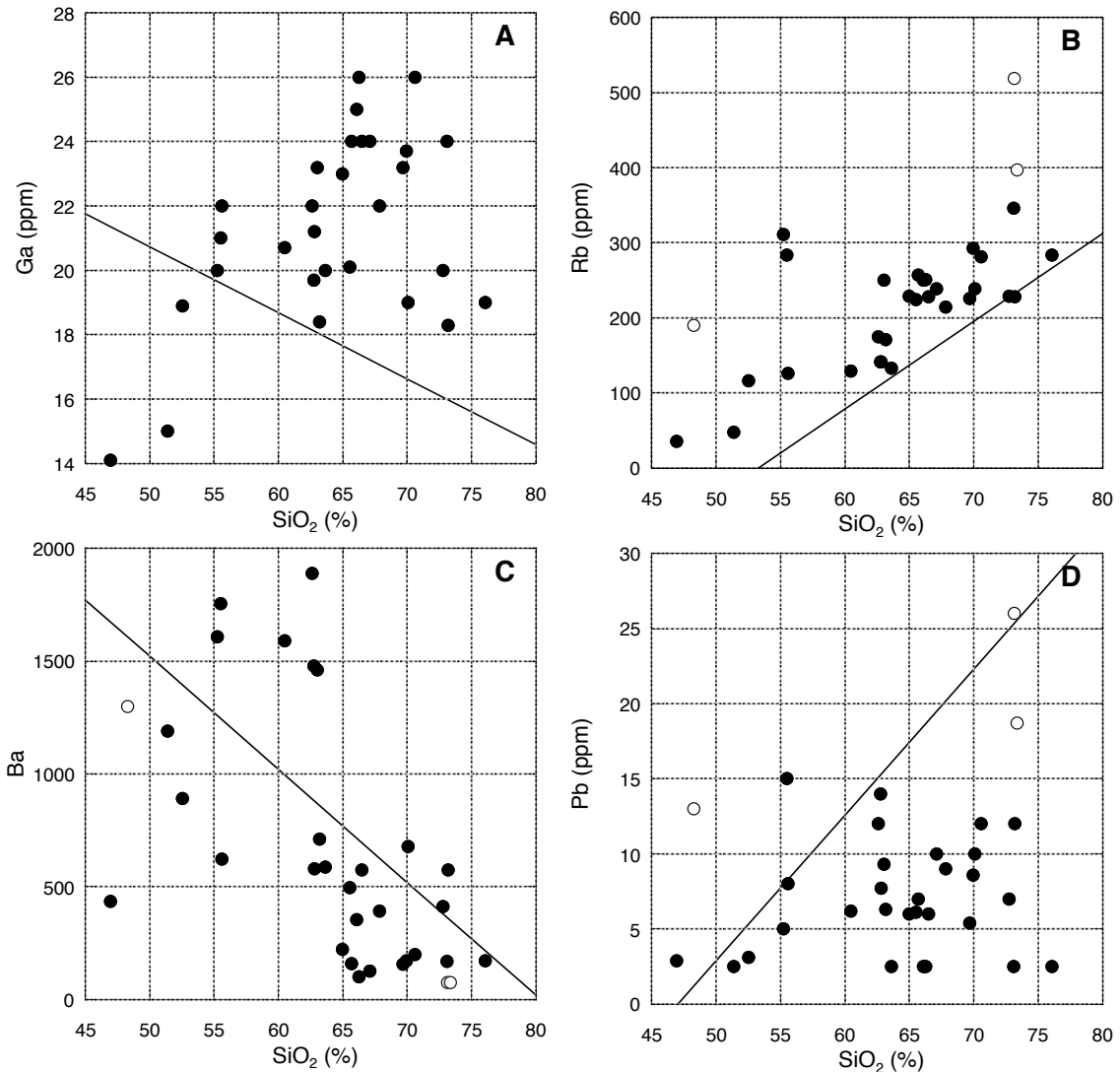K_2O contents are plotted in the shoshonite and high

Fig. 5   Harker diagrams for Ga, Rb, Ba and Pb.

K-series areas (Fig. 4C) and are higher than those of the Okueyama granitoids. Three biotite monzogranites and two gabbroids are as low as the Okueyama trend. Dolerite dike is plotted in the shoshonite field, but the two rhyolite dikes are less potassic, plotted in the high-K field. Molecular ratio of sodium and potassium against alumina (NK/A) is constantly much higher than that of the Okueyama pluton (Fig. 4D).

Trace elements which replace Al_2O_3 in feldspars show unusual trend. Gallium (Ga^{3+}, 0.62Å, Mason, 1966), for example, does not follow the amount of Al_2O_3 (Al^{3+}, 0.50Å) and is much higher in felsic rocks than mafic rocks, which is completely different from common distribution trend of calc-alkaline rocks that follow Al_2O_3 contents as seen in the Okueyama pluton. Except for two gabbroids, the Ga contents range from 18 to 26 ppm (Fig. 5A), which are much higher than those of the Okueyama granitoids. This relative abundance was used to define the granitoids as A type by Imaoka and Nakashima (1994), although the geologic environment

is not anorogenic but orogenic.

Rubidium (Rb^+, 1.47Å) which replaces K^+ (1.33Å) in K-feldspar shows the same distribution trend as that of the Okueyama granitoids, but the contents are higher (Fig. 5B). Barium (Ba^{2+}, 1.34Å) contents are similar to those of the Okueyama granitoids, decreasing in the content with increasing SiO_2 in general (Fig. 5C). However, the contents are much lower in the rocks with 47-55 wt.% and 63-73 wt.% SiO_2 ranges, but higher in the rocks with 55-63 wt.% SiO_2 range, as compared with the average trend of the Okueyama pluton. Trace amounts of lead (Pb^{2+}, 1.20Å) that takes K-position in K-feldspar, are much lower than those of the Okueyama pluton (Fig. 5D), which ranges from 14 to 40 ppm Pb in the common granodioritic phase and 40 to 70 ppm Pb in the uppermost leucocratic phase (see Ishihara and Chappell, 2010).

CaO contents are generally lower than the average of the Okueyama pluton in the main syenitic rocks (Fig. 6A). On the contrary, Na_2O contents are much higher

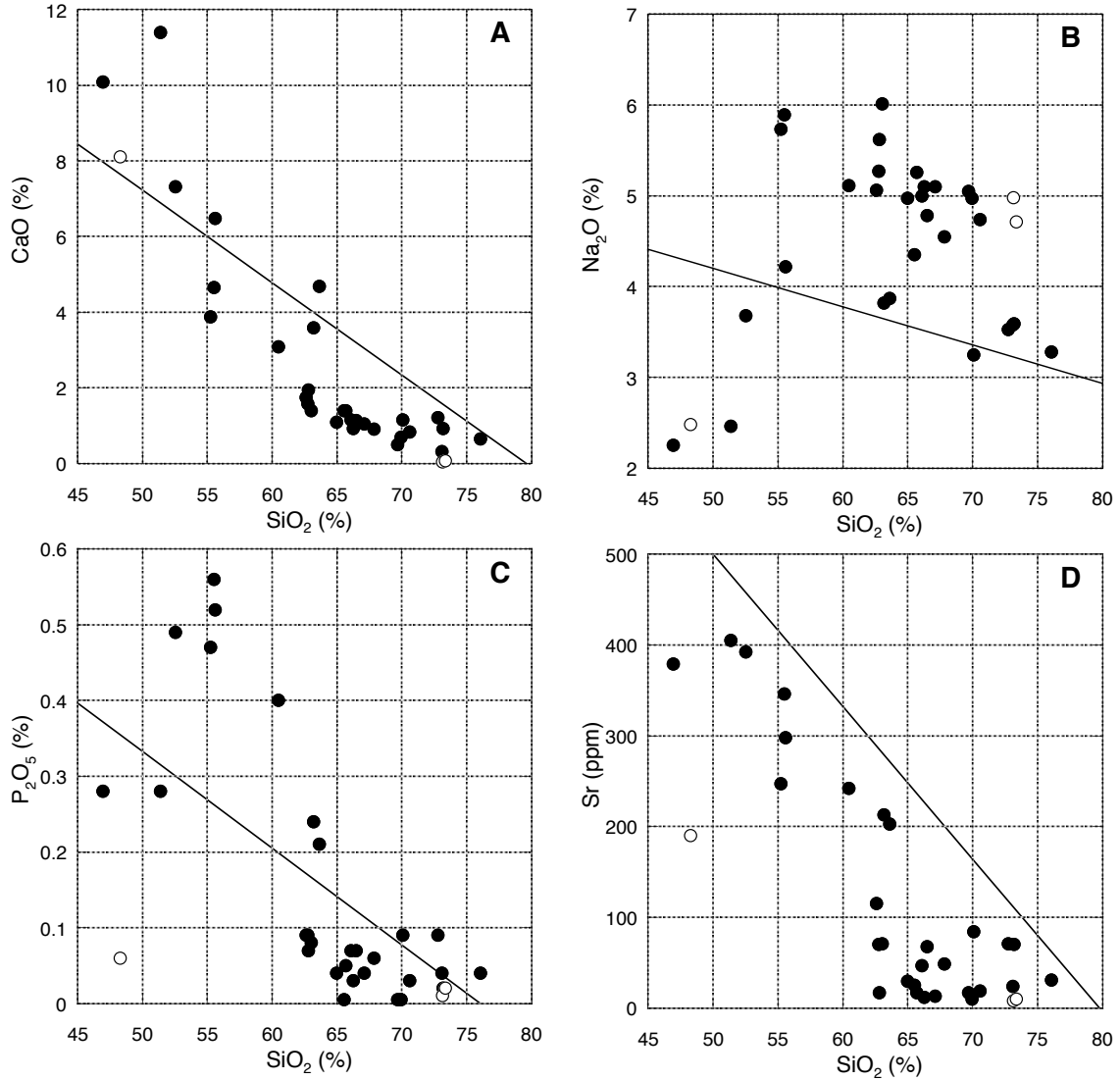Fig. 6   Harker diagrams for CaO, Na₂O, P₂O₅ and Sr.

than the average contents especially on the SiO$_2$ 55-70 wt.% rocks (Fig. 6B). Two gabbroids high in CaO content are very low in Na$_2$O content. Thus, these two rocks (58A102 and AZR1) must contain very calcic plagioclase. P$_2$O$_5$ contents are very high at around SiO$_2$ 55%, but most of syenitic rocks are lower than the average content of the Okueyama pluton (Fig. 6C). About strontium (Sr^{2+}, 1.12Å), it follows CaO content implying its occurrence in plagioclase (Ca^{2+}, 0.99Å); but the contents are very low in the granodiorite-granite phase (SiO$_2$ 63-76 wt.%). Distribution of Sr is always lower than that of the average value of the Okueyama body (Fig. 6D).

Total Fe$_2$O$_3$ contents are slightly lower than the average content of the Okueyama granitoids, but MnO contents are very similar or slightly higher than the average contents of the Okueyama pluton (Figs. 7A, B). Two dikes have similar distribution. Both MgO and TiO$_2$ contents are different having higher values at low silica side than the Okueyama average, but depleted in

high silica range of 63 to 73 wt.% (Figs. 7C, D). One gabbro, AZR1 (Ishihara and Murakami, 2006), is very high in MgO (12.5 wt.%), implying high magnesian source rock in the upper mantle for this rock. About zinc (Zn^{2+}, 0.75Å) replacing ferrous iron (Fe^{2+}, 0.78Å) and Mg^{2+} (0.72Å), the contents are similar to the average content of the Okueyama pluton but variable at the low silica range rocks (Fig. 7E). About copper (Cu^{2+}, 0.73Å), the contents are generally higher in mafic rocks but are lower in the high silica range rocks than the average of the Okueyama granitoids (Fig. 7F).

Among the other trace element, characteristics of the Cape Ashizuri pluton are abundance of HFSE (high-field-strength elements), notably Zr, Hf, Nb, Ta, Y, REE, Th and U, and also F. The HFSE-bearing accessory minerals occur generally as euhedral forms scattered in the rock-forming minerals, but fluorite, the source of fluorine, is typically seen as rounded forms associated with mafic silicates, especially of biotite.

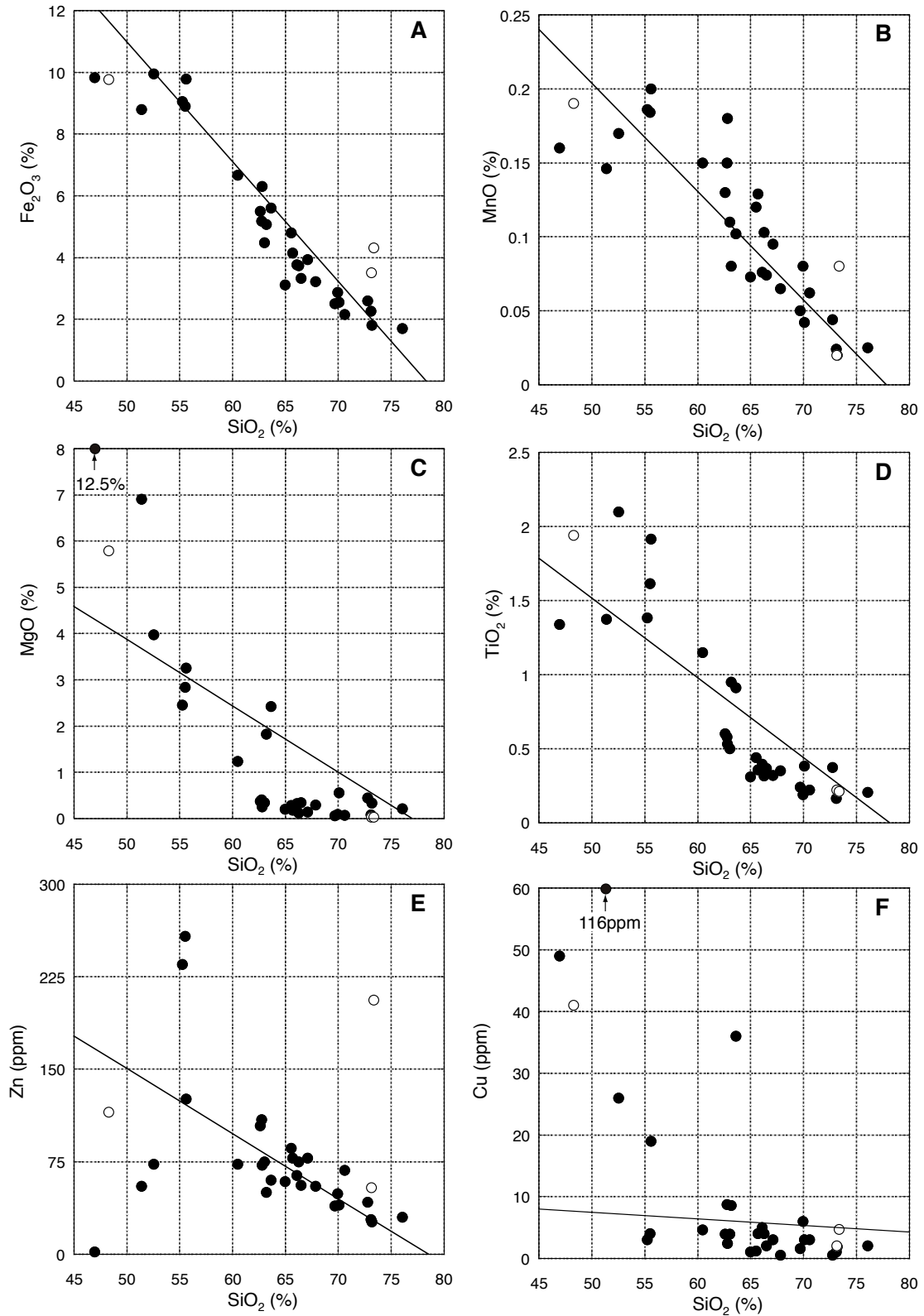The Zr contents show unique distribution pattern.

Fig. 7　Harker diagrams for Fe$_2$O$_3$, MnO, MgO, TiO$_2$, Zn and Cu.

They are low at low-silica range and are highest around 66 wt.% SiO$_2$, then decrease to the higher silica contents (Fig. 8A). The highest values were obtained on 58A142 and drill-core samples (solid triangle).

As a whole, Zr contents are the highest at 65-67 wt.% SiO$_2$ rocks, similarly to the pattern observed in the Boggy Plain pluton of the Lachlan Fold Belt, Southeast Australia, which was considered as one of the
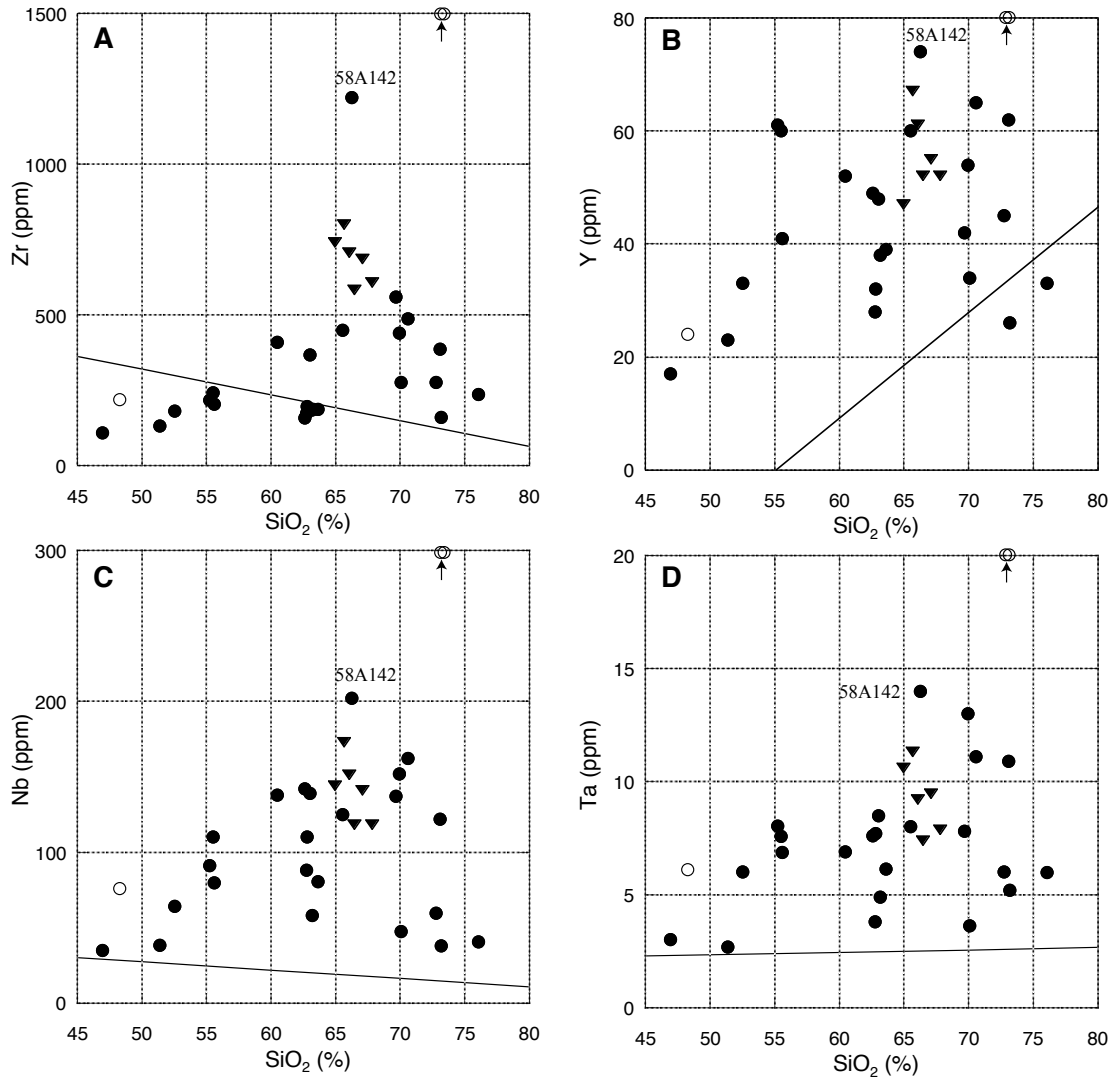
Fig. 8 Harker diagrams for Zr, Y, Nb, and Ta. Solid triangle for the six drill core samples for Figs. 8 and 9.

typical patterns for the high temperature I-type granites (Chappell *et al.*, 2004). The whole contents of Zr are much higher than the average of the Okueyama granitoids, which agree to the experimental data implying that solubility of zircon is much higher in peralkaline melt than metaluminous or peraluminous melt (Linnen and Keppler, 2002). The highest content is 1,220 ppm, which is the highest among the Japanese granitoids.

Contents of Y, Nb and Ta are high and are similar to that of Zr (Figs. 8B, C, D). The contents are much higher in the Cape Ashizuri granitoids than in the Okueyama granitoids (Figs. 8B, C), which agrees to alkalinity control of solubility of $MnNb_2O_6$ in granitic melts (Linnen and Keppler, 1997). Again, the highest peaks are around 66 wt.% SiO_2 (Fig. 8C). Distribution of Ta is very similar to that of Nb in the Harker diagram (Fig. 8D) for similar ionic radius and charge (Nb^{+5}, 0.69Å, Ta^{+5}, 0.68Å). In all the Zr, Y, Nb, and Ta diagrams, the post-plutonic rhyolite dikes are very high in these elements plotted at the outside of the diagrams.

Both Th and U contents are much higher than the averages of the Okueyama granitoids, and increase with increasing silica contents (Figs. 9A, B). Both La and Ce contents are lower than the averages of the Okueyama pluton at gabbroic composition, but are higher than the averages in the high-silica rocks, with the highest peak at 66 wt.% SiO_2 (Figs. 8E, F), similarly to the patterns of Zr and Nb.

3.2 Binary diagrams

Binary diagrams were made on Zr and other related elements. Zirconium in igneous rocks is contained in zircon ($ZrSiO_4$); zircon forms a complete solid solution with hafnon (Linnen and Keppler, 2002). Therefore, Zr (Zr^{+4}, 0.72Å) - Hf (Hf^{+4}, 0.71Å) pair has the highest correlation coefficient of R = 0.98 (Fig. 10A). Hoshino *et al.* (2010) analyzed zircon from monzogranite phase (No. 152) of the northern part of the plutonic body, and found that the core has 0.93 wt.% HfO_2 but the rim contains 1.94 wt.% HfO_2, implying that hafnon com-
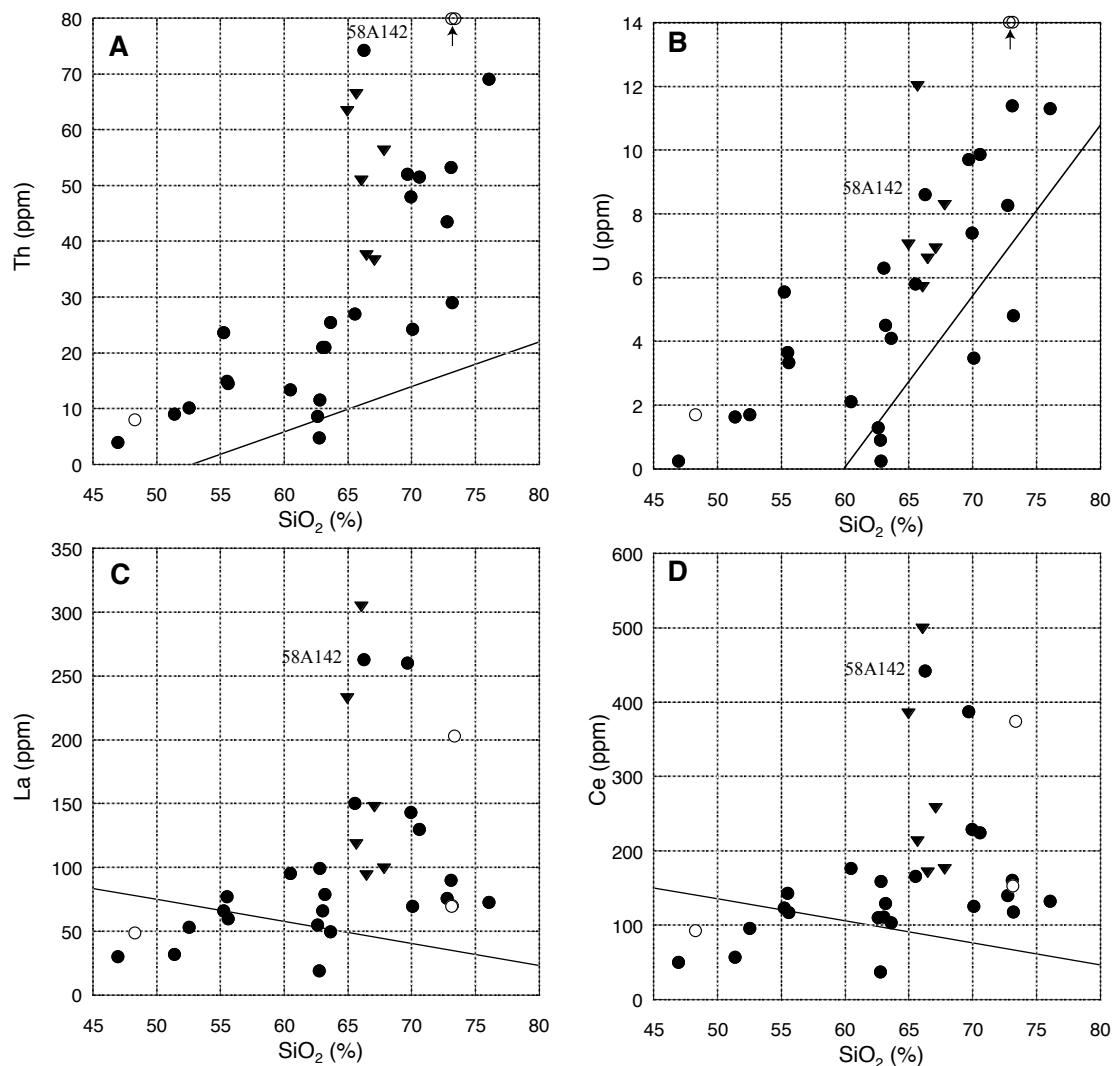
Fig. 9 Harker diagrams for Th, U, La, and Ce. Six drilled samples are shown by solid triangle.

ponent tends to be concentrated in a later zircon phase. Generally speaking, the core of given zircon is concentrated by 0.19 wt.% Y_2O_3, 0.21 wt.% Yb_2O_3, 0.12 wt.% FeO, 0.31 wt.% ThO_2 and 0.43 wt.% UO_2 (Hoshino *et al.*, 2010).

Correlation coefficient of the bulk Zr with Ce is the next high as R = 0.83 (Fig. 10B), which can be expected from the patterns in the Harker diagrams of Figures 8A and 8B. The LREE components should be contained not in zircon but other accessory minerals, such as allanite, monazite and titanite. The correlation coefficients of Zr with Nb, Th, Y and U are lower as 0.79, 0.76, 0.71 and 0.59, respectively. Niobium was detected in ilmenite up to 4.4 wt.% Nb_2O_3 by Nakashima and Imaoka (1998). They also recognized in the studied pluton trace amounts of Nb-oxide such as fergusonite, samarskite, columbite and pyrochlore, which could contain some other elements as Y, Ce, Ta, Fe and Ti. Both Th and U are contained in zircon, but their correlation coefficient against Th and U are as low as R = 0.76 (Fig. 10E) and

0.59 (Fig. 10F), respectively.

Among the other heavy elements, the highest correlation coefficient of 0.99 is seen on the La-Ce pair (Fig. 11B), La-Nd (Fig. 12A) and HREE-Dy (Fig. 12C). The high correlation coefficients are observed in Y-Dy (0.97, Fig. 12D), Th-U (0.90, Fig. 11D), Nb-Ta (0.88, Fig. 11A), and Nb-Y (0.83, Fig. 11C). The correlation coefficient of La-Dy pair is only 0.63 (Fig. 12B), implying LREE and HREE occur rather independently depending upon the host REE-bearing minerals.

3.3 REE contents and REE patterns

REE contents of the studied samples are listed in Table 1. The total REE contents vary from 141 ppm of gabbro to 1,046 ppm of the quartz syenite of the drill-core sample at -145.2 meter (DH145.2). Y content is the highest (74 ppm) in the highest Zr rock of 58A142. LREE/HREE ratio is as low as 8.0 to 9.0 in the mafic rocks, but increase in quartz syenite and monzogranite up to 23.1 (DH96.3). Eu anomaly is generally absent
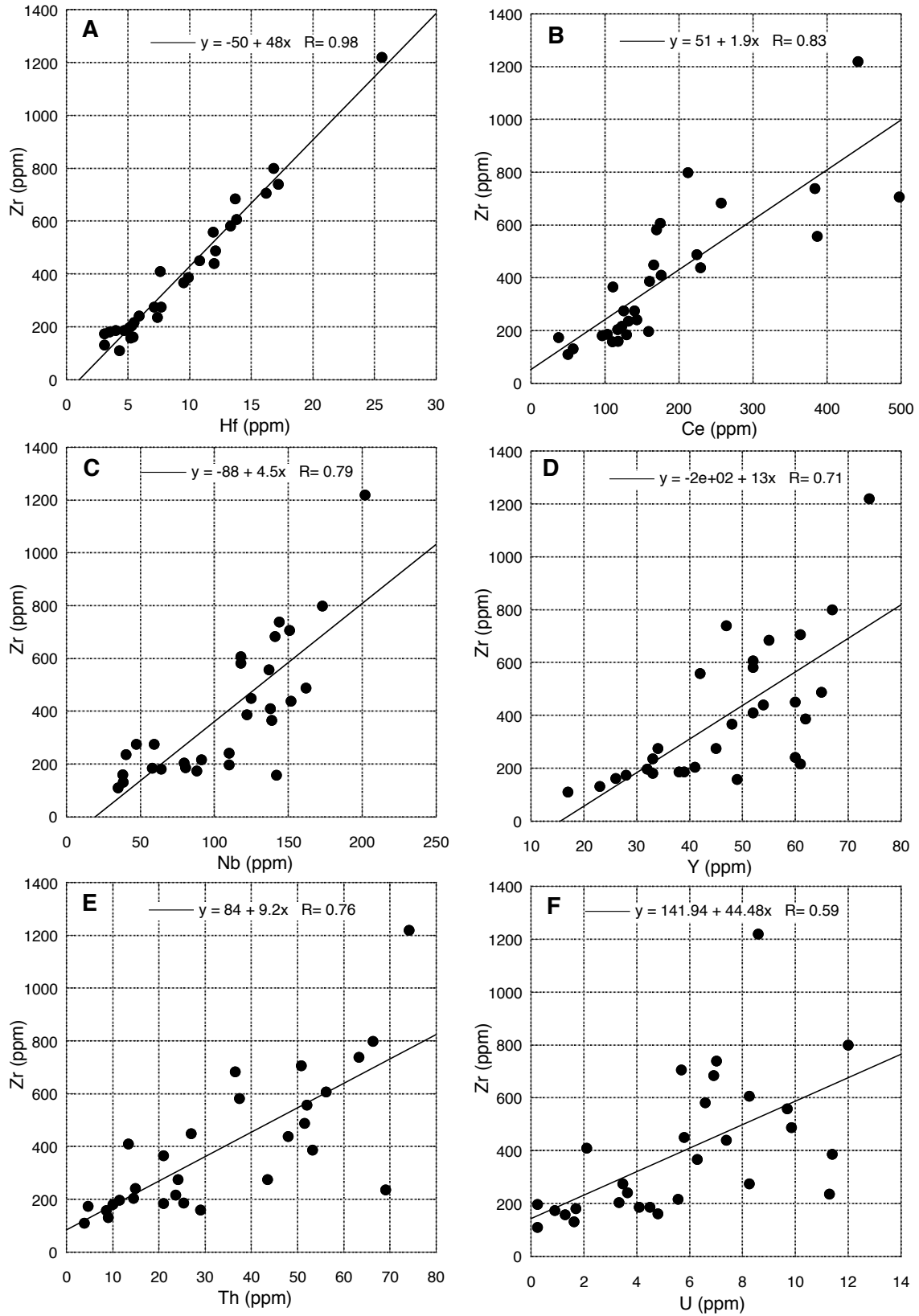
Fig. 10 Binary diagrams for Zr vs. Hf, Ce, Nb, Y, Th and U. Straight line implying the best fit line. The correlation coefficient is also shown.
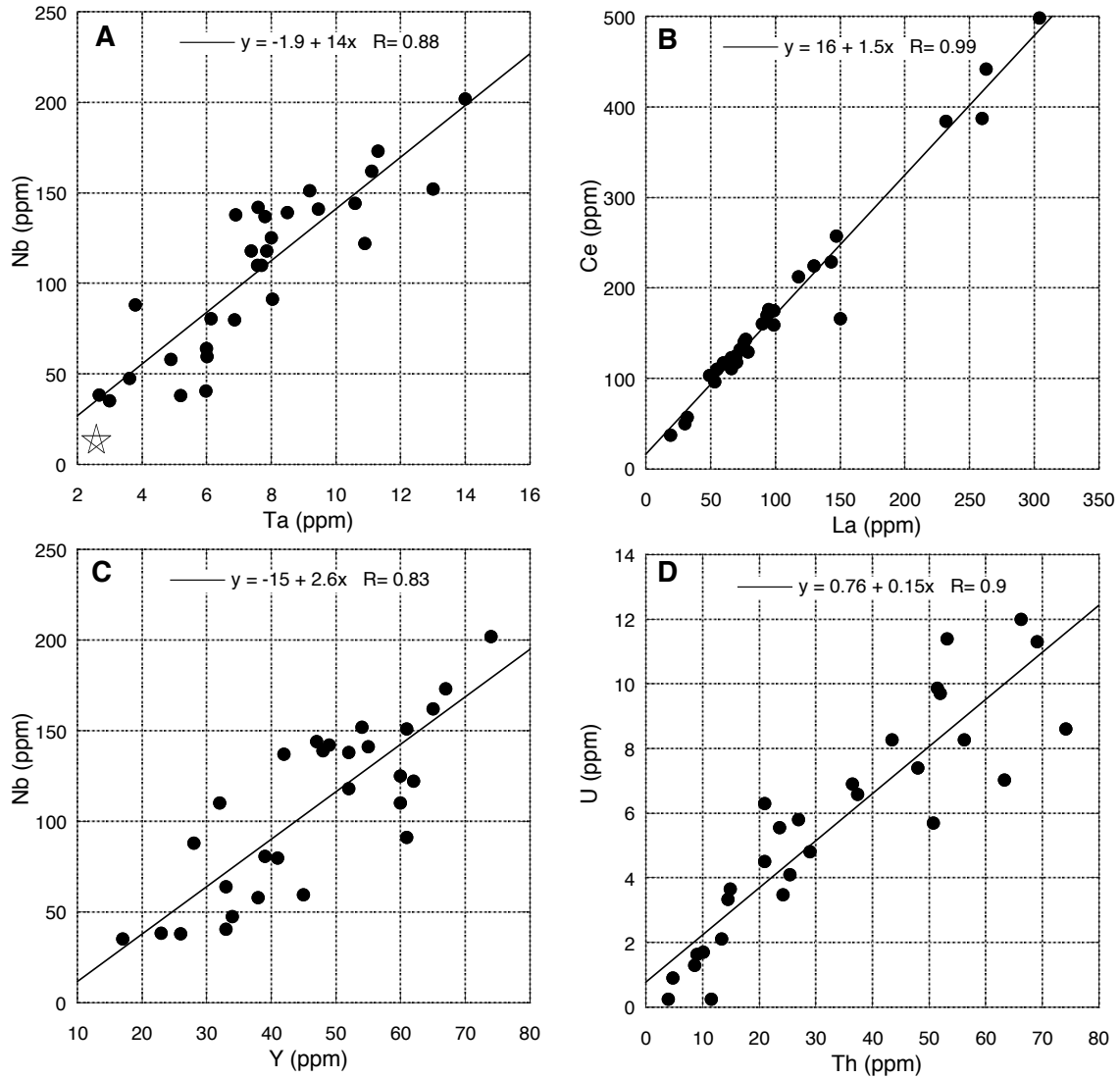
Fig. 11 Binary diagrams for Nb-Ta, Ce-La, Nb-Y and U-Th. Straight line implying the best fit line. The correlation coefficient is also shown.

below 55 wt.% SiO_2 but is seen above this value.

REE pattern of the studied rocks are shown in Figures 13 A to D. The 58A102 gabbro shows the lowest and flat pattern (Fig. 13A). In increasing with silica and potassium contents, the REE contents increase and the negative Eu anomalies also increase. The 58A142 sample with 66.3 wt.% SiO_2 has the largest negative Eu anomaly (Fig. 13A). The same is also seen on the 58A124 point where two mafic monzonites with 55.2-55.5 wt.% SiO_2 mingled with felsic quartz syenite with 70.6 wt.% SiO_2. The monzonites have no but quartz syenite has Eu-negative anomaly (Fig. 13B). It could mean that Ca^{2+} of an early crystallized plagioclase was substituted by Eu^{2+}, thus stayed in mafic counterpart left behind at depth.

Quartz syenites from the drill core have the highest REE contents and the largest negative Eu anomaly (Fig. 13C), including 58A152 monzogranite which intrudes into gabbroids near the Cape Ashizuri. They are considered to have generated from mafic igneous source rocks by small degrees of partial melting. In the other high silica rocks of monzogranite (58A118, 58A130 and 69AZ01), their REE patterns are similar to those of the quartz syenite (Fig. 13D), but they occur in the northernmost part of the Cape Ashizuri pluton and interacted with the intruded Shimanto sedimentary rocks. They have lower NK/A ratio and are lower in the REE contents. These granites may have been formed by interaction between the quartz syenitic magma and partial melting of the sedimentary wall rocks.

Feldspars in igneous rocks have large positive Eu-anomalies. The Eu-anomaly of plagioclase decreases with increasing fO_2 and increasing temperature (Hanson, 1980). This means that Eu is divalent in a reduced magma and preferentially replaces Ca^{2+} position in plagioclase. In Figure 13A, the rock of 51.4 wt.% SiO_2 has no and the rocks of 55.6 and 63.6 wt.% SiO_2 have small Eu-anomalies, but the rocks of 66.3-76.1
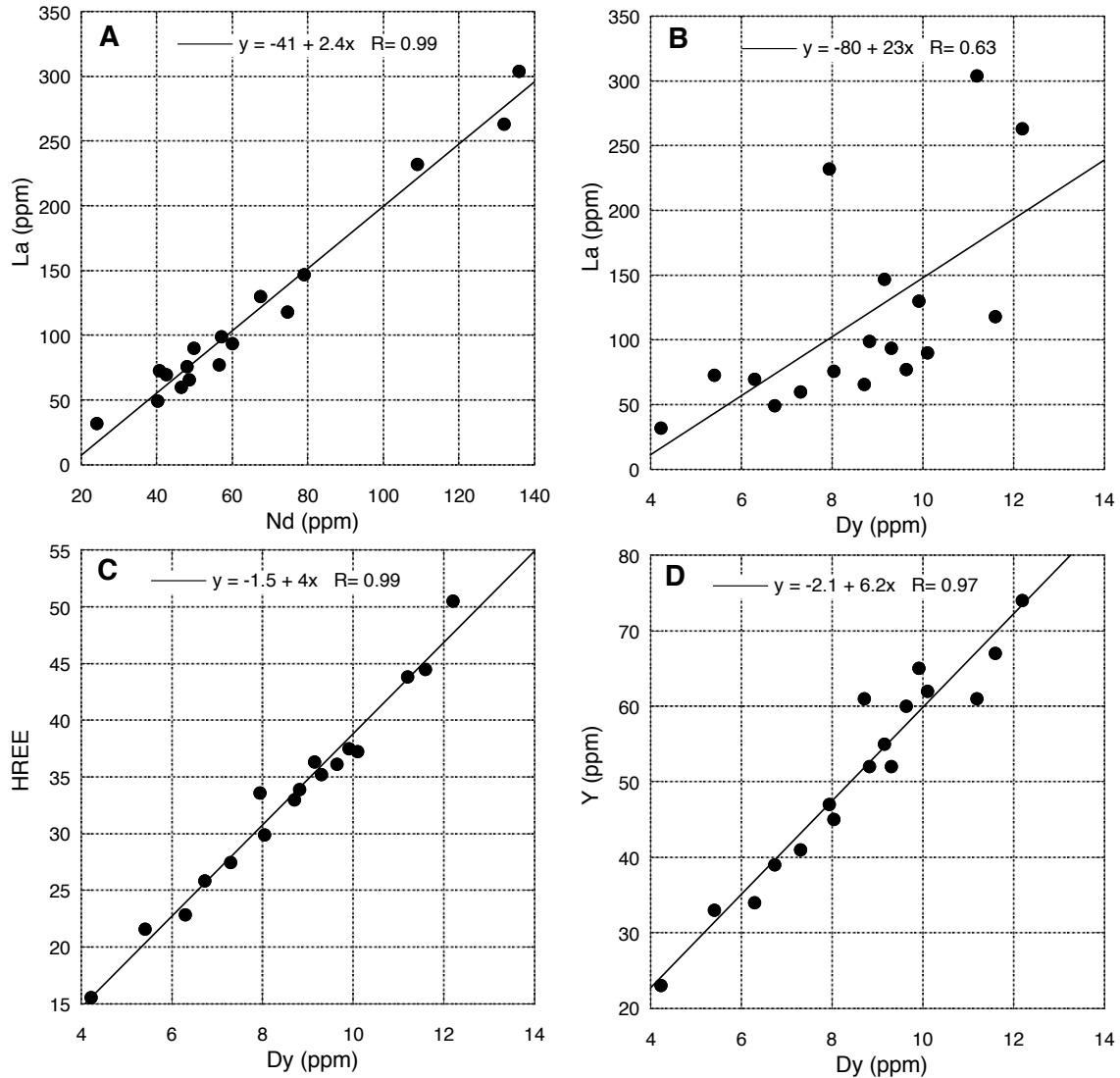
Fig. 12 Binary diagrams for La-Nd, La-Dy, HREE-Dy and Y-Dy. Straight line implying the best fit line. The calculated correlation coefficients are also shown.

wt.% SiO_2 have a distinct Eu-negative anomaly. These could be interpreted that Eu was enriched in calcic plagioclase crystals of calcic and mafic magmas, which crystallized at depth and left behind when the alkaline granitoids intruded upward.

4. Chemical compositions of selected rare minerals

The Cape Ashizuri granitoids are characterized by many rare accessory minerals, and zircon and titanite may be visible by naked eyes. Besides euhedral crystals, zircon shows many strange textures, which may be due to resorption and other reasons. Hayashi and Akai (2011) studied zircon from two localities of quartz syenite and granite, and classified its textures into three types, as Resorption disturbance, Local disturbance, and Hafnon-like disturbance. Ti-rich ferriallanite was studied by Nagashima *et al.* (2011).

Thorite and uranothorite can be found radiometric survey (Hayashi *et al.*, 1969), and Zn- and Nb-ilmenite, and columbite, euxenite, fergusonite, samarskite, and a pyrochlore-like mineral occur in syenite (Nakashima and Imaoka, 1998). We also studied accessory minerals of the quartz syenite with the highest Zr content (58A142) and a moderate one (DH96.3) and one monzogranite (58A124F), and analyzed Mn- and Nb-ilmenite, zircon, allanite, titanite, fergusonite and chevkinite by an electron probe microanalyzer (EPMA) with the method described in Hoshino *et al.* (2006, 2010). The results are shown in Tables 2 to 7.

4.1 Ilmenite

Ilmenite is commonly contained in both ilmenite-series and magnetite-series granitoids. The ilmenites in ilmenite-series granitoids of the Outer Zone granites (Osumi and Takakumayama plutons) have MnO contents of 5 to 19 wt.%, which tends to increase toward
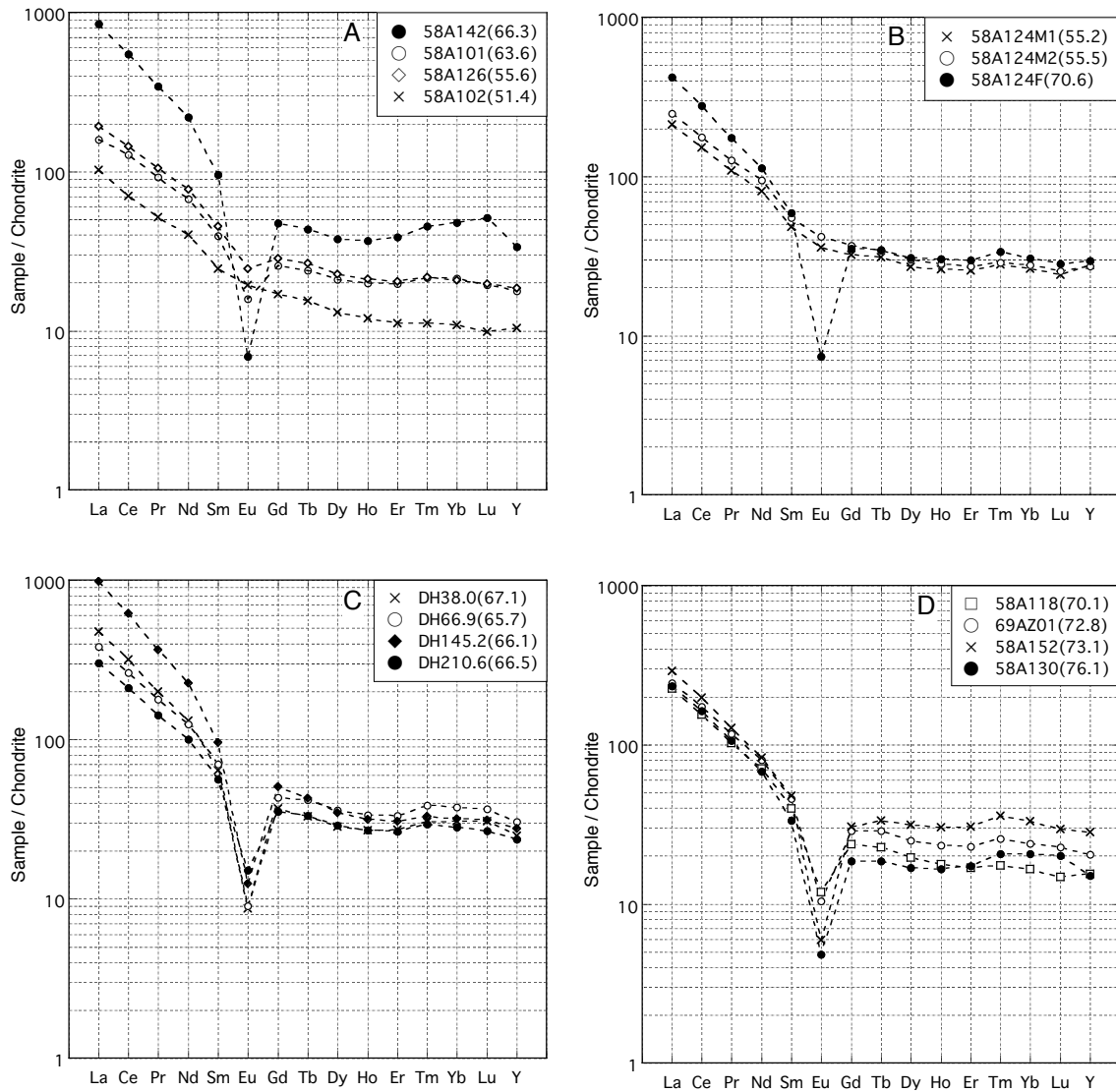
Fig. 13 Selected REE patterns of the studied plutonic rocks.

the margin of crystals (Tsusue, 1973). Tsusue and Ishihara (1974) found common occurrences of hemo-ilmenite in the magnetite-series granitoids in the Sanin Belt of the Inner Zone of SW Japan, but no such minerals are observed in the Ashizuri-misaki magnetite-series granitoids, implying relatively lower oxygen fugacity of the Cape Ashizuri pluton than typical magnetite-series granitoids.

In the Cape Ashizuri body, Nakashima and Imaoka (1998) reported 1.8 to 4.6 wt.% MnO and up to 4.4 wt.% Nb_2O_5 in the ilmenites of the quartz syenite, where Nb is substituting octahedral site of Ti. Our results are shown in Table 2. MnO contents are as high as 4.3-5.7 wt.% in the 58A142 quartz syenite, but as low as 1.7-1.8 wt.% in the DH96.3 quartz syenite. The 58A124 monzogranite has intermediate values of 2.2 and 2.4 wt.% MnO.

The Nb_2O_5 contents are higher, 2.0 to 3.8 wt.% , in the quartz syenites than 0.27 wt.% of the 58A124 mon-

zogranite (Table 2). The high value is seen at rim of ilmenite crystals, which implies that the niobium was added during the latest magmatic stage of the magma crystallization.

4.2 Zircon

Zircons of the granitic terrains in Japan were studied by Hoshino *et al.* (2010), and classified into (HREE)-U-Th-poor type 1, which is hosted in granitoids themselves, and HREE-U-Th-rich type 2, which occurs generally in granitic pegmatites. Within the type 1, zircons are composed of (A) low REE-Th-U subtype and (B) high REE-Th-U-F subtype, the latter of which tends to occur in the well fractionated granites of the Sanyo Sn-W mineralized belt, such as Naegi Granite, Tanakami Granite, and Kurashiki Granite of southern Okayama Prefecture (Ishihara and Murakami, 2006).

Zircons from the Cape Ashizuri pluton are charac-

Table. 2   Chemical composition of ilmenites of selected monzogranite and quartz syenites.

Sample no.	58A124F: monzogranite		58A142: quartz syenite				DH96.3: quartz syenite			
Spot Loc.	1. core		1. core		2. rim		1. core		2. rim	
n	7	100%	4	100%	2	100%	2	100%	4	100%
TiO_2	45.30	49.18	43.97	46.26	41.45	43.62	43.26	45.38	42.80	44.94
FeO	44.18	47.96	44.71	47.03	43.96	46.26	47.72	50.06	48.20	50.61
MnO	2.16	2.35	4.27	4.49	5.72	6.02	1.78	1.87	1.74	1.82
CaO	0.20	0.22	0.07	0.07	0.07	0.07	0.03	0.04	0.01	0.01
Nb_2O_5	0.27	0.29	2.04	2.15	3.84	4.04	2.52	2.65	2.50	2.62
Total	92.11	100.00	95.06	100.00	95.03	100.00	95.33	100.00	95.24	100.00

Table. 3   Chemical composition of zircons of selected monzogranite and quartz syenites.

Sample No.	58A124F: monzogranite				58A142: quartz syenite				DH96.3: quartz syenite				
	Euhedral crystal		Corroded crystal		Corroded	Euhedral crystal		Euhedral	Zoned		X	Y	Z
Spot Loc.	1. core	2. rim	1. core	2. rim		Bright	Dark		Dark	Bright	Single phase crystals		
n	2 (1, 2)	2 (3, 4)	2 (5,6)	2(7,8)	3(9–11)	2 (12,14)	2 (13,15)	2(16,17)	2(18–19)	2(20–21)	3(22–24)	2(25–26)	2(27–28)
SiO_2	34.19	34.09	33.90	33.60	34.93	34.07	34.61	34.57	35.25	35.75	34.69	35.15	35.40
ZrO_2	62.95	61.06	62.88	61.26	64.69	62.75	64.19	64.33	65.09	62.00	63.53	65.40	65.03
HfO_2	2.36	2.47	1.45	1.90	1.36	1.09	1.32	1.03	1.45	1.62	1.08	1.43	1.02
Y_2O_3	0.17	0.67	0.53	0.90	0.12	1.00	0.37	0.26	0.06	0.08	0.56	0.07	0.11
Total	99.67	98.29	98.76	97.65	101.10	98.91	100.49	100.19	101.84	99.46	99.86	102.05	101.56
HfO_2/ZrO_2*100	3.75	4.06	2.30	3.10	2.10	2.61	2.06	1.61	2.23	2.61	1.70	2.19	1.57
Y_2O_3/ZrO_2*1000	2.70	11.00	5.40	14.70	1.90	1.13	5.76	3.98	0.92	12.74	8.82	1.07	1.69

Table. 4   Chemical composition of allanites of selected quartz syenite.

Sample No.	58A142: quartz syenite					DH96.3: quartz syenite	
Spot Loc.	G, 1–5	G, 6–7	G, 8–9	10–14	H, 15–18	I. 19–23	24–25
n	5	2	2	5	4	5	2
SiO_2	31.50	30.86	30.99	31.36	31.19	31.33	30.25
TiO_2	3.08	3.71	3.92	2.73	2.63	3.14	3.17
Al_2O_3	8.97	7.43	7.29	9.44	9.24	9.93	9.38
FeO	19.56	20.30	20.50	19.42	19.81	18.49	18.32
MnO	0.37	0.36	0.41	0.42	0.44	0.32	0.29
CaO	9.53	8.99	9.10	9.66	9.55	9.64	9.41
La_2O_3	7.95	8.27	7.84	7.61	7.93	7.61	8.24
Ce_2O_3	12.92	13.09	12.96	12.95	13.09	12.54	12.26
Pr_2O_3	1.08	0.94	1.10	1.20	1.08	0.95	0.99
Nd_2O_3	2.92	2.75	3.00	3.18	3.18	2.83	2.60
Total REE	25.38	25.81	25.50	25.41	25.74	24.58	25.23
ThO_2	0.16	0.38	0.54	0.17	0.05	0.57	0.54
Total	98.04	97.07	97.63	98.13	98.19	97.35	95.42

For G to I, see Plate II

Table. 5   Chemical composition of titanites of selected quartz syenite.

Sample No.	58A124F: monzogranite			
Spot Loc.	1	2	3 core	3 rim
n	3	5	3	2
SiO_2	30.29	30.52	29.99	30.02
TiO_2	30.73	30.14	29.71	28.78
Al_2O_3	2.49	2.79	2.44	1.60
FeO	1.52	1.65	1.72	2.50
CaO	34.18	34.03	33.20	32.72
La_2O_3	0.03	0.03	0.09	0.05
Ce_2O_3	0.20	0.18	0.45	0.41
Pr_2O_3	0.02	0.04	0.04	0.07
Nd_2O_3	0.04	0.06	0.21	0.14
ThO_2	0.02	0.04	0.04	0.01
Y_2O_3	0.07	0.06	0.16	0.21
ZrO_2	0.19	0.18	0.18	0.10
Nb_2O_5	0.29	0.31	0.71	2.70
Total	100.06	100.02	98.95	99.31

terized by their abundance and ragged shapes, which could be euhedral zircons broken, resorbed and/or corroded in later stages (A-F, Plate II). These zircons belong to the subtype A of the type 1 by Hoshino *et al.* (2010), because REE, U and Th are below the detection limits (Table 3), but yttrium is contained up to 1.0 wt. % Y_2O_3. The Y-bearing phase is seen brighter than Y-free phases. Yttrium tends to be depleted in the core and enriched in the rim (see Table 3); $Y_2O_3/ZrO_2 \times 1,000$ of the core zircon ranges from 1.57 to 3.75, while the rim zircon varies from 2.7 to 14.7. This mode of occurrence indicates that the yttrium was added into the zircon crystals from the remaining fluid phase in the latest magmatic stage.

The most common impurity in the zircons is hafnium, which goes up to 2.42 wt.% HfO_2. Hafnium tends to be rich in the core of single crystal, indicating its closest geochemical affinity with zirconium. The $HfO_2/ZrO_2 \times 100$ ratio varies from 1.61 to 3.75 in the main

Table. 6 Chemical composition of fergusonites of the 58A142 quartz syenite.

Sample No.	58A142: quartz syenite					
Spot Loc.	core: 1−3	rim; 4−5	core,6−7	rim, 8−9	10, 11	12, 13
n	3	2	2	2	2	2
SiO_2	4.40	8.04	5.21	2.60	4.23	0.48
TiO_2	0.76	0.14	0.94	0.35	0.91	0.94
FeO	2.11	5.09	2.29	0.66	1.55	0.31
CaO	1.43	2.52	1.46	1.72	1.53	2.22
La_2O_3	0.41	0.13	0.39	0.19	0.33	0.54
Ce_2O_3	2.18	0.86	2.46	2.18	2.19	3.17
Pr_2O_3	0.47	0.19	0.47	0.63	0.42	0.76
Nd_2O_3	2.77	2.40	2.92	4.47	3.15	3.61
Sm_2O_3	1.25	1.80	1.35	2.33	1.44	1.35
Gd_2O_3	2.75	3.91	3.00	4.21	2.97	2.90
Tb_2O_3	0.36	0.54	0.46	0.53	0.41	0.36
Dy_2O_3	2.85	3.49	3.05	3.30	2.61	2.86
Er_2O_3	1.74	1.85	1.73	1.66	1.50	1.80
Yb_2O_3	1.40	2.48	0.98	1.96	1.33	1.51
Lu_2O_3	0.34	0.60	0.28	0.53	0.34	0.41
Ta_2O_5	1.17	1.18	0.77	1.21	0.83	0.84
Y_2O_3	13.52	18.20	13.40	16.70	13.13	16.99
Nb_2O_5	42.77	38.40	39.30	44.36	41.70	46.38
ThO_2	4.84	1.85	7.22	4.43	7.64	6.98
UO_2	4.31	1.45	3.13	1.61	2.93	3.24
Total	91.84	95.11	90.81	95.60	91.14	97.66

Table. 7 Chemical composition of chevkinite of the 58A142 quartz syenite.

Sample No.	58A142		
Spot Loc.	1−2	3−4	5−6
n	3	3	2
SiO_2	20.63	20.59	20.56
TiO_2	14.70	15.05	14.35
Al_2O_3	0.46	0.45	0.46
FeO	11.87	11.66	11.75
CaO	4.18	4.34	3.89
La_2O_3	12.47	12.77	12.48
Ce_2O_3	20.96	21.05	21.19
Pr_2O_3	1.66	1.51	1.63
Nd_2O_3	5.56	5.37	5.57
Y_2O_3	0.45	0.39	0.37
ZrO_2	0.62	0.78	0.46
Nb_2O_5	2.82	2.58	3.29
ThO_2	1.40	1.19	1.24
Total	97.80	97.72	97.24

phase of the zircon crystals.

4.3 Allanite

Allanites occur in anhedral forms in the studied granitoids (G-I, Plate II). This mineral in granitic rocks are known to have MnO-poor chemistry, less than 2 wt.% MnO, in the magnetite-series granitoids, while MnO-rich ones, more than 2 wt.% MnO, are common in the ilmenite-series granitoids (Hoshino *et al.*, 2006). The MnO-poor allanites are relatively rich in LREE, while the MnO-rich ones tend to have enrichment in middle rare earth elements (MREE). This relationship is expressed by the coupled substitution $[Mn^{2+} + (MREE, HREE^{3+}) = Ca^{2+} + LREE^{3+}]$ (Hoshino *et al.*, 2006).

Allanites were found in two quartz syenites, zircon-rich one (58A142) and drill core sample (DH96.3); the both belong to MnO-poor type due to low MnO content (<0.44 wt.% MnO). This is consistent with the host granitoid belonging to a magnetite series. Allanites in these quartz syenites are very rich in LREE; the total rare earth contents of LREE range from 25.4 to 25.8 wt.% on the 58A142 quartz syenite, and 24.6 to 25.2 wt.% on the DH96.3 quartz syenite (Table 4). On the other hand, thorium content varies greatly from 0.05 to 3.7 wt.% ThO_2 for the 58A142 quartz syenite, depending upon grains.

4.4 Titanite

Coarse-grained euhedral titanites are commonly seen in felsic phase of the magma mingled part at the 58A124 locality. Their analyzed crystals are shown in Plate III and chemical compositions are indicated in Table 5. The chemical compositions are rather homogeneous, but one euhedral crystal has a bright rim rich in FeO, LREE, Y_2O_3 and Nb_2O_5 (C in Plate III), which is the latest crystallized phase of the magmatic fractionation. Thus, these components are considered to have added during the latest stage of the solidification.

4.5 Fergusonite and chevkinite

Fergusonite is seen in the 58A142 quartz syenite. This mineral occurs as anhedral crystals (D-F in Plate III), having brighter rims (e.g., E in Plate III). The compositions are heterogeneous, depending upon crystals as seen in Table 6. In the core vs. rim variations, Th, U and LREE are depleted in the rim of fergusonite, while HREE and Y are enriched in the rim.

Chevkinite was first found in Japan by Imaoka and Nakashima (1994) in quartz syenite of this pluton. We also identified this mineral in the zircon-rich rock of the 58A142 quartz syenite, and its chemical compositions are shown in Table 7. A distinct difference between the two results is seen on the thorium contents; Imaoka and Nakashima (1994) reporting 4.84 wt.% ThO_2.

5. Genetic consideration on the Cape Ashizuri pluton

Miocene alkaline body of the Cape Ashizuri is composed of both quartz undersaturated and oversaturated igneous rocks, similarly to other alkaline rock province (e.g., Oslo region, Neumann ,1980). They are composed of gabbroic and granitic rocks in both the main plutonic stage and post-plutonic subvolcanic stages, as mentioned previously. The lowest silica rock is 47.0 wt.% SiO_2, which contains 12.5 wt.% MgO (AZR1,
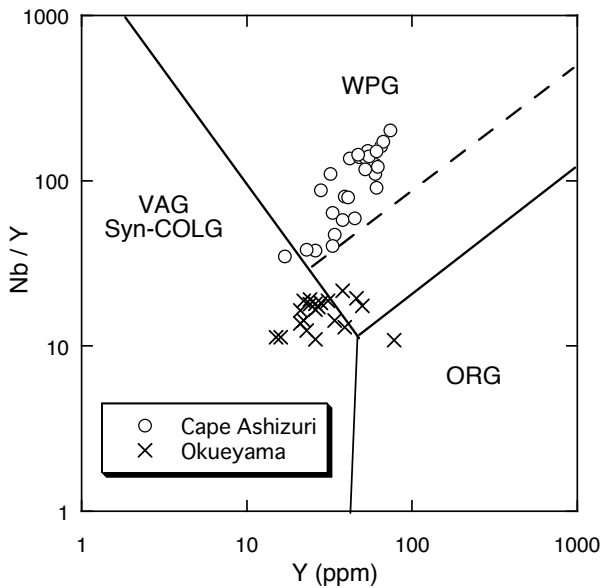
Fig. 14 Nb/Y vs. Y plot of the Cape Ashizuri and Okueyama plutonic rocks.

Ishihara and Murakami, 2006). This rock must have originated from a deep and mafic source rock in the upper mantle, and therefore moved upward invading through the subducting Philippine Plate, mafic lower crust and overlying accretionary complex of the Shimanto Supergroup during a certain period of the Miocene time, having severe interaction locally with the magmas from crustal sources.

All the other Miocene granitic rocks in the Outer Zone belong to the ilmenite-series composed of both I- and S-types. Some amounts of the sedimentary rocks of the accreted prism were considered mixed with the magmas from the depth; thus formed I- or S-type magma depending upon their mixing ratio. The Okueyama granodiorite-granite pluton is one typical example of I-type ilmenite-series having the exposure of 96 km^2. If these granitoids are plotted on the Nb/Y vs. Y diagram to discriminate their tectonic settings (Fig. 14), the Cape Ashizuri granitoids stay in the within-plate-granite (WPG) area, but the Okueyama granitoids are located mostly in the volcanic arc granite (VAG) area, although the two plutons occur in typical volcanic arc setting.

The Okueyama granitic body is vertically zoned being granodiorite at the lowest part and changing its composition upward to monzogranite, then aplitic granite containing pegmatite at the top 200 m, and thus differentiated vertically (Takahashi, 1986). They are composed of quartz-oversaturated rocks, except for a small part at 680 m above sea level, which is composed of monzonite (MT680, see Appendix I of Ishihara and Chappell, 2010). The Cape Ashizuri pluton, on the other hand, is horizontally zoned being alkaline monzo-syenitic rocks in the southern part and quartz over-saturated monzogranite in the northern part, and the

gabbroids occurring between them (Fig. 2). They are considered products of different intrusive bodies but genetically related.

The gabbroic rock with the lowest silica of 47.0 wt.% SiO$_2$ and highest magnesium as 12.5 wt.% MgO, has the alkali contents of 2.25 wt.% Na$_2$O and 1.23 wt.% K$_2$O, thus belonging to an alkaline gabbroid. Alkaline granitoids can be differentiates of the alkaline gabbroid, if much larger host gabbroid hidden underneath the present body. Another possibility, which seems more probable, is small degree of partial melting of igneous lower continental crust below the Shimanto accretionary complex by the heat brought up by the alkaline gabbroic magma. Because degree of the melting was small, alkaline feldspar components of alkalis and gallium, also fluorine moved selectively to the melt phase, and thus Ga-F-rich alkaline granitic magma was formed. Experimentally, zircon solubility is strongly enhanced by addition of NaSi$_3$O$_7$ to water. The same may be expected on K-silicate. Thus, the alkaline-rich magmas tend to contain abundant zirconium.

High-field strength elements (HFSE) such as Zr, Hf, Nb, Ta, Y, REE and W, are generally concentrated in residual melts during solidification of granitic magmas, as the best observed in the aplitic dike of the Naegi Granite (Ishihara and Murakami, 2006). It means that when the syenitic magma was generated in the lower continental curst below the Cape Ashizuri, the HFSE-rich melt, together with much fluorine, must be the first one to move to the melt phase together with some feldspar components. Thus, the HFSE-rich alkaline granitoids were formed.

The northern half of the Cape Ashizuri pluton is a quartz-oversaturated monzogranite having abundant modal quartz but low Ga contents less than 19 ppm. Thus, it is normal ilmenite-series granite having low magnetic susceptibility, similarly to the other ilmenite-series granitoids of the Outer Zone whose interaction with the accreted sediments are best shown by elevated δ^{18}O values (Ishihara and Matsuhisa, 1999). Sedimentary blocks and enclaves from the Shimanto accretionary complex are commonly observed in this granite area. This could be intermingled part at depth of the alkaline granitic magma with the shale and sandstones of the accretionary complex, which may have been stacked more than 10 km along the Outer Zone. Presence of sedimentary enclaves and higher initial Sr isotopic ratio support that interpretation.

6. Economic evaluation of the REE-rich granites

Similar REE and Zr-rich alkaline granites occur sporadically in many places in the world. Since these granites have A-type characteristics, they occur generally in an-orogenic environment like in Nigeria (Kinnaird *et al.*, 1985), Namibia (Schmitt *et al.*, 2002), Thor Lake in Canada (Ishihara and Watanabe, 2007) and Baerzhe of the Inner Mongolia (Ishihara and Murakami, 2007),

yet they are seen also in orogenic environment like the studied Cape Ashizuri complex and Bokan Mountain complex in Alaska (Philpotts *et al.*, 1994).

The Bokan Mountain complex of Jurassic age (151-171 Ma) occurs as intrusive rocks in the early Paleozoic accretionary complex of eugeosynclinal sediments in the southeastern Alaska. It has a circular form with 6 km diameter, composed of aegirine granite porphyry at margin and riebeckite granite porphyry in the center (Thompson *et al.*, 1982). The U-Th-REE mineralization is associated with the first collapse of the ring dike formation. The ore deposits occur in pipe-like bodies, as lenses in sheared zones and in vein quartz.

Economically more important REE-rich alkaline granites occur in anorogenic environments in Saudi Arabia, Mongolia and Canada. These granites are rich in Zr, Y, and REE. Microgranite-hosted Ghurayyah type may be the highest in HREE contents (Drysdall *et al.*, 1984). Many of these REE-rich granites have received REE enrichment by both magmatic and hydrothermal processes (Kovalenko *et al.*, 1995; Salvi and Williams-Jones, 2005). It is interesting to find hydrothermal alteration zones in and around the Cape Ashizuri plutonic and subvolcanic bodies.

7. Conclusions

The Cape Ashizuri plutonic complex having an exposed area of 12 km^2 is a unique alkaline plutonic complex, composed of magnetite-series and ilmenite-series granitoids occurring in the Shimanto accretionary sedimentary terrain where all the other Miocene granitic rocks belong to calc-alkaline ilmenite-series granitoids. The Cape Ashizuri plutonic complex has a variety of rock facies, but is grouped into three as (1) gabbroids, (2) alkaline granites with low quartz contents, which are distributed in the southern half of the body, and (3) quartz-oversaturated calc-alkaline monzogranite, exposed in the northern half in contact with the sedimentary wall rocks. These rocks, particularly of alkaline granitoids, are rich in Zr, REE, Nb-Ta, and Th-U, which are contained in the rock-forming minerals of ilmenite, titanite, allanite, fergusonite, chevkinite, uranothorite and others

The alkaline granitoids would have been generated at the lower crust of mafic igneous source rocks by heat brought up by the gabbroic magmas from the upper mantle. A small degree of the partial melting was a main cause to produce HFSE and F dominant magmas. The quartz-oversaturated monzogranite in the northern half would be a mixed magma of the alkaline granitic magma from the depth and local magma generated with interaction of the sedimentary wall rocks of the Shimanto Supergroup.

References

Chappell, B. W., White, A. J. R., Williams, I. S. and Wyborn, D. (2004) Low- and high-temperature granites. *Proc. Royal Soc. Edinburgh, Earth Sci.*, **95**, 125-140.

Cullers, R. L. and Graf, J. L. (1984) Rare earth elements in igneous rocks of the continental crust: Intermediate and silicic rocks – Ore petrogenesis. *Rare Earth Element Geochemistry* (P. Henderson ed.), Elsevier, Amsterdam, 275-316.

Drysdall, A. R., Jackson, N. J., Ramsay, C. R., Douch, C. J. and Hackett, D. (1984) Rare element mineralization related to Precambrian alkali granites in the Arabian Shield. *Econ. Geol.*, **79**, 1366-1377.

Hanson, G. N. (1980) Rare earth elements in petrogenetic studies of igneous systems. *Ann. Rev. Earth Planet. Sci.*, **8**, 371-406.

Hayashi, H. and Akai, J. (2011) Unusual internal textures and trace element chemistry of zircon from Cape Ashizuri Ring Complex, Kochi, SW Japan. *Petrol. Mineral.*, **40**, 1-12 (in Japanese with English abstract).

Hayashi, S., Ishihara, S. and Sakamaki, Y. (1969) Uranium in the decomposed granitic rocks at the Cape Ashizuri, Kochi Prefecture, with special reference to the green uranothorite. *Rept. Geol. Surv. Japan*, no. 232, 93-103 (in Japanese with English abstract).

Hoshino, M., Kimata, M., Shimizu, M., Nishida, N. and Furukawa, T. (2006) Allanite-(Ce) in granitic rocks from Japan: genetic implications of patterns of REE and Mn enrichment. *Can. Mineral.*, **44**, 45-62.

Hoshino, M., Kimata, M., Nishida, N., Shimizu, M. and Akasaka, T. (2010) Crystal chemistry of zircon from granitic rocks, Japan: Genetic implications of HREE, U and Th enrichment. *N. Jb. Mineral. Abh.*, **187/2**, 167-188.

Iizumi, S. and Murakami, N. (1980) Sr isotopic ratio of the Ashizuri-misaki ring complex. *Abstract Issue for 92nd Annual Mtg., Geol. Soc. Japan*, 338 (in Japanese).

Imaoka, T. and Nakashima, K. (1994) Chevkinite in syenites from Cape Ashizuri, Shikoku Island, Japan. *N. Jb. Mineral. Mh.*, **H.8**, 358-366.

Imaoka, T. Nakashima, K. and Murakami, N. (1991) Gallium in A-type granites from the Cape Ashizuri, Kochi Prefecture, Southwest Japan. *Japan. Assoc. Mineral. Petrol. Econ. Geol.*, **86**, 354-363 (in Japanese with English abstract).

Ishihara, S. (1979) Lateral variation of magnetic susceptibility of the Japanese granitoids. *Jour. Geol. Soc. Japan*, **85**, 509-523.

Ishihara, S. and Chappell, B. W. (2010) Chemical

compositions of the Miocene granitoids of the Okueyama, Hoei mine and Takakumayama plutons, Outer Zone of SW Japan. *Bull. Geol. Surv. Japan*, **61**, 17-38.

Ishihara, S. and Matsuhisa, H. (1999) Oxygen isotopic constraints on the geneses of the Miocene Outer Zone granitoids in Japan. *Lithos*, **46**, 523-534.

Ishihara, S. and Murakami, H. (2006) Characteristics of REE distribution in granitoid of SW Japan: Miocene plutonic rocks at Ashizuri-misaki and late Cretaceous granitoids of the Sanyo Belt of SW Japan. *Bull. Geol. Surv. Japan*, **57**, 89-103 (in Japanese with English abstract).

Ishihara, S. and Murakami, H. (2007) HREE concentration in the Baerzhe Granites, Inner Mongolia, China. *Resource Geol.*, **57**, 137-142 (in Japanese with English abstract).

Ishihara, S. and Watanabe, Y. (2007) Hydrothermal REE deposits: An example of the Thor Lake property. *Resource Geol.*, **57**, 65-70 (in Japanese with English abstract).

Ishihara, S., Teraoka, Y., Terashima, S. and Sakamaki, Y. (1985) Chemical variation of Mesozoic-Cenozoic sandstone and shale across the western Shikoku district. *Bull. Geol. Surv. Japan*, **36**, 85-102.

Ishihara, S., Tanaka, T., Terashima, S., Togashi, S., Murao, S. and Kamioka, H. (1990) Peralkaline rhyolite dikes at the Cape Ashizuri: A new type of REE and rare metal mineral resources. *Mining Geol.*, **40**, 107-115.

Kinnaird, J. A., Bowden, P., Ixer, R. A. and Odling, N. W. A. (1985) Mineralogy, geochemistry and mineralization of the Ririwai complex, Northern Nigeria. Jour. *African Earth Sci.*, **3**, 185-222.

Kovalenko, V. I., Tsaryeva, G. M., Goreglyad, A. V., Yarmolyuk, V. V., Troitsky, V. A., Hervig, R. L. and Farmer, G. L. (1995) The peralkaline granite-related Khaldzan-Buregtey rare metal (Zr, Nb, REE) deposit, Western Mongolia. *Econ. Geol.*, **90**, 530-547.

Linnen, R. L. and Keppler, H. (1997) Columbite stability in granitic melts: consequences for the enrichment and fractionation of Nb and Ta in the Earth's crust. *Contrib. Mineral. Petrol.*, **128**, 213-227.

Linnen, R. L. and Keppler, H. (2002) Melt composition control of Zr/Hf fractionation in magmatic processes. *Geochim. Cosmochim. Acta*, **66**, 3293-3301.

Mason, B. (1966) *Principles of Geochemistry. 3rd ed.*, 329 p.

Murakami, H. and Ishihara, S. (2006) REE geochemistry of weathered soil within Miocene granitoids in the Ashizuri-misaki area, SW Japan: Possibility as REE resources. *Chikyukagaku (Geochemistry)*, **40**, 147-165 (in Japanese with English abstract).

Murakami, N. and Imaoka, T. (1985) Rapakivi granite. *Jour. Geol. Soc. Japan*, **91**, 179-194 (in Japanese

with English abstract).

Murakami, N. and Masuda, Y. (1984) Trace elements in the Tertiary igneous rocks from Cape Ashizuri, Kochi Prefecture, Southwest Japan. Japan. Assoc. Mineral. Petrol. *Econ. Geol.*, **79**, 318-328.

Murakami, N. and Matsuo, H. (1963) Petrological studies on the metasomatic syenites in Japan. Part 1. Syenites of the Cape of Ashizuri, Kochi Prefecture. Japan. Assoc. Mineral. Petrol. *Econ. Geol.*, **50**, 93-109 (in Japanese with English abstract).

Murakami, N., Imaoka, T. and Uozumi, S. (1989) Ring complex of the Cape of Ashizuri, and its mode of emplacement, Kochi Prefecture, Southwest Japan. *In Collapse Basins*. Monogr. 36, Assoc. Geol. Collab., 115-142 (in Japanese with English abstract).

Murakami, N., Kanisawa, S. and Ishikawa, K. (1983) High fluorine content of Tertiary igneous rocks from the Cape of Ashizuri, Kochi Prefecture, Southwest Japan. Japan. Assoc. Mineral. Petrol. *Econ. Geol.*, **78**, 497-504 (in Japanese with English abstract).

Nagashima, M., Imaoka, T. and Nakashima, K. (2011) Crystal chemistry of Ti-rich ferriallanite-(Ce) from Cape Ashizuri, Shikoku Island, Japan. *Amer. Mineral.*, **96**, 1870-1877.

Nakashima, K. and Imaoka, T. (1998) Niobian and zincian ilmenites in syenites from Cape Ashizuri, Southwest Japan. *Mineral. Petrol.*, **63**, 1-17.

Neumann, E. R. (1980) Petrogenesis of the Oslo region larvikites and associated rocks. *Jour. Petrol.*, **21**, 499-531.

Philpotts, J. A., Taylor, C. D. and Baedecker, P. A. (1994) Rare-earth enrichment at Bokan Mountain, Southeast Alaska. Geologic Studies in Alaska by the U.S. Geol. Surv., 89-100.

Salvi, S. and Williams-Jones, A. E. (2005) Alkaline granite-syenite deposits. In Linnen, R. and Samson, I., eds., *Rare-element geochemistry and mineral deposits*. Geol. Assoc. Canada, Short Course Notes 17, 315-341.

Schmitt, A. K., Tbumbull, R. B., Dulski, P. and Emmermann, R. (2002) Zr-Nb-REE mineralization on peralkaline granites from the Amis complex, Brandberg (Namibia): Evidence for magmatic pre-enrichment from the melt inclusions. *Econ. Geol.*, **97**, 399-413.

Shibano, T. (1958) Un-utilized iron mineral resources in the Ashizurimisaki District. *Un-utilized Mineral Resources No. 5*, Ministry of International Trade and Industry, 168-172 (in Japanese).

Shibata, K. and Ishihara, S. (1979) Initial $^{87}Sr/^{86}Sr$ ratios of plutonic rocks from Japan. *Contrib. Mineral. Petrol.*, **70**, 381-390.

Shibata, K. and Nozawa, T. (1982) Radiometric age map of Japan: Granitic rocks. Scale 1:3,000,000. Geol. Surv. Japan.

Shinjoe, H., Orihashi, Y. and Sumii, T. (2010) U-Pb

zircon ages of syenitic and granitic rocks in the Ashizuri igneous complex, southwestern Shikoku: Constraint for the origin of forearc alkaline magmatism. *Geochem. Jour*., **44**, 275-283.

Suzuki, T. (1938) *Explanatory text of the geological map of Japan. Scale 1:75,000, Sukumo* (in Japanese with English abstract).

Takahashi, M. (1986) Anatomy of a middle Miocene Valles-type caldera cluster: Geology of the Okueyama volcano-plutonic complex, Southwest Japan. Jour. *Volc. Geothermal Res*., **29**, 33-70.

Teraoka, Y. (1979) Provenance of the Shimanto geosynclinals sediments inferred from the sandstone compositions. *Jour. Geol. Soc. Japan*, **85**, 753-769

Teraoka, Y., Okumura, K., Suzuki, M. and Kawakami, K. (1999) Clastic sediments of the Shimanto Supergroup in Southwest Japan. *Bull. Geol. Surv. Japan*, **50**, 559-590 (in Japanese with English abstract).

Thompson, T. B., Pierson, J. R. and Lyttle, T. (1982) Petrology and petrogenesis of the Bokan granite complex, southeastern Alaska. *Geol. Soc. America, Bull*., **93**, 898-908.

Tsusue, A. (1973) The distribution of manganese and iron between ilmenite and granitic magma in the Osumi Peninsula, Japan. *Contrib. Mineral. Petrol*., **40**, 305-314

Tsusue, A. and Ishihara, S. (1974) The iron-titanium oxides in the granitic rocks of Southwest Japan. *Mining Geol*., **24**, 13-30 (in Japanese with English abstract).

Wilke, M., Schmidt, C., Dubrail, J., Appel, K., Borchert, M., Kvashnina, K. and Manning, C. E. (2012) Zircon solubility and zirconium complexation in $H_2O + Na_2O + SiO_2 \pm Al_2O_3$ fluids at high pressure and temperature. *Earth Planet. Sci. Letters*, **349-350**, 15-25.

足摺岬の付加体に貫入するジルコンと希土類元素に富むアルカリ深成岩類

石原舜三・星野美保子

要　旨

　西南日本外帯の足摺岬火成岩体は露出面積 12 km^2 の小岩体であるが，その南部は斑レイ岩および狭義の閃長岩・石英閃長岩から閃長花崗岩に至る幅広いアルカリ花崗岩類，その北部は四万十帯に接する石英に富む黒雲母モンゾ花崗岩で構成される複合岩体である．化学分析値をハーカー図上で検討すると，黒雲母モンゾ花崗岩の 3 個を除き A/CNK<1.0，即ちメタアルミナスの領域に，また K$_2$O-SiO$_2$ 図上ではショショナイトー高カリウム系列上にプロットされる．Na$_2$O や Rb にも富んでいる．ガリウム量は斑れい岩を除き 18 ppm Ga 以上と多く，A タイプ的な傾向を持つ．足摺岬花崗岩類の最大の特徴は HFSE (high-field strength elements) に富むことにある．Zr は最大で 1,220 ppm 含まれ，Hf (<25.6 ppm)，Nb (<202 ppm)，Ta (<14 ppm)，LREE (<1,002 ppm)，HREE (<50.5 ppm)，Y (<74 ppm)，Th (<74.2 ppm) にも富んでいる．またフッ素 (<0.43 wt.% F) が多く含まれる．

　これらの微量成分は多数の副成分鉱物に含まれるが，一般的な鉱物はジルコン，チタン鉄鉱，褐廉石，チタン石などである．ジルコンはもっとも普遍的にみられ，まれに肉眼で識別できることもある．ジルコニウムの最大含有量を持つ 58A142 試料中のジルコンは，2.4 wt.% 以下の HfO$_2$，1.0 wt.% 以下の Y$_2$O$_3$ を含む．58A142 試料のチタン鉄鉱は 4.3-5.7 wt.% MnO を含むが，その他の石英閃長岩のチタン鉄鉱は低い値 (1.7-1.8 wt.% MnO) を持つにすぎない．チタン鉄鉱中のニオブは 3.8 wt.% Nb$_2$O$_5$ 以下であり，チタン鉄鉱の縁に濃集するので，マグマ期最末期に熱水から添加されたものと考えられる．褐廉石は他形結晶として見られ，磁鉄鉱系花崗岩類に特徴的なマンガンに乏しい特徴 (0.44 wt.% MnO) を持つ．また，褐廉石は軽希土類元素に富み，24.6-25.8 wt.% LREE の範囲で比較的一定であるが，トリウム (0.05-3.7 wt.% ThO$_2$) は変化に富む．

　足摺岬岩体の斑れい岩は最も苦鉄質な岩相で 47.0 wt.% SiO$_2$，12.5 wt.% MgO であり，上部マントルにその起源をもつものと思われる．閃長岩類は 55-60 wt.% SiO$_2$ で低い Sr 初生値 (0.7035) を持つことから，大陸地殻下部の苦鉄質岩を出発物質としているが，マグマの発生量が小規模であった為に，結果的にアルカリや HFSE に富んだと考えられる．北部の黒雲母花崗岩はこのマグマが四万十層群の堆積岩類を深所で同化して生成したと考えられる．足摺岬岩体の石英閃長岩類と関連岩脈類は異常な Zr, REE, Y を含むので，関連する熱水性鉱床を発見することは，REE 含有鉱床探査上のために重要である．

Plate IA   Southern coastal view toward the Cape Ashizuri where alkaline granitoids are well exposed along the coastal cliff.
Plate IB   Gabbroic blocks mingled with alkaline granitoids at the Cape Ashizuri, the same photo as one of the postcard set "Granites in Japan" by the Geological Museum, GSJ.
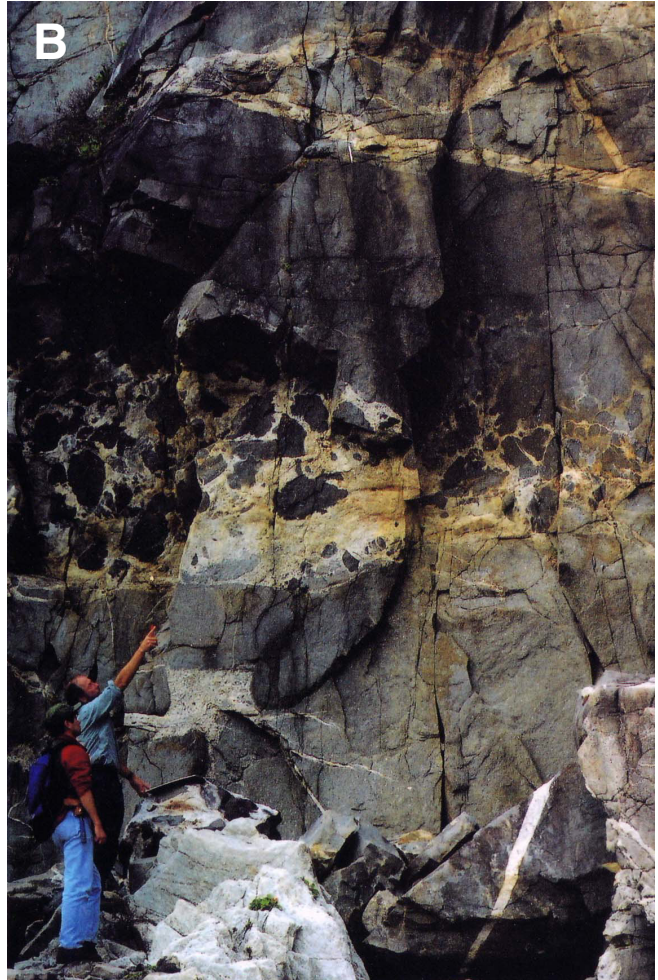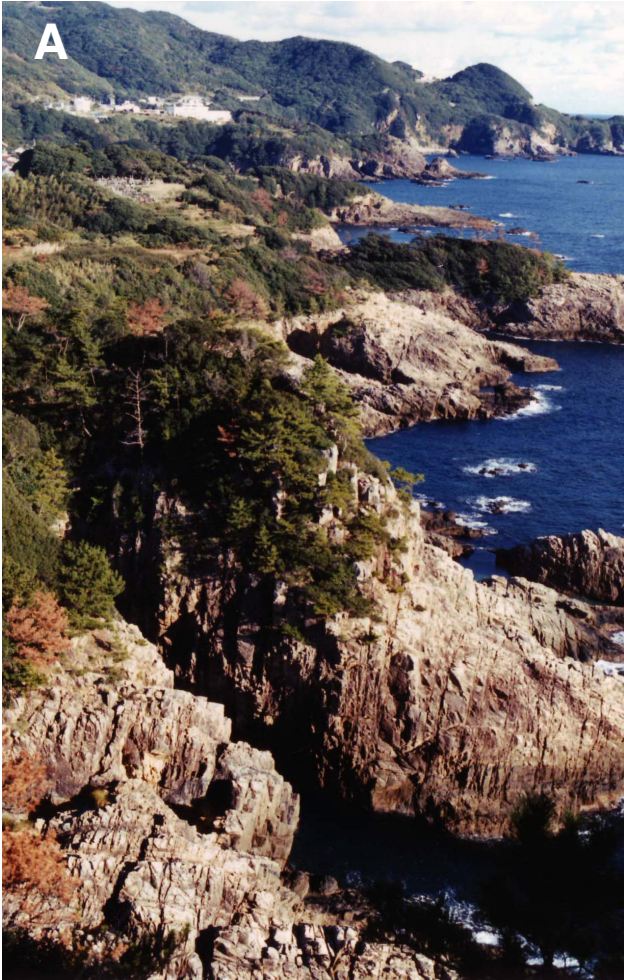
Plate II   Analyzed zircon (A-F) and allanite (G-I) crystals by EPMA. The white bar indicates 0.1 mm.
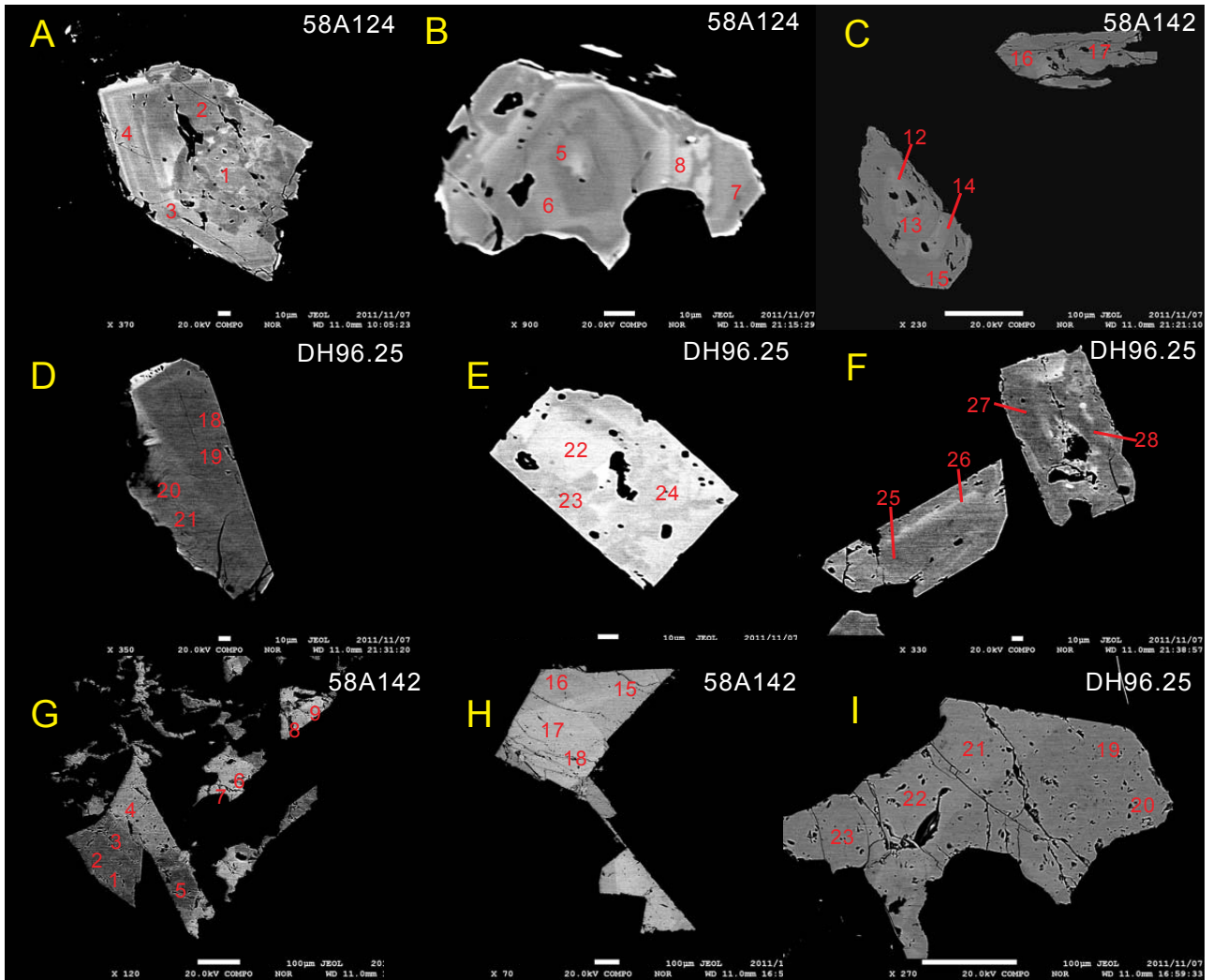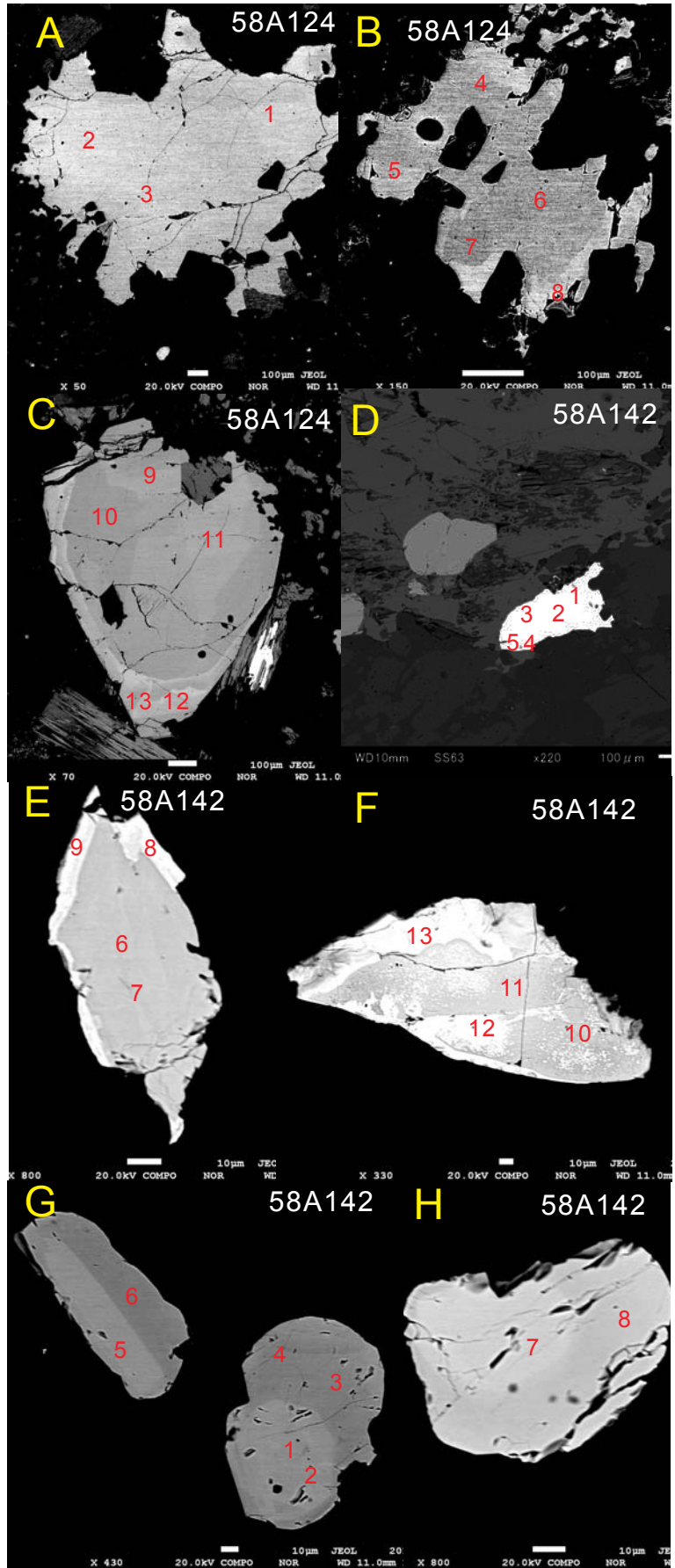
Plate III Analyzed titanite (A-C), fergusonite (D-F) and chevkinite (G-H) crystals by EPMA. The white bar indicates 0.1 mm.

論文 - Article

滋賀県琵琶湖南方・田上花崗岩体中の細粒暗色包有岩

中野聰志 [1, *]・大橋義也 [2]・石原舜三 [3]・河野俊夫 [4]

Abstract: Microgranular dark-colored enclaves from medium-grained porphyritic biotite granites in the Tanakami Granite pluton were studied petrographically, geochemically and mineralogically. Many of them are ball-like in form with a diameter of ~1~20~ cm. They consist mainly of fine-grained plagioclase, quartz, biotite and several accessory minerals together with porphyritic plagioclase (mainly) and quartz (subordinately). The maximum biotite content is ca. 27 % in mode analysis. The occurrence of alkali feldspar is limited to be as small patches seemingly replacing plagioclase interiors. Their occurrence, textures, bulk rock chemistry, REE patterns, mineral textures and its chemistry seem to be totally consistent with the idea that they are not a product of magma mixing but is a product of early-stage crystallization from the magma forming the medium-grained porphyritic biotite granites as the host rock. The MME often occurs with aplite-pegmatite facies (dykes), which suggests some common circumstances such as relatively rapid cooling conditions catalyzed by some volatile components.

Keywords: Tanakami Granite, MME, occurrence, geochemistry, mineralogy, volatile, rapid cooling, early crystallization

要 旨

琵琶湖周辺の優白質花崗岩体中には珍しい細粒暗色包有岩（MME）の産出を，琵琶湖南方の田上花崗岩体を構成する中−粗粒黒雲母花崗岩と中粒斑状黒雲母花崗岩中で確認した．それらの大きさは 1 cm 程度から最大 20 cm 強であり，形はほぼ球状から楕円状であるがやや細長いものもある．有色鉱物として黒雲母のみ含む (最大約 27 %)．本地域の MME は，アプライト・ペグマタイトとしばしば共存している．中粒斑状黒雲母花崗岩中の MME について，全岩化学分析 (主成分元素，REE を含む微量元素) を行うとともに，鉱物集合状態と鉱物組織の観察ならびに鉱物化学組成 (長石類，黒雲母，イルメナイト) の解析を行った．これらの結果は，産状や組織等のデータとともに，本 MME がよく知られているマグマ混合による産物であるとの考えではなくて，中粒斑状黒雲母花崗岩マグマからの早期晶出による産物であるとの考えに

より整合的であるように思われる．MME とアプライト・ペグマタイトとの共存は，MME の成因における揮発性成分の重要な役割を示唆する．

1．はじめに

田上花崗岩体は，山陽−苗木帯に属し，琵琶湖南部周辺に分布する白亜紀末環状岩体を構成する花崗岩体の中で最も南部に位置する (第 1 図)(周琵琶湖花崗岩団体研究グループ，2000；中野ほか，2003)．石原・村上 (2006) は，田上花崗岩体中の新名神高速道路建設工事現場・金勝山トンネル西口付近の玉石から，「苦鉄質包有岩」(SiO_2 = 57.62 %，石英閃緑岩) を見いだし，その特徴を記載した．一方，京都東南部図幅作成の過程で，上記包有岩の母岩である中粒斑状黒雲母花崗岩中のみならず田上花崗岩体の主岩相である中−粗粒黒雲母花崗岩中にも，細粒暗色包有岩が広い範囲で散在することが

[1] 滋賀大学教育学部理科教育講座 (Department of Natural Science, Faculty of Education, Shiga University, Hiratsu 2−5−1, Otsu 520−0862, Japan)

[2] 岐阜県中津川市立坂本中学校 (Sakamoto Junior High School, Sendanbayashi, Nakatsugawa 509−9131, Japan)

[3] 産業技術総合研究所特別顧問 (Special Adviser, National Institute of Advanced Industrial Sience and Technology, Central 7, Higashi 1−1−1, Tsukuba 305−8567, Japan)

[4] 滋賀大学教育学研究科共同研究員 (Joint Researcher, Graduate School of Education, Shiga University, Hiratsu 2−5−1, Otsu 520−0862, Japan)

* Corresponding author: S. NAKANO, E−mail：nakano@edu.shiga−u.ac.jp
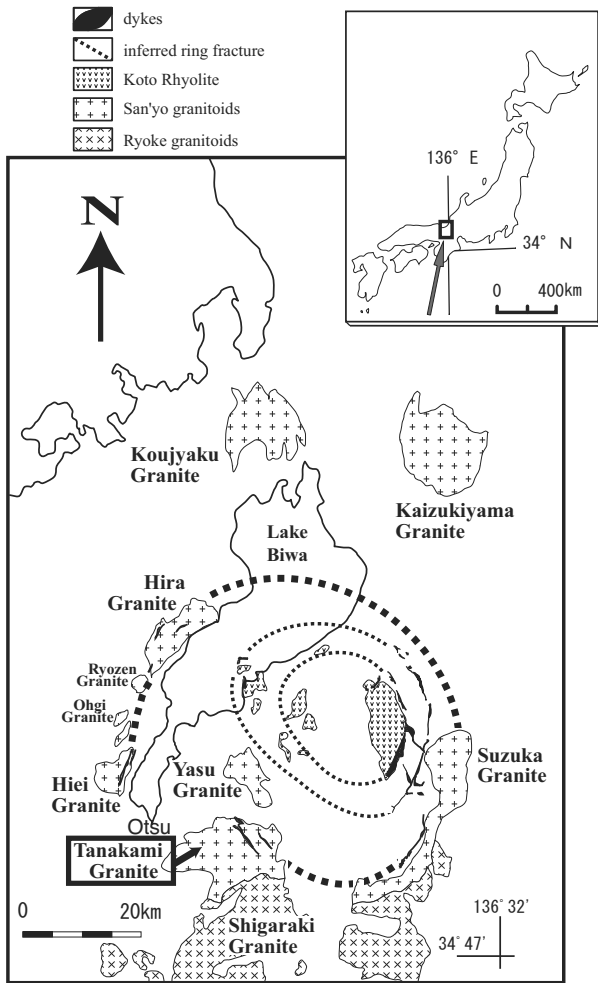
第1図　琵琶湖周辺の花崗岩質岩体分布図.

Fig. 1　Index map showing the locations of granite plutons around Lake Biwa, central Japan.

確認された (中野，2013) ので，それらを本研究の対象とした．今回の試料は，上記の「苦鉄質包有岩」ほど苦鉄質ではなくトーナル岩質であり (SiO$_2$ = 63.39−70.02 %)，含まれる有色鉱物 (黒雲母) の割合もそれほど高くない (最大約 27 %)．本細粒暗色包有岩は，以下に紹介する最近一般的に使用されている MME (または ME) の範疇に入る．すなわち，MME は，苦鉄質火成包有岩 (mafic magmatic enclaves (Barbarin, 2005))，苦鉄質細粒包有岩 (mafic microgranular enclaves (Barbarin and Didier, 1992))，あるいは細粒火成包有岩 (microgranular magmatic enclaves (Slaby et al, 2004, 2008)) の略号であり，最近では mafic enclaves (Wada et al., 2004) や microgranular enclaves (Donaire et al., 2005；Esna−Ashari et al., 2011) とされる場合がある．MME は，マグマ混合の産物とされる場合が多い (Vernon, 1990；Sergi, 1997；Wiebe et al., 1997；Perugini et al., 2003；Barbarin, 2005；Kocak et al., 2011；ほか) が，マグマからの早期晶出物と考えられている例も多い (例えば，Fershtater and Borodina (1977)，Best and

Christiansen (2001)，Esna−Ashari et al., 2011 を参照)．いずれにせよ，MME は花崗岩体中に包有される細粒の火成岩 (様) 組織を有する苦鉄質鉱物に富む岩石である．したがって，本研究での田上花崗岩体中の細粒暗色包有岩を，以下 MME と記述する．

　MME の研究は，花崗岩体を形成したマグマの熱史を知る上で重要な意味がある (Donaire et al, 2005；Esna−Ashari et al., 2011；参照)．日本においても黒部川花崗岩体 (Wada et al., 2004)，対馬花崗岩体 (Shin et al., 2009)，山陰帯花崗岩体 (薬師寺ほか，2012) 等での詳しい研究例が報告されている．しかし，これまで，琵琶湖周辺の花崗岩体からは，貝月山花崗岩体での暗色包有岩 (多くは堆積岩起源，まれに閃緑岩質)(杉井・沢田，1999) と野洲花崗岩体での細粒−中粒等粒状の暗色包有物 (最大径 10 cm) の簡単な記載がある (細野・牧野，2002) のみである．本稿では，田上花崗岩体を構成する中−粗粒黒雲母花崗岩中の MME について，その産状や構造，全岩化学組成，構成鉱物の化学組成について記載し，その成因について言及する．ただし，石原・村上 (2006) に報告のある苦鉄質包有物岩は，角閃石が含まれず黒雲母が多く含まれている点は共通であるが，これまでのところ径約 1 m の玉石として単独で確認されているのみであり，化学的性質において今回対象とした MME とは異なる点があり，現時点においては例外的なものとする．

2.　地質概説

　滋賀県の琵琶湖周辺には，江若岩体，貝月山岩体，野洲岩体，鈴鹿岩体，田上岩体，比叡岩体，比良岩体といった白亜紀末の優白質の花崗岩体と，活動年代が未確定の花崗閃緑岩−トーナル岩質の仰木岩体，霊仙岩体が地表に分布している (第 1 図) とともに，雄琴や瀬田川沿いの地下に伏在している (橋本ほか，2000；中野，2013)．これらの各花崗岩質体は近年それぞれ詳しく研究が行われてきた (周琵琶湖花崗岩団体研究グループ，1982，1997，2000，2005，2008；中野ほか，2003；中野，2013)．

　琵琶湖南部周辺には，上記岩体のうち田上，比良，比叡，野洲，鈴鹿の花崗岩体が分布している．これらはいずれも山陽帯の花崗岩類に属しており，各花崗岩体は琵琶湖南部において長径約 60 km，短径や約 40 km の環状に配列し，当時のコールドロン形成に関係した環状岩体であると考えられている (沢田ほか，1994)．このコールドロンは，当初「湖東コールドロン」と命名された (西川ほか，1979，1983；西堀ほか，1991) が，沢田ほか (1994) はそれをはるかに上回る大規模なコールドロンを推定した (第 1 図)．その後の研究により，沢田ほか (1994) の提唱したコールドロンは，新たに「琵琶湖コールドロン」と命名された (周琵琶湖花崗岩団体研究グループ，2000；
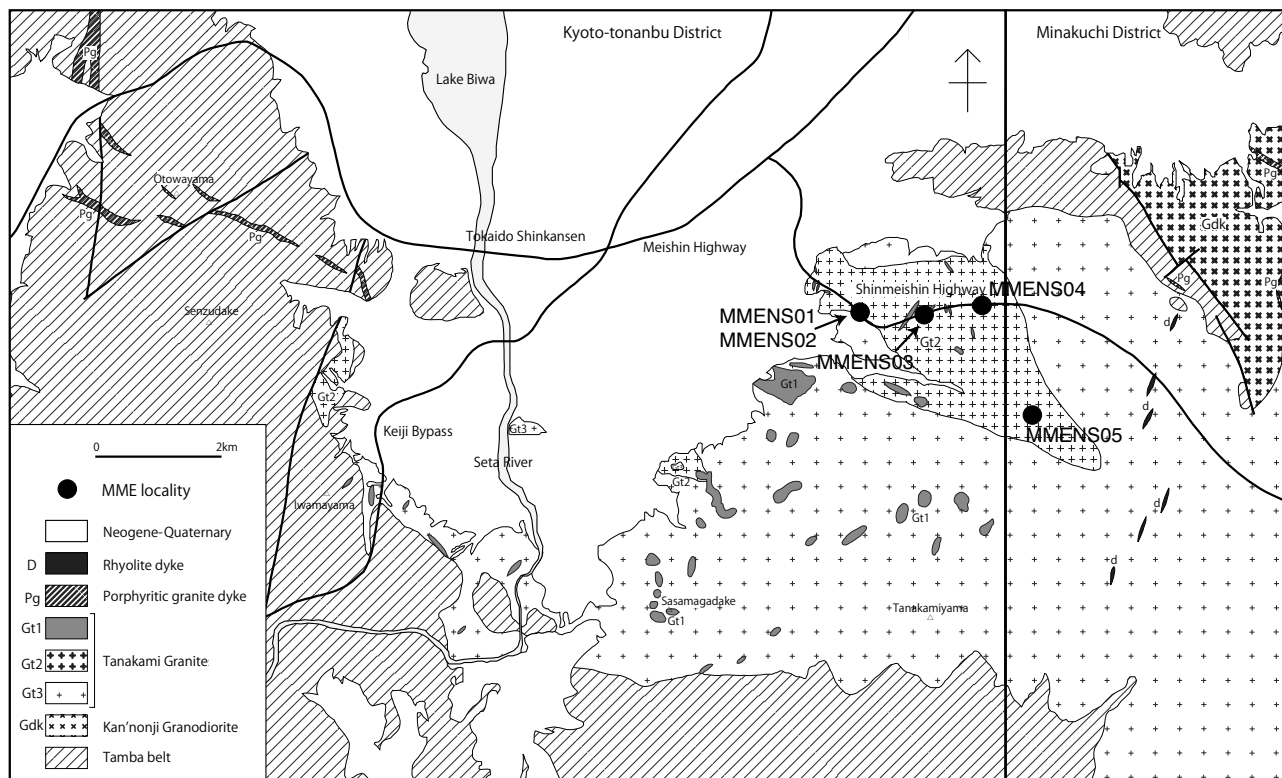
第2図 MME試料採取地点を示す田上花崗岩体の地質図．地質図の凡例は，中野 (2013) にしたがっている (以下の図においても同様)：Gt3 (中−粗粒黒雲母花崗岩)・Gt2 (中−粗粒斑状黒雲母花崗岩)・Gt1 (細粒−細粒斑状黒雲母花崗岩).

Fig. 2 Geological map of the Tanakami Granite pluton showing the sampling points of MME. The abbreviations, Gt3 (medium- to coarse-grained biotite granite), Gt2 (medium- to coarse-grained porphyritic biotite granite) and Gt1 (fine-grained to fine-grained porphyritic biotite granite), are according to Nakano (2012)(these abbreviations are the same in the later corresponding figures).

琵琶湖基盤地質研究会，2001）．一方，比叡花崗岩体は，その活動時期や化学的性質の違いから，「琵琶湖コールドロン」形成に関与した他の環状花崗岩体の活動とは異なる火成活動の産物であることが最近明らかにされるとともに，琵琶湖周辺の白亜紀火成活動史の再検討の必要性が提起された (周琵琶湖花崗岩団体研究グループ，2008)．この観点から，現在，比良岩体と比叡岩体の間に位置する仰木花崗閃緑岩体の研究が進められている (貴治ほか，準備中).

田上花崗岩体は東西約20 km，南北約6-8 kmの分布域を持つ花崗岩体 (第2図) で，田上−信楽山系と呼ばれる標高500-600 mの山地を形成している．田上花崗岩体で最も広い分布域を有するのは中−粗粒黒雲母花崗岩であり，多くのペグマタイトや熱水変質長石鉱床を胚胎している (中野ほか，2006)．田上岩体を構成するのは，そのほかに岩体東北部に分布する細−中粒斑状黒雲母花崗岩，岩体北西部に分布する中−粗粒斑状黒雲母花崗岩，岩体西部に点在する細粒−細粒斑状黒雲母花崗岩とされた (周琵琶湖花崗岩団体研究グループ，2000；中野ほか，2003)．しかし，その後の研究を経て，中野 (2013) は，田上岩体の構成を中−粗粒黒雲母花崗岩 (Gt3)，中−粗粒斑状黒雲

母花崗岩 (Gt2)(粗粒相は一部)，細粒−細粒斑状黒雲母花崗岩 (Gt1：アプライト (IUGSの用語法 (Le Maitre，2002) にしたがい細粒非顕晶質花崗岩)，ペグマタイト，細粒−細粒斑状花崗岩脈等を含む) の3岩相とした (第2図)．本稿では，田上花崗岩体の岩相区分を中野 (2013) にしたがっており，本文中のみならず図表中及びその説明文中において，Gt3・Gt2・Gt1の記号も多用した．MMEは，岩体北西部の中−粗粒斑状黒雲母花崗岩中と主岩相である中−粗粒黒雲母花崗岩中に分布する．後者の存在は最近明らかになった (中野，2013) が，風化のため解析試料の採取ができていない．なお，田上花崗岩体西縁部は日本の三大ペグマタイト産地の一つとして良く知られている (大林，2002；河野ほか，2008；Rakovan et al., 2009；角谷ほか，2012；中野，2013).

3. 岩石試料

第2図に示すように，岩体北西部に分布する中−粗粒斑状黒雲母花崗岩 (Gt1：中野，2013) 分布域からMMEを採集した．それらの周囲の母岩はいずれもほぼ中粒質である．なお，MMENS05試料 (大戸川河床) を除きいずれ

のMME試料も，露頭から直接採取したものではなく新名神高速道路建設中の工事ルート上に集積されていた玉石から採取したものである．ただし，付近の露頭でも同じ産状が確認されている．既に述べたように，MMEは笹間ヶ岳周辺をはじめとする中-粗粒黒雲母花崗岩 (Gt3：中野，2013) 中の各所にも見出されるが，いずれも風化が進んでおり分析用の試料としての採取は今後の課題である．

多数採取したMME試料のうち，代表的な4地点中の玉石から採集したMMEからそれぞれ1試料を選び (試料番号MMENS01-MMENS04) それに大戸川河床露頭からの試料 (MMENS05) を加え以下の解析試料とした．母岩である中-粗粒斑状黒雲母花崗岩についても多数岩石試料を採集した．この中-粗粒斑状黒雲母花崗岩の岩石記載や以下で述べるMMEと共存するアプライト等の岩石記載は，中野 (2013) に与えられている．なお，中野 (2013) では，アプライトは細粒非顕晶質黒雲母花崗岩として，ペグマタイトや脈岩類とともに細粒-細粒斑状黒雲母花崗岩 (Gt1) 岩相のなかに一括されている．

4. 研究方法

MME4試料の全岩化学組成は，Activation Laboratories Ltd. (Canada) により重量法 ($H_2O\pm$)，IR法 (Total S)，FUS-ICP法 (SiO_2ほか主成分，Scほか微量元素)，FUS-MS法 (REEほか微量元素) で求められた．鉱物組織観察，鉱物組成分析等には，電子マイクロプローブアナライザー (EMPA：滋賀大学教育学部設置，日本電子JXA8800M) を使用した．そのうち定量分析は，加速電圧15kV・試料電流20 nAで行った．補正方法はBence and Albee法による．EMPAマッピングは，加速電圧15 kV・試料電流50 nAで行った．他の分析条件は，Nakano *et al.* (2001) やNakano and Makino (2010) 等と同じである．

5. MME の記載岩石学的特徴

5.1 肉眼的特徴

田上花崗岩体産のMMEの野外での産状は，中野 (2013) によって概略的に与えられている．多い場合でも 1 m^2 中に数個程度であるが，母岩中の各所に広範に散在している．

中-粗粒斑状黒雲母花崗岩中に見られるMMEの形状は，一般的には断面では円形や楕円形である (第3図)．立体的には主に球状と卵型状と考えられる．しかし，まれに細長いレンズ状のもの (5 cm) や不規則形状のものがある (10 cm内外)．長径10 cm前後のサイズのものが目立つが，全体としては長径約 1 cm- 最大20 cm強のサイズ変化がある．1 cm程度あるいはそれより小さいものは，黒雲母クロット (周琵琶湖花崗岩団体研究グループ，1982, 2000；

中野ほか，2003) と紛らわしくなる．母岩である中-粗粒斑状黒雲母花崗岩との境界は明瞭であるが，母岩側，MME側共にほとんどの場合特別なゾーンは見られない．ただし，まれにMMEの最外縁部が相対的により黒い場合がある．また，MMEの周りの母岩が部分的に粗粒 (ペグマティティック) になる場合があるとともに，黒雲母のレイアリング (layering) がMMEと近接する場合がある．観察露頭として代表的な地点である大戸川河床では，中-粗粒斑状黒雲母花崗岩中に，大きさが約 1 cmから約 15 cmのMMEが点在している (第3図)．この露頭において，幅約 15 cmのアプライト脈から 30 cmほどのところにMMEが存在している．これらの共存関係は他の場所でもしばしば観察され，まれに両者が接している場合もある．

本MMEの肉眼的な岩相としては，細粒 (1 mm以下) 石基中に点在する斜長石斑晶が特徴的である．まれに，石英の融食斑晶が点在している場合がある．また，斑晶が見当たらない場合もある．実際のモード組成や顕微鏡観察では斜長石の割合が大きいにもかかわらず，細粒石基に黒雲母粒子が散在しているため全体として黒色に見えている．斑晶斜長石の形状は自形-半自形に見える粒子もあるが，石基との境界は単純に平面状ではなく，角が丸みを帯びたり湾曲したりかなりの凹凸を有して石基と入り組んでいる場合が多い．

本稿の対象ではない中-粗粒黒雲母花崗岩中にも，笹間ヶ岳-堂山地域においてMMEが散在している (中野，2013)．本地域は，上記中-粗粒斑状黒雲母花崗岩分布域とともに，ペグマタイト多産地域である．中-粗粒斑状黒雲母花崗岩中の場合と同じくアプライト・ペグマタイトや黒雲母シュリーレンと共存しているほか，それに加えてこれらの近辺には球状花崗岩が伴われている (中野，2013)．中-粗粒黒雲母花崗岩とMMEとの境界はいずれも明瞭である．大きさや形は，中-粗粒斑状黒雲母花崗岩中のMMEとほぼ共通である．母岩とともに風化が進んでおり，これまでのところ野外観察に留まっている．

5.2 鏡下での特徴

構成鉱物の粒径は0.1-0.5 mm程度である．MMEを構成する石基の主成分鉱物は石英，斜長石，黒雲母である．石英の大きさは0.1-0.5 mm程度であり，他形である．自形-半自形の石基斜長石の長径は0.2-1.0 mm程度であり，コア-リムの累帯構造が発達しており，そのうちコア部はソーシュライト化している．斜長石のソーシュライト化した部分にはアルカリ長石小片が散在している．黒雲母の長径は0.1-0.3 mm程度である．

MME中に含まれる石英斑晶 (長径2-7 mm程度) であり，融食され丸みをおびた形である．斜長石斑晶は一般に大きさ2-10 mm程度である．MMENS03には多くの斑晶が
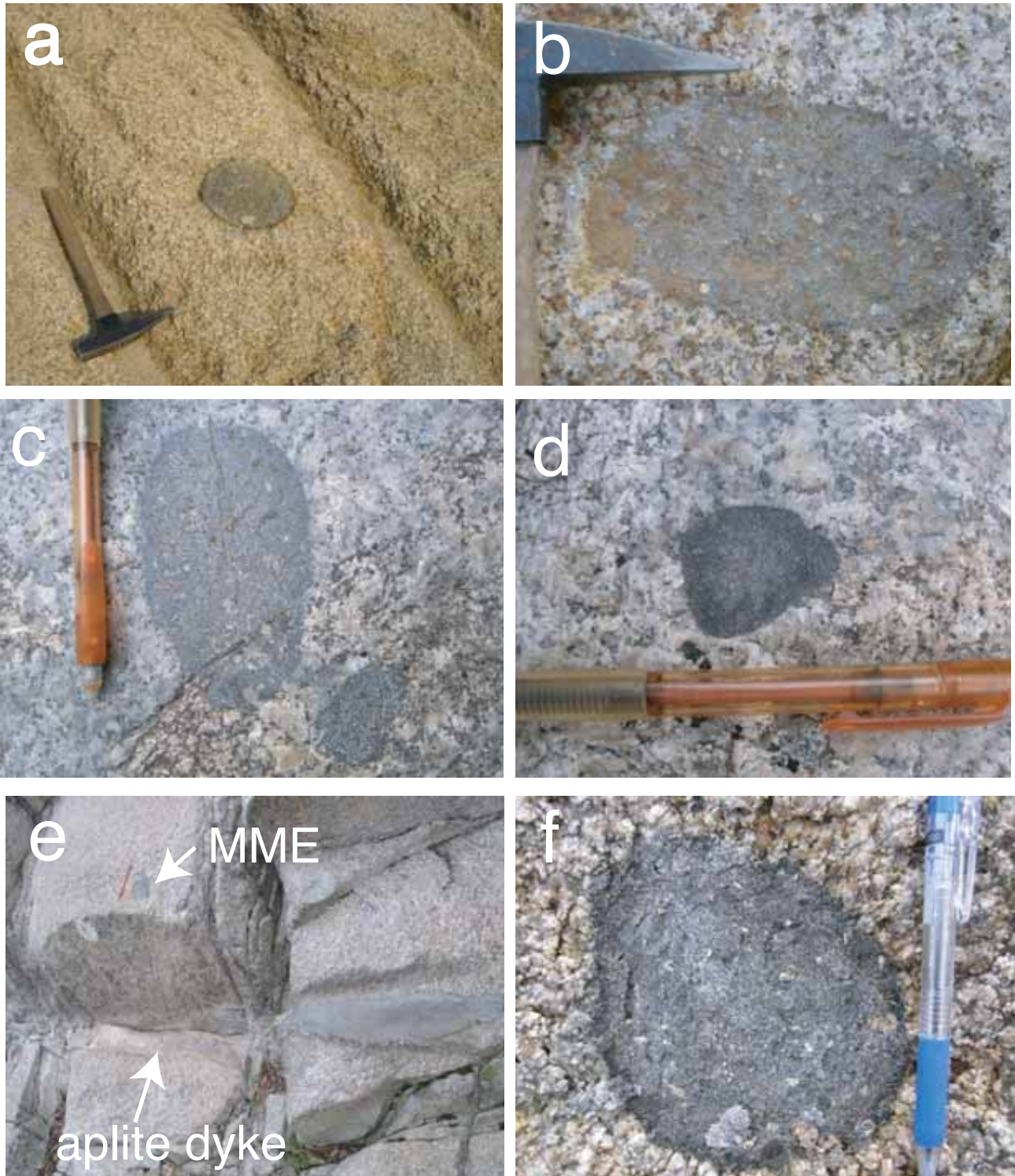
第3図　MMEの露頭写真．a，b：MMENS01 and MMENS 02，c：MMENS03，d：MMENS04，e：MMENS05 (以上，中－粗粒斑状黒雲母花崗岩 (Gt2) 中)，f：中－粗粒黒雲母花崗岩 (Gt3) 中のMME.

Fig. 3　Photographs of MME in outcrops, a, b: MMENS01 and MMENS 02，c: MMENS03，d: MMENS04，e: MMENS05 (a-e in medium- to coarse-grained porphyritic biotite granite (Gt2)), f: MME in medium- to coarse-grained biotite granite (Gt3).

存在し，10 mm以上の大きな斑晶もある (第4図，第11図)．斜長石斑晶は，コア－リムの関係に若干の振動パターンが加わった累帯構造を示すが，コア部は変質しており（ソーシュライト化）そこに不定形の微粒アルカリ長石及び間隙充填の石英や細粒黒雲母等が存在している．以下に，今回解析したMME試料について個別に鏡下の特徴
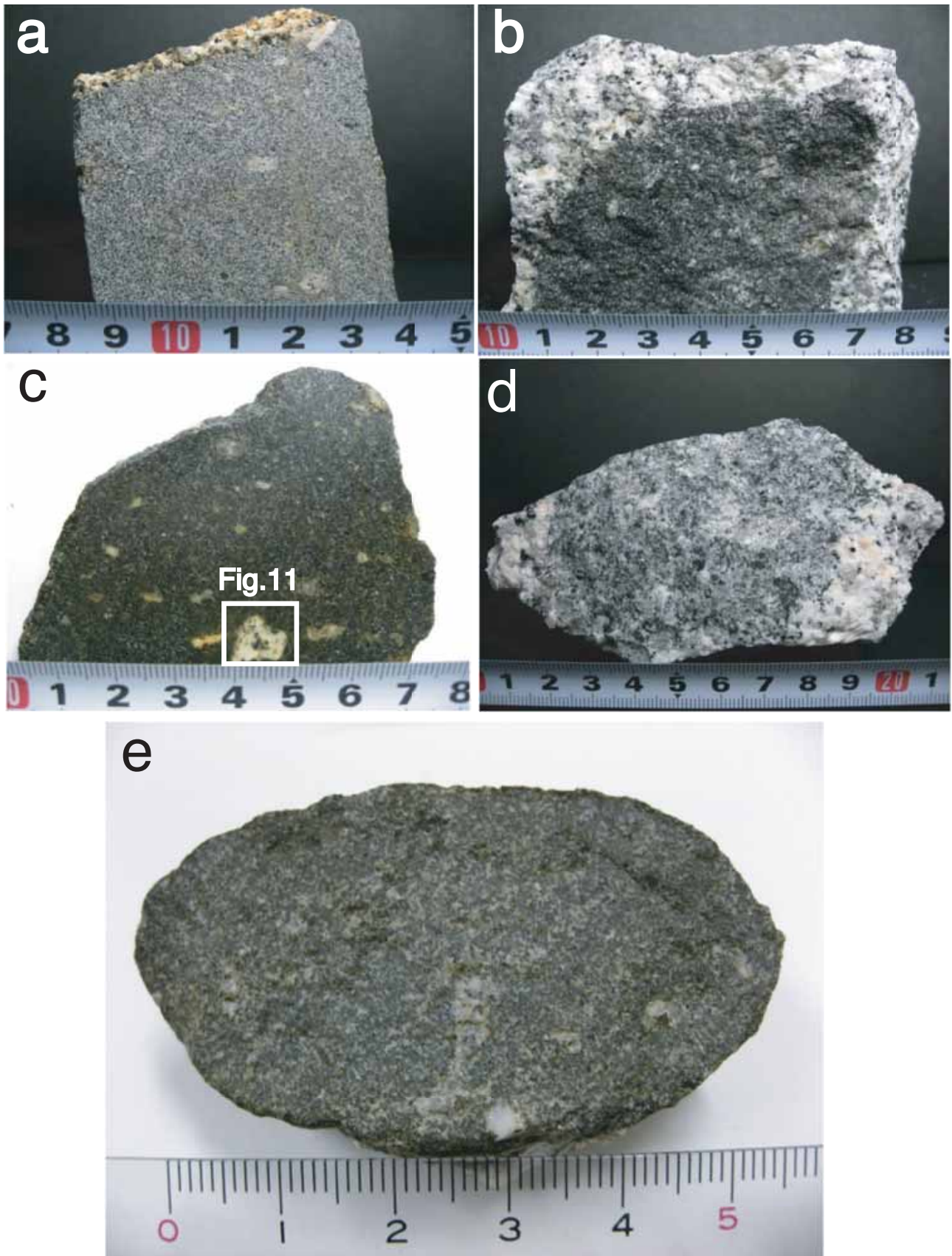
第4図　田上MME試料の接写写真．a：MMENS01,b：MMENS02，c：MMENS03，d：MMENS04，e：MMENS05.

Fig. 4　Close up photographs of the Tanakami MME samples investigated in this study. a: MMENS01, b: MMENS02, c: MMENS03, d: MMENS04, e: MMENS05.
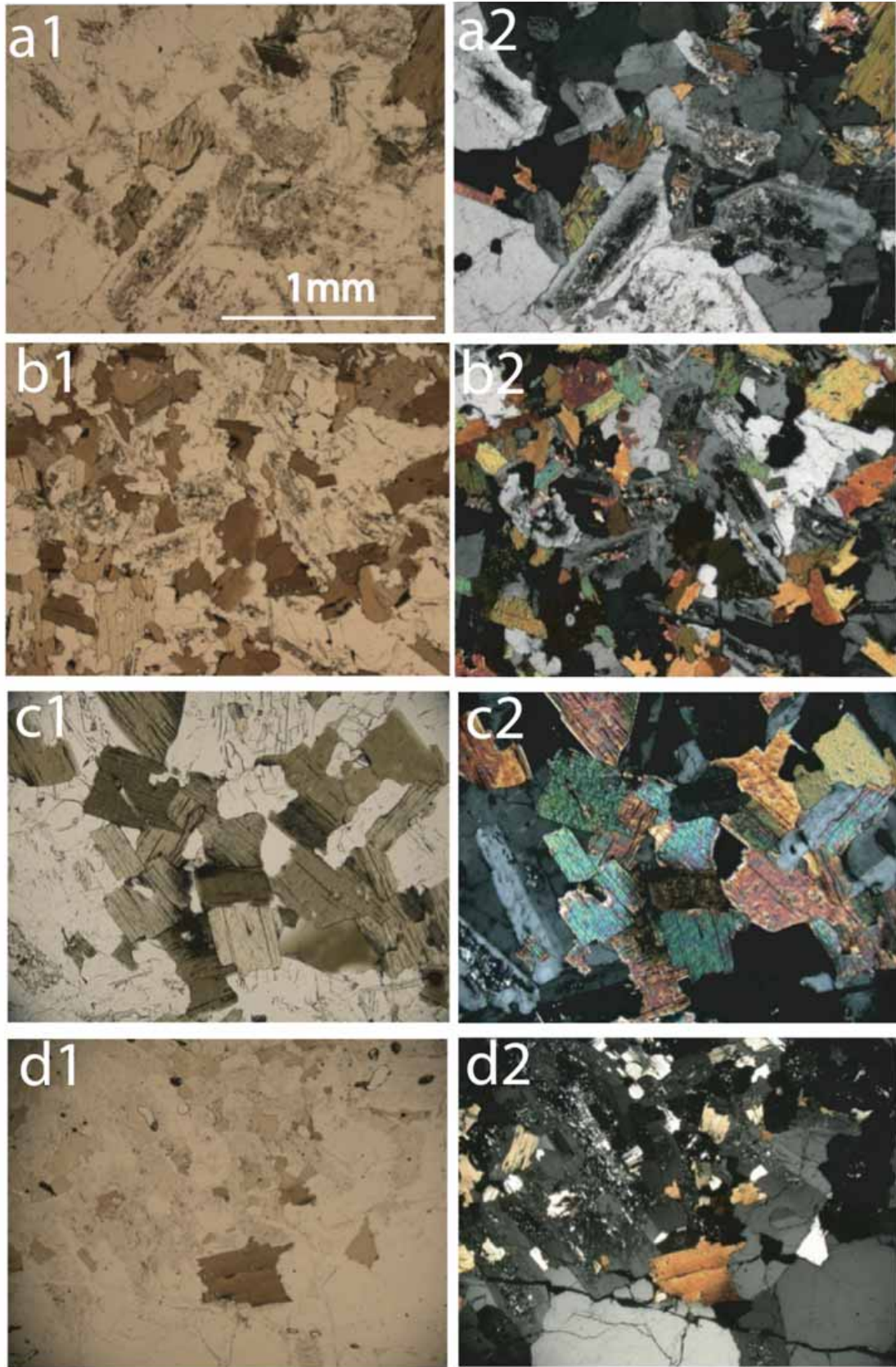
第5図　田上MME試料の薄片顕微鏡写真．a：MMENS01，b：MMENS02，c：MMENS03，d：MMENS04．番号1の写真は単ニコル，
　　　　番号2の写真は直交ニコル．

Fig. 5　Microphotographs of thin sections of the Tanakami MME samples. a: MMENS01, b: MMENS02, c: MMENS03, d: MMENS04.
　　　　Photos numbered as 1 are under one nicol and those numbered as 2 are under crossed nicols.

を述べる.

MMENS01 (第 4 図a, 第 5 図a)

　他のMMEと比較すると, 斜長石, 石英が多く, 黒雲母は少ない. また, 斜長石, 石英の大きさが 0.7 mm前後と大きい. そのため肉眼では白と黒の細かいまだら模様に見える. 5 mm前後の斜長石の斑晶と 1 mmほどの黒雲母の斑晶を含有する. 母岩である中粒斑状黒雲母花崗岩との境界部は明瞭である.

　鏡下では, 斜長石の大きさは 0.2-1 mm程度であり, 自形で伸長方向に成長し, 累帯構造が発達している. 累帯構造のコア部はソーシュライト化している. 石英は 0.3-1 mmで, 他形で間隙充填的に存在している. 黒雲母は短冊状のものや不規則型があり, 大きさは 0.1-0.8 mmほどである.

MMENS02 (第 4 図b, 第 5 図b)

　長径約 10 cmで, 断面の形状はひずんだ楕円状である. 他のMMEと比較すると, 全体的に細粒で, 黒雲母に富む. 肉眼では緻密な黒色状の塊に見える. 大きさ 3 mm前後の斑晶状の石英をわずかに含む.

　鏡下では自形斜長石の累帯構造が発達しており, 大きさは 0.3 mm前後である. 石英は他形で間隙充填的であり, 大きさは長径 0.1 mm以下のものから 0.7 mmほどである. 黒雲母は 0.1 mm以下のものから 0.4 mm程度のものがある.

MMENS03 (第 4 図c, 第 5 図c)

　長径 20 cmほどの細粒緻密なMMEである. 斜長石と石英の斑晶を多く含む. 斜長石の斑晶は 5 mm前後のものが多いが, 長径が約 1.4 mmの大きな斑晶もある (第 10図). 斑晶内部に存在する黒雲母集合部分を肉眼で確認できる. 斑晶状他形石英は大きさ 5 mm前後である.

　鏡下では, 径 10 mmを超える斜長石斑晶 (第 10 図) は, 他の斑晶 (他地点及び本地点) のこれまで触れてきた内部組織と異なり, 多数の 0.5 mm前後の短冊状斜長石が集まっているように見える). 既に述べたように, 斑晶内部に 0.1 mm以下の黒雲母が濃集している部分があり, 肉眼で黒色部に見える. 斑晶コア部には, 石英や微細な黒雲母, アルカリ長石, ジルコン, イルメナイト, 蛍石が存在しており, 黒雲母は緑泥石化している. 共存しているジルコンやイルメナイトは大きさ 10 μm程度, 蛍石は長径 100 μmを超える.

MMENS04 (第 4 図d, 第 5 図d)

　構成鉱物の粒度が粗いので, 個々の鉱物粒子が肉眼でもわかる. MME中にさらに 0.5 mm前後の黒雲母が濃集する部分 (クロット) が見られる.

　鏡下では, 斜長石, 石英共に大きさが 0.4-1 mmほどで, 他のMMEと比較すると, 鉱物粒子のサイズが相対的に大きい. 自形斜長石は, コア部がソーシュライト化しているものは少なく比較的新鮮である. 石英は他形で間隙充填的に存在する. 黒雲母の大きさは長径 0.5 mm前後で

ある.

MMENS05 (第 3 図e, 第 4 図e)

　本MMEは長径約 5 cmで断面は楕円形をしている. 2 mm前後の他形の石英斑晶を含んでいる. 石基の斜長石は自形で, 大きさは 0.5-0.8 mmで, 他の田上花崗岩中MMEと比較すると大きい. 石英は他形で間隙充填的であり, 大きさは 0.1-0.5 mmほどである. 黒雲母は短冊状のものが多く, 大きさは 0.1 mm以下のものから 0.3 mm程度と比較的小さい.

5.3 顕微鏡モード組成

　モード組成の測定値を第 1 表と第 6 図に示す. MMEに含まれる鉱物は石英と斜長石が約 40 ％で, 黒雲母は 20 ％前後であり, トーナル岩の組成を示す. MMEの中でもMMENS04は黒雲母の占める割合が 15.3 ％と相対的に少ない. 黒雲母の多いMMENS02はその割合が 26.6 ％である. MMEのアルカリ長石は斜長石中に小さく点在しているためカウントできていない.

6. 全岩化学組成

6.1 全岩主成分組成

　田上花崗岩体を構成する各岩相の全岩化学組成 (中野, 2013) に, 本稿の対象であるMMEの全岩化学組成を加えて第 2 表と第 3 表に示す. MMEのSiO_2の平均値は 66.1 wt% (分析数：4個), MME, 中-粗粒斑状黒雲母花崗岩 (Gt2), 中-粗粒黒雲母花崗岩 (Gt3), 細粒-細粒斑状黒雲母花崗岩 (Gt1)(アプライトを含む) の順にSiO_2の値が高くなっている. MMEと中-粗粒斑状黒雲母花崗岩のSiO_2平均値では 7 ％の差があるが, MMENS01サンプルは 70.04 wt%とSiO_2に富み母岩に近い値である. また, MMENS01サンプルはTiO_2, Fe_2O_3, MgOが他の田上花崗岩体中のMMEに比べて低く, 中-粗粒斑状黒雲母花崗岩に近い値を示す. 一方, MMENS02サンプルはSiO_2が 63.39 wt%と最も低い値である. 一方, 石原・村上 (2006) のMMEのSiO_2含有量は, 今回の試料より極めて低い.

　主成分元素の変化図 (ハーカー図) を第 7 図に示す. TiO_2, Al_2O_3, Fe_2O_3, MnO, MgO, CaO, P_2O_5は, SiO_2の増加に伴って, すなわちMME・中-粗粒斑状黒雲母花崗岩・中-粗粒黒雲母花崗岩・細粒-細粒斑状黒雲母花崗岩 (アプライトを含む) の順で減少している. Al_2O_3, P_2O_5は直線的に変化するが, Fe_2O_3, MnO, MgO, CaO, K_2O, TiO_2は曲線的に変化している. 一方, K_2Oは中-粗粒黒雲母花崗岩と細粒-細粒斑状黒雲母花崗岩では若干のばらつきがあるがほぼ直線的に増加する. Na_2Oは, どの岩相もほぼ 3.5-4.0 ％と一定でありSiO_2との間に相関がみられない. なお, 石原・村上 (2006) が記載したMME (MNK50) は, 多くの酸化物でこれらの変化曲線 (回帰曲線) の外挿線から大きく外れた位置にあり, 本研究でのMMEとは

第1表　田上MMEの顕微鏡モード組成.
Table 1　Modal analyses of the Tanakami MME under a petrographic microscope.

（%）	MME				Medium-grained Porphyritic bt gr (Gt2)		Aplite (Gt1)	
	MMENSO1	MMENSO2	MMENSO3	MMENSO4	KTM01	KTM06	MMENS05	Hirano
Quartz	40.2	37.9	39.2	37.9	36.0	37.5	54.2	47.1
Alkali feldspar	0.0	0.0	0.0	0.0	30.7	28.1	32.2	37.4
Plagioclase	41.3	35.2	38.7	45.6	27.0	28.4	12.0	14.5
Biotite	18.5	26.6	22.0	15.3	6.3	6.0	1.6	1.0
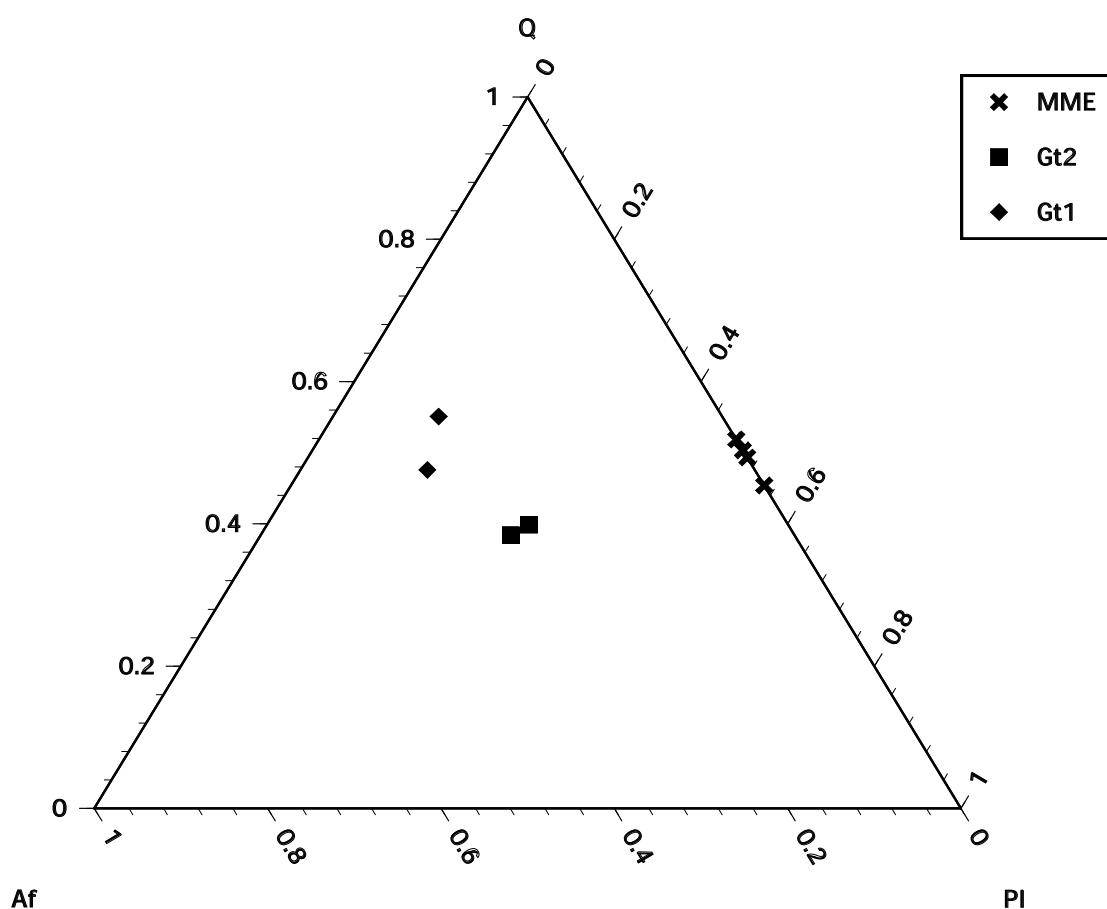
第6図　Q（石英）–Af（アルカリ長石）–Pl（斜長石）三成分モード組成図.
Fig. 6　Modal compositions on the Q (quartz)-Af (alkali feldspar)-Pl (Plagioclase) ternary diagram.

異質な岩石といえる.

6.2 REE含有量

　石原ほか (2005) は，田上花崗岩体水口図幅域の田上花崗岩体東半部構成岩相のREE含有量とその分布パターンについて次のように述べている：「その含有量は高く，179–290 ppmであり，特に重希土類に富んでお

り，イットリウムは40–114 ppmに達する」．この特徴は，第3表に示されている水口図幅西隣の京都東南部図幅域に相当する田上花崗岩体西半部からの各岩相試料についての分析値にもほぼ共通である．ただし，中野 (2013) の細粒–細粒斑状黒雲母花崗岩 (Gt1) のKTF01-04 (細粒斑状黒雲母花崗岩脈2本とアプライト岩脈2本) の軽希土類は41–84 ppmと石原ほか (2005) の相当岩 (3試料)

第 2 表　田上 MME と田上花崗岩体構成岩相の全岩化学組成（主成分）. Gt3（中一粗粒黒雲母花崗岩）・Gt2（中一粗粒斑状黒雲母花崗岩）・Gt1（細粒−細粒斑状黒雲母花崗岩）の記号は中野（2013）にしたがっている（第 3 表も同様）. 下段の Q・Or・Ab・An の数値はノルム組成を示す. 表中の − は未測定を示す.

Table 2 Bulk rock compositions (major elements) of MME and each constituent rock facies of The Tanakami Granite pluton. Chemical analyses were made by Act Lab. The abbreviations, Gt3 (medium- to coarse-grained biotite granite), Gt2 (medium- to coarse-grained porphyritic biotite granite) and Gt1 (fine-grained to fine-grained porphyritic biotite granite), are according to Nakano (2012) (these abbreviations are the same in Table 3). In the lower column, the values of Q, Or, Ab and An values are normative ones calculated. -: not determined.

This study

	KTC05	KTM01	KTM02	KTM03	KTM04	KTM05	KTM06	KTM08	KTM09	KTF01	KTF02	KTF03	KTF04	MMENS01	MMENS02	MMENS03	MMENS04
Rock facies	Gt3	Gt2	Gt2	Gt2	Gt2	Gt2	Gt2	Gt2	Gt2	Gt1	Gt1	Gt1	Gt1	MME	MME	MME	MME
SiO_2	75.68	73.24	73.80	72.16	73.38	71.44	73.75	71.64	74.09	77.65	75.75	77.59	76.02	70.02	63.39	65.10	65.86
TiO_2	0.03	0.16	0.16	0.10	0.19	0.20	0.17	0.18	0.17	0.05	0.05	0.02	0.02	0.33	0.70	0.78	0.61
Al_2O_3	13.08	13.54	13.10	13.88	13.81	13.75	13.45	13.60	13.51	12.56	12.53	12.56	12.75	14.30	15.55	15.60	14.85
$Fe_2O_3(T)$	1.70	2.54	2.41	1.69	3.07	3.14	2.73	2.96	2.56	1.35	1.22	0.65	0.99	3.82	7.97	6.79	6.96
MnO	0.06	0.08	0.06	0.05	0.08	0.08	0.07	0.07	0.07	0.04	0.04	0.01	0.04	0.10	0.24	0.15	0.17
MgO	0.03	0.23	0.25	0.18	0.29	0.30	0.23	0.24	0.27	0.07	0.07	0.05	0.02	0.53	1.20	1.17	1.08
CaO	0.33	1.51	1.44	1.17	1.53	1.69	1.52	1.58	1.36	0.53	0.59	0.55	0.63	2.14	2.88	2.87	2.70
Na_2O	4.25	3.58	3.47	3.69	3.94	3.87	3.61	3.62	3.70	3.93	3.94	4.18	3.36	3.75	4.09	4.13	3.95
K_2O	4.11	4.32	4.33	4.90	3.71	3.52	3.97	4.01	4.45	4.32	4.23	4.30	5.56	3.64	2.59	2.25	2.14
P_2O_5	0.02	0.05	0.05	0.03	0.07	0.06	0.05	0.06	0.06	0.02	0.02	0.08	<0.01	0.13	0.22	0.25	0.19
Total S	<0.01	<0.01	<0.01	<0.01	<0.01	<0.01	<0.01	<0.01	0.01	0.01	<0.01	0.02	<0.01	-	-	-	-
LOI	0.43	0.78	1.04	0.62	0.46	0.82	0.47	0.52	0.50	0.41	0.43	0.45	0.31	1.56	1.83	1.85	1.67
H_2O^+	0.40	0.50	0.50	0.40	0.50	0.70	0.50	0.60	0.50	0.40	0.40	0.20	0.10	-	-	-	-
H_2O^-	0.10	0.20	0.10	0.20	0.10	0.20	0.20	0.10	0.10	<0.10	<0.10	<0.10	<0.10	-	-	-	-
Total (wt%)	99.71	100.03	100.10	98.46	100.54	98.90	100.02	98.48	100.74	100.94	98.87	100.46	99.70	>101.00	100.70	101.00	>101.00
Norm Q	34.5	32.5	33.7	29.3	32.8	32.3	34.1	31.7	32.4	37.1	35.3	35.8	33.9	29.3	22.3	25.3	27.8
Or	24.3	25.5	25.6	29.0	21.9	19.6	23.5	23.7	26.3	25.5	25.0	25.4	32.9	21.5	15.3	13.3	12.7
Ab	36.0	30.3	29.4	31.2	33.3	32.8	30.6	30.6	31.3	33.3	33.3	35.4	28.4	31.7	34.6	35.0	33.4
An	1.5	7.2	6.8	5.6	7.1	8.0	7.2	7.5	6.4	2.5	2.8	2.2	3.1	9.8	12.9	12.6	12.2

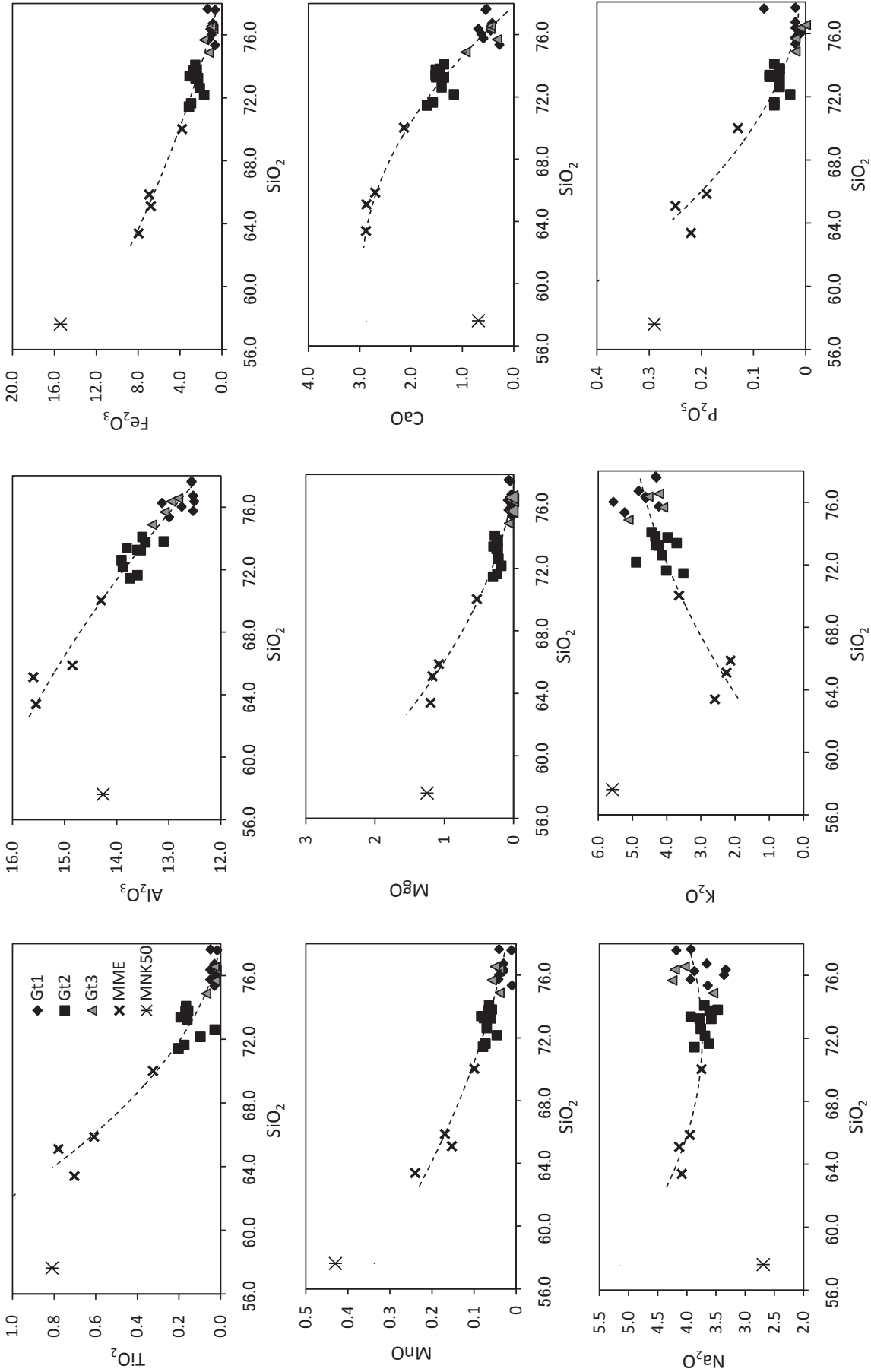| Reference	CRGGLB* (2000)			Ishihara et al. (2005)						Ishihara and Murakami (2006)
Sample No.	III	IV	V	TKM01	TKM03	TKM04	TKM01	TKM05	TKM06	MNK50
Rock facies	Gt3	Gt2	Gt1	Gt3	Gt3	Gt1	Gt2	Gt1	Gt1	MME
SiO_2	76.55	72.61	76.26	76.36	74.87	76.36	73.25	75.35	76.73	57.62
TiO_2	0.03	0.03	0.03	0.02	0.07	0.05	0.16	0.03	0.03	0.81
Al_2O_3	12.82	13.91	13.13	12.95	13.32	12.51	13.60	12.99	12.53	14.26
Fe_2O_3	0.19	0.45	0.88	0.82	1.26	1.08	2.28	0.64	0.85	15.42
FeO	0.75	1.50	n.d.	-	-	-	-	-	-	-
$Fe_2O_3(T)$	1.02	2.12	0.88	0.82	1.26	1.08	2.28	0.64	0.85	15.42
MnO	0.05	0.07	0.03	0.04	0.04	0.03	0.06	0.01	0.03	0.43
MgO	0.03	0.22	0.03	0.02	0.07	0.08	0.25	0.02	0.03	1.25
CaO	0.45	1.41	0.45	0.46	0.94	0.69	1.36	0.28	0.42	0.69
Na_2O	4.04	3.76	3.87	4.21	3.55	3.33	3.78	3.64	3.66	2.69
K_2O	4.23	4.14	4.61	4.54	5.12	4.62	4.23	5.23	4.82	5.59
P_2O_5	-	0.05	0.01	0.01	0.02	0.02	0.07	0.02	0.02	0.29
S	-	-	-	-	-	-	-	-	-	0.03
LOI	0.59	1.32	-	0.03	0.03	0.03	0.03	0.03	0.03	1.41
H_2O^+	-	-	-	0.32	0.50	1.04	0.62	1.55	0.79	0.15
H_2O^-	-	-	-	0.06	0.02	0.22	0.13	0.23	0.10	0.06
CO_2	-	-	-	0.08	0.12	0.09	0.12	0.10	0.10	-
Total (wt%)	99.73	99.47	99.30	99.91	99.92	100.14	99.93	100.11	100.13	100.64
Norm Q	34.4	31.7	35.1	33.5	32.6	37.8	32.0	33.6	36.1	18.1
Or	25.0	24.5	27.2	26.8	30.3	27.3	25.0	30.9	28.5	33.0
Ab	34.2	31.8	32.8	35.6	30.0	28.2	32.0	30.8	31.0	22.8
An	4.4	6.7	2.2	2.2	4.5	3.3	6.3	1.3	2.0	1.5

* CRGGLB=Collaborative Research Group for the Granites around Lake Biwa

第3表　MMEと田上花崗岩体構成岩相の全岩化学組成（微量成分）．表中の－は未測定を示す．

Table 3　Bulk rock compositions (trace elements) of MME and each constituent rock facies of The Tanakami Granite pluton. Chemical analyses were made by Act Lab. in Canada. –: not determined.

Reference	Nakano (in press)													Ishihara et al. (2005)						This study				*
Sample No.	KTC05	KTM01	KTM02	KTM03	KTM04	KTM05	KTM06	KTM08	KTM09	KTF01	KTF02	KTF03	KTF04	TKMO2	TKMO3	TKMO1	TKMO4	TKMO6	TKMO6	MMENS01	MMENS02	MMENS03	MMENS04	MNK50
Rock facies	Gt3	Gt2	Gt2	Gt2	Gt2	Gt2	Gt2	Gt2	Gt2	Gt1	Gt1	Gt1	Gt1	Gt3	Gt3	Gt2	Gt1	Gt1	Gt1	MME	MME	MME	MME	MME
F	1100	1500	1300	1000	2200	1800	1200	2000	1400	1100	1000	700	1500	1550	730	1120	830	480	590	-	-	-	-	-
Li	-	-	-	-	-	-	-	-	-	-	-	-	-	87	36	60	18	10	17	-	-	-	-	-
Sc	9	7	6	4	8	8	7	7	7	5	5	6	5	-	-	-	-	-	-	9	19	14	11	-
Be	4	4	4	3	9	9	4	4	4	6	6	15	12	-	-	-	-	-	-	11	9	4	3	-
Rb	375	242	224	242	263	274	199	216	243	300	308	290	342	334	172	219	250	355	319	264	362	218	261	588
Sr	5	121	111	82	118	129	124	143	87	24	20	20	7	4	63	101	33	5	19	189	167	150	130	11
Rb/Sr	75.0	2.0	2.0	3.0	2.2	2.1	1.6	1.5	2.8	12.5	15.4	14.5	48.9	83.5	2.7	2.2	7.6	71.0	16.8	1.4	2.2	1.5	2.0	53.5
Cs	13.6	11.7	9.2	7	14.6	15.3	11.7	13.9	9.1	7.6	6.5	7.7	41.5	16.4	2.8	8.4	2.6	2.3	5.6	21.2	39.8	9.7	9.1	25.3
Ba	17	564	459	436	327	504	513	499	338	66	49	121	38	20	330	415	144	16	37	502	311	380	266	267
Zr	42	142	115	78	120	151	148	145	113	62	74	92	86	62	101	145	85	72	85	173	177	222	196	466
Hf	2.9	4.9	4.4	3.6	4.6	4.8	5	5	4.8	3.5	4.3	6.2	5.6	3.1	3.6	4.6	3.8	4.6	4.2	5.4	5.4	6.1	5.7	17.6
Nb	19	11	10	9	14	18	11	10	14	13	14	32	19	13.3	9.9	13.7	10.7	25.0	10.3	12.8	28.3	13.7	15.1	141
Ta	4.8	1.7	1.7	1.8	3	3.6	2.3	1.5	2.5	3.4	3.7	6.5	8.7	2.4	0.9	2.0	2.2	4.5	1.8	2.31	5.75	1.61	1.24	6.87
V	6	11	11	5	17	13	10	9	19	24	<5	<5	<5	<2	<2	5	<2	<2	<2	32	99	84	58	38
Cr	240	<20	<20	180	20	<20	140	<20	<20	130	<20	<20	<20	2	<2	5	6.2	1.7	4.1	<20	<20	<20	<20	<20
Co	<1	1	3	1	4	2	2	2	2	<1	<1	<1	<1	5.3	4.3	7.8	4.8	2.4	5.7	7	7	9	8	7
Ni	<20	<20	<20	<20	<10	<20	<20	<20	<20	<20	<20	<20	<20	<0.7	1.30	<0.7	<0.7	3.40	0.70	<20	<20	<20	<20	<20
Cu	<10	<10	30	<10	<10	10	<10	<10	<10	<10	<10	<10	<10	<0.4	31	<0.4	3.90	0.60	<0.4	<10	<10	<10	<10	<2
Zn	30	50	30	<30	40	50	50	40	40	<30	30	<30	<30	21	29	43	36	16	18	70	80	90	130	296
Pb	16	25	12	19	15	28	23	11	16	31	21	36	58	24	26	19	20	25	39	23	24	28	23	17
Ga	23	18	18	19	19	17	19	17	20	18	19	19	18	19	16	18	15	21	17	18	19	17	20	38.0
Ge	<5	2	2	1	2	3	2	2	2	6	2	2	4	2.9	1.9	2.4	2.2	3.2	3.1	2.6	3.1	2.2	2.4	3.0
As	<5	<5	<5	<5	6	<5	<5	<5	<5	<2	<5	8	<5	<0.5	<0.5	<0.5	0.3	<0.6	<0.6	<5	<5	<5	<5	<5
Se	-	-	-	-	-	-	-	-	-	-	-	-	-	0.3	0.5	0.2	<0.1	0.2	0.2	-	-	-	-	0.5
Mo	6	<2	<2	4	<2	<2	3	<2	<2	<2	<2	<2	<2	<0.2	<0.2	<0.2	<0.2	<0.2	0.30	<2	<2	<2	<2	3.3
Ag	<0.5	<0.5	<0.5	<0.5	<0.5	<0.5	<0.5	<0.5	<0.5	<0.5	<0.5	<0.5	<0.5	-	-	-	-	-	-	-	-	-	-	<1
In	<0.2	<0.2	<0.2	<0.2	<0.2	<0.2	<0.2	<0.2	<0.2	<0.2	<0.2	<0.2	<0.2	-	-	-	-	-	-	-	-	-	-	<0.3
Sn	<5	5	5	6	6	14	6	5	4	4	4	3	22	6	1	-	2	−1	2	7	12	4	4	25
Sb	<0.5	1.2	0.5	<0.5	0.7	1	1.3	1.2	<0.5	0.8	0.5	2.9	<0.5	-	1	-	-	-	-	3.2	1.3	1.6	2.7	1.5
La	12	40.4	27.6	25.9	22.1	27.3	35.1	29	28.3	9.9	9.7	6.3	8	15.7	24.2	24	24.4	23	16.4	32.4	28.1	35.8	52.9	90.2
Ce	35.1	82.2	57	51.5	48.1	56.6	71.2	58.9	52.9	24.2	23.8	15.1	19.6	38.1	52	49.7	36.7	25.3	38.7	65.7	57.3	55.9	74.8	204
Pr	3.85	9.21	6.86	6.49	5.93	7.01	8.18	6.98	7.17	3.50	3.46	2.45	2.72	4.82	6.08	5.68	5.65	7.49	5.13	7.74	6.6	7.89	10.9	29.4
Nd	18.3	32.3	26	25.2	25.1	27.6	29.2	25.6	29.3	19.7	19.9	11	11.1	21.8	24.8	22.6	22	35	23	31.2	28.7	30.8	38.9	144
Sm	5.4	6.8	6.1	6.1	6.7	8.2	6.4	5.9	7.5	6.8	6.8	5.7	5.2	7.72	6.39	6.28	5.99	13.5	7.33	8.12	7.77	7.87	8.85	49.1
Eu	<0.05	0.68	0.62	0.48	0.59	0.65	0.7	0.71	0.51	0.13	0.12	0.08	<0.05	0.04	0.36	0.574	0.247	0.114	0.085	0.999	0.749	0.67	0.699	0.164
LREE	74.65	171.59	124.18	115.67	108.52	127.36	150.78	127.09	125.68	64.23	63.78	40.63	46.62	88.18	113.83	108.83	94.99	104.40	90.65	146.16	129.22	138.93	187.05	516.86
Gd	6.3	6.7	6.7	7	8.3	9.5	6.6	6.8	10	9.9	10.5	6.3	7.8	9.35	6.45	7.35	6.91	16.1	8.92	9.73	9.14	8.64	8.81	88.1
Tb	1.3	1.3	1.3	1.3	1.6	1.9	1.2	1.3	1.7	2.3	2.4	1.9	2	1.95	1.15	1.6	1.44	3.24	2	1.88	1.77	1.56	1.46	20.4
Dy	8.9	8.5	8.4	8.7	11.1	12.8	7.8	8.3	11.7	17.5	18.3	13.5	14.9	11.8	6.72	10	9.54	19.8	13.1	11.8	11.4	9.16	8.17	142
Ho	2	1.9	1.9	1.9	2.5	2.6	1.7	1.8	2.7	4.1	4.3	3	3.5	2.37	1.32	2.06	2	3.83	2.73	2.4	2.38	1.83	1.56	32.0
Er	6.3	6.2	6.1	6.3	7.9	8.2	5.5	5.8	8.6	13.5	14	10.4	11.9	7.84	4.24	6.93	7.03	12.5	9.38	7.3	7.37	5.41	4.55	99.4
Tm	0.99	0.95	0.94	0.95	1.27	1.43	0.87	0.89	1.32	2.16	2.23	1.98	2.29	1.32	0.674	1.14	1.18	2.05	1.56	1.19	1.17	0.85	0.704	14.1
Yb	6.5	6.1	6	6	8.3	9.9	5.8	5.7	8.6	14.1	14.7	15	17.2	8.15	3.91	7.12	7.47	12.4	9.42	7.95	8.24	5.58	4.59	78.4
Lu	0.92	0.88	0.86	0.86	1.18	1.45	0.84	0.81	1.28	1.99	2.1	2.36	2.64	1.29	0.624	1.11	1.18	1.89	1.46	1.17	1.27	0.812	0.683	10.5
HREE	33.21	32.83	32.2	33.01	42.15	47.78	30.31	31.4	44.9	65.65	68.53	56.04	62.23	121.97	65.39	103.91	103.05	185.81	132.87	43.42	42.74	33.84	30.53	484.9
Y	50	54	52	52	71	85	48	50	73	115	114	134	125	77.9	40.3	66.6	66.3	114	84.3	72.1	75.5	54.2	46.8	792
HREE+Y	83.21	86.83	84.2	85.01	113.15	132.78	78.31	81.4	117.9	180.65	182.53	190.04	187.23	199.87	105.69	170.51	169.35	299.81	217.17	115.52	118.24	88.04	77.33	1276.9
L/HREE	0.90	1.98	1.47	1.36	0.96	0.96	1.93	1.56	1.07	0.36	0.35	0.21	0.25	0.72	1.74	1.05	0.92	0.56	0.68	3.37	3.02	4.11	6.13	0.40
W	4	2	<1	1	2	<1	2	<1	2	<1	<1	<1	2	-0.5	-0.5	-0.5	-0.5	17.0	-0.5	25.1	14.6	9.3	18	2.2
Tl	1.6	3.5	1	1.2	2.2	1.2	2.8	1.8	1.1	3.6	2.2	1.2	1.3	2.9	1.5	1.8	1.9	2.6	2.6	2.29	1.67	2.17	2.53	5.17
Bi	0.6	59.2	0.5	0.6	42.5	<0.4	52.7	27.2	0.7	38.3	27.7	13.5	1.2	<0.3	1	20.5	0	1	<0.3	1.6	0.4	0.3	1.7	<0.1
Th	21.7	17.3	16.5	13.5	18.2	20.5	16.4	14.6	14.1	25.4	26.8	25.5	29.7	24.2	18.0	20.5	29.0	30.1	25.1	17.8	13.1	10.8	11.6	192
U	4.8	4.9	5	3.5	4.9	6.7	4.3	3.4	4.4	13.2	13.3	9.7	9.7	3.6	3.1	5.3	4.3	4.1	6.0	4.93	4.32	3.35	2.32	41.2
Th/U	4.5	3.5	3.3	3.9	3.7	3.1	3.8	4.3	3.2	1.9	2.0	2.6	3.1	6.7	5.8	3.9	6.7	7.3	4.2	3.6	3.0	3.2	5.0	4.7
(ppm)																								

* = Ishihara and Murakami (2006)

第 7 図　MME と田上花崗岩体各岩相のハーカー図（全岩化学組成変化図）．図中の破線は，石原・村上 (2006) の MME（＊印）を除く分析値に対してマイクロソフト・エクセルにより求めた近似（回帰）二次曲線を示す．

Fig. 7　Variation diagrams of bulk rock compositions of the Tanakami granites (Harker's diagrams). Each broken line shows each regression quadratic curve for each distribution pattern except for the MME (symbol=*) of Ishihara and Murakami (2006), which was obtained by the software "Microsoft Excel".
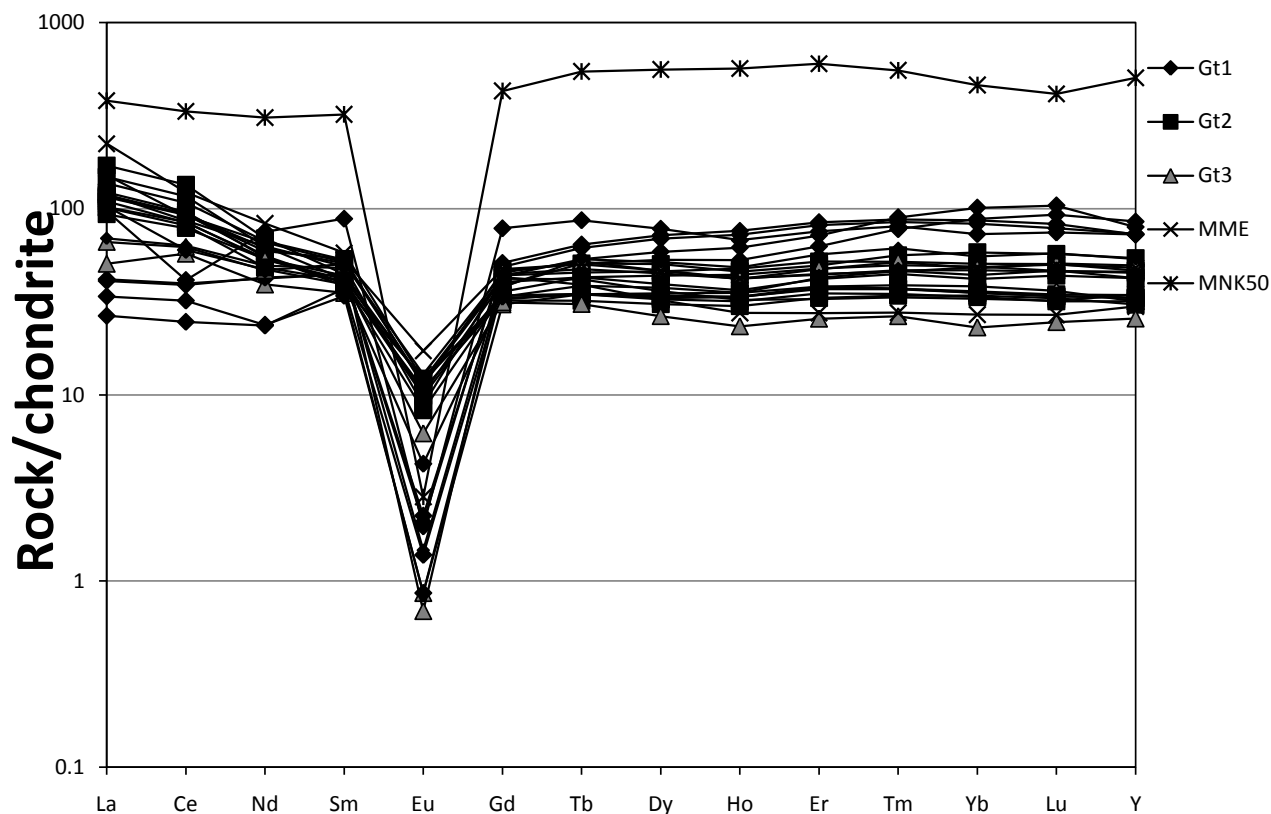
第8図　全岩化学組成図 (REE)．a：MMEと田上花崗岩体構成岩相のREEパターン図 (コンドライト規格化)．
Fig. 8　Spider diagram showing the contents of REE in bulk rock compositions. Plotted data are normalized using the chondrite values.

の91–104 ppmと比べるとかなり低い．

　MMEを含めての第3表に示されている分析値について，それらのコンドライト規格化した希土類元素の存在パターン (REEパターン) を第8図に示す．コンドライト規格化には，Sun and McDonough (1989)のコンドライト組成値を用いた．今回のMMEのREEは，相対的に軽希土類に富み重希土類に乏しいので，そのコンドライト規格化パターンはやや右下がりになっている．母岩の中–粗粒斑状黒雲母花崗岩 (Gt2) のREEパターンもほぼ同じパターンを示しており，両者のパターンはほぼ同じ範囲で重複している．ただし，MMEの方が，共通に見られるEuの負異常の落ち込みがやや小さい．これらのREEパターンは，比叡花崗岩のパターンに比較的近いものとなっている．主岩相の中–粗粒黒雲母花崗岩 (Gt3) のREEは，田上花崗岩体の中では，軽希土類においても重希土類においても相対的に含有量が少なくなっているが，パターンとしては同じようにやや右下がりである．細粒–細粒斑状黒雲母花崗岩 (Gt1) のREEは，軽希土類においてはかなり含有量が少ない場合も含めて平均的に少なくなっている一方，重希土類においては最も多い含有量であるので，全体のパターンとしては以上のパターンと逆にやや右上がりとなっている．なお，今回対象としたMMEのREEパターンと異なり，石原・村上 (2006) の

MNK50は，「希土類元素総量は非常に高く(1,804 ppm)，特にY (792 ppm)に富み，Dyは142 ppm」であり，例外的な含有量でやや右上がりのREEパターンを示している．

6.3ノルム組成

　全岩化学組成より求めたノルムAb–An–Or比とノルムQ–Ab–Or比は既に示した第2表に付記してあるが，第9図として示す．MMEは，ノルムAb–An–Or三角図では田上花崗岩体を構成する岩相中最もAnに富む組成を示し，ノルムQ–Ab–Or三角図では最もAbに富む．MMEは，ノルムAb–An–Or三角図，ノルムQ–Ab–Or三角図ではOr成分が産出される．ただし，関連岩相中では最も低いOr成分を示している．MMEの母岩である中–粗粒斑状黒雲母花崗岩は，ノルムAb–An–Or三角図において，主岩相の中–粗粒黒雲母花崗岩に比べるとよりAn成分に富む領域にプロットされる．細粒斑状黒雲母花崗岩とアプライトは粗粒黒雲母花崗岩よりもOr成分に富む領域にプロットされる．ノルムQ–Ab–Or三角図では，田上花崗岩体の各岩相ともにほぼ同じような領域にプロットされる一方，MMEのみがそれらとやや離れた領域にプロットされる．すなわち，Q成分はほとんど変わらないがAb：Or比が多少異なっている．
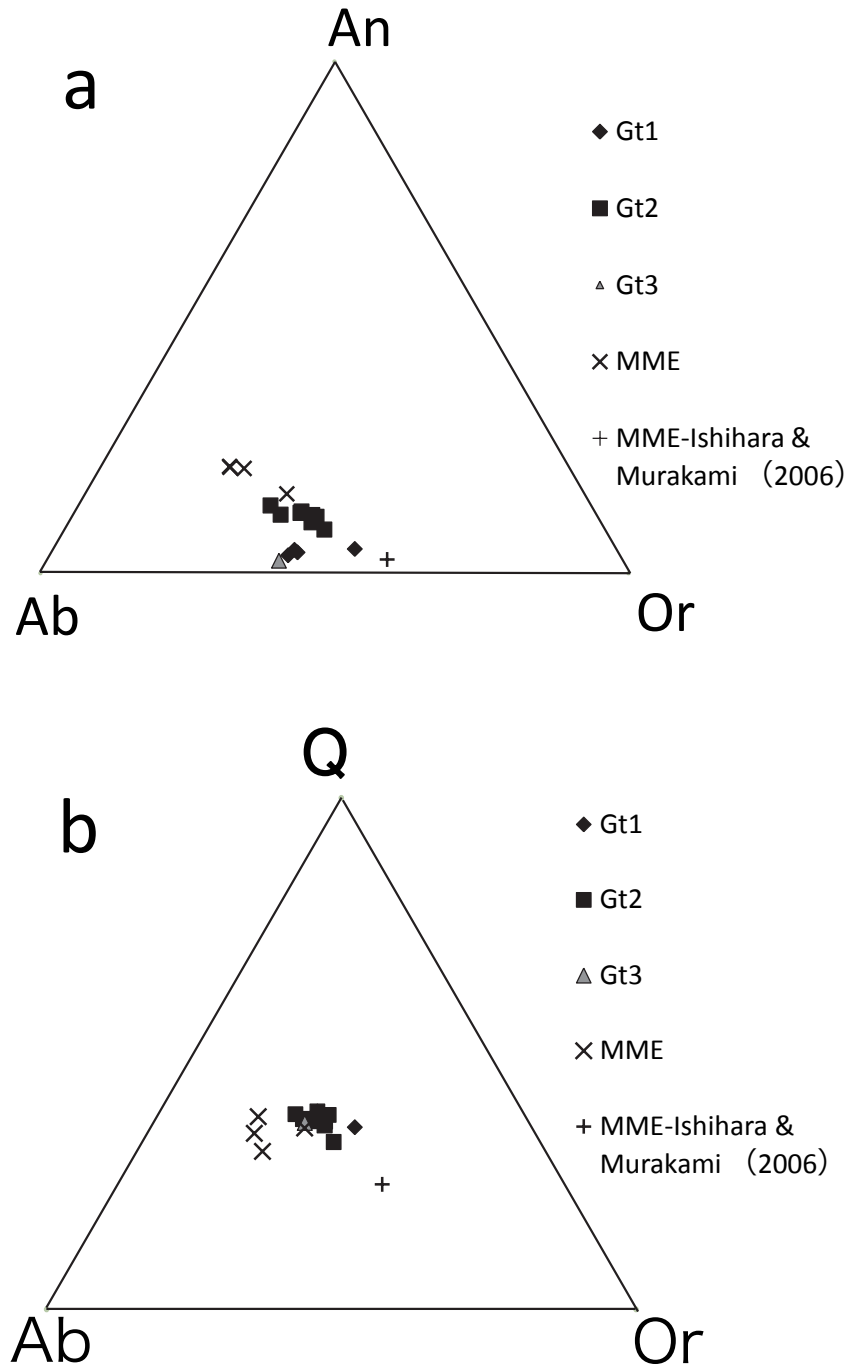
第9図　ノルム組成図. a：An–Ab–Or図，b：Q–Ab–Or図.
Fig. 9　Normative compositions of the rock samples. a: An-Ab-Or ternary compositions and b: Q-Ab-Or ternary compositions.

7.　造岩鉱物の組織と化学組成変化

7.1 斜長石

　第10図に各岩相中斜長石のAb成分の組成範囲を示す.
MME母岩の中−粗粒斑状黒雲母花崗岩中の斜長石の化学
組成はAb$_{60}$An$_{39}$Or$_{0.8}$−Ab$_{99}$An$_{0.4}$Or$_{0.5}$，中−粗粒黒雲母花崗
岩では，Ab$_{68}$An$_{30}$Or$_{1.8}$−Ab$_{98}$An$_{1.2}$Or$_{0.9}$という結果が得られ
た. 中−粗粒斑状黒雲母花崗岩中斜長石と中−粗粒黒雲

母花崗岩中斜長石は類似した化学組成を示すが，後者の
方がややAb成分に富む. 個別に得られたMME中の斜長
石の化学組成は，Ab$_{52}$An$_{47}$Or$_{0.7}$−Ab$_{88}$An$_{10}$Or$_{1.5}$ (MMENS01)，
Ab$_{52}$An$_{47}$Or$_{0.5}$−Ab$_{91}$An$_{6}$Or$_{2.4}$ (MMENS01)，Ab$_{44}$An$_{56}$Or$_{0.7}$−
Ab$_{83}$An$_{15}$Or$_{2.1}$ (新名神工事位置指標st.362：KTM03 (中
野, 2013) 地点西)，Ab$_{45}$An$_{55}$Or$_{1.0}$−Ab$_{96}$An$_{4}$Or$_{0.4}$ (MMENS03)，
Ab$_{55}$An$_{44}$Or$_{1.1}$−Ab$_{86}$An$_{13}$Or$_{1.5}$ (新名神工事位置指標st.368：
KTM02 (中野, 2013) 地点西)，Ab$_{55}$An$_{44}$Or$_{0.9}$−Ab$_{80}$An$_{18}$Or$_{2.0}$
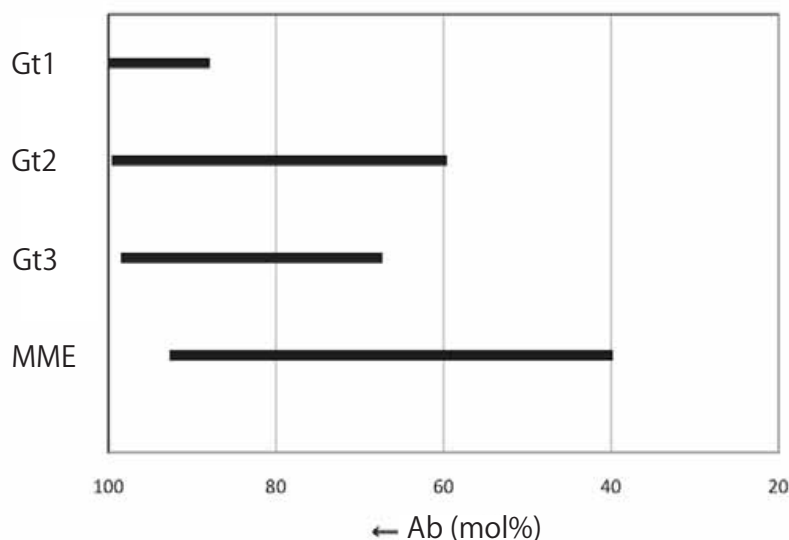
第10図　MME及び田上花崗岩体構成岩相中斜長石の組成比較図.
Fig. 10　Plagioclase compositions of MME and each constituent rock facies of the Tanakami Granite pluton.

(MMENS04)，$Ab_{45}An_{54}Or_{1.2}$–$Ab_{92}An_7Or_{0.7}$ (MMENS04t)，$Ab_{40}An_{59}Or_{0.8}$–$Ab_{84}An_{15}Or_{1.9}$ (MMENS04tl)，$Ab_{47}An_{53}Or_{0.7}$–$Ab_{92}An_7Or_{0.7}$ (MMENS05) である．MME中の斜長石は短冊状をしており，コア–リムの累帯構造を示す (第11図)．累帯構造のコアはAn成分に富み，リムほどAb成分に富む．コアの組成は曹灰長石を示し，リムの組成値はサンプルによって幅があり，灰曹長石の組成を示すもの (MMENS01・st.362・st.368・MMENS04・MMENS04tl) と，曹長石の組成を示すもの (MMENS02・MMENS03・MMENS04t・MMENS05) とがある．MMEを構成する斜長石は，母岩である中–粗粒斑状黒雲母花崗岩や中–粗粒黒雲母花崗岩と比較すると，An成分に富みAb成分に乏しい (第10図)．

MME中の斜長石斑晶についても (MMENS03サンプル中の長径14 mmほどの斜長石斑晶とst.368中の斜長石斑晶)，その化学組成を調べた．第10図の斑晶のコア部の化学組成は$Ab_{72}An_{27}Or_{0.8}$–$Ab_{96}An_3Or_{0.2}$であり，他のMME中の斜長石斑晶よりも，よりAb成分に富み曹長石化している．この大きい斑晶は短冊状の (0.5 mm前後) 斜長石結晶が集合した組織を示しているのが注目されるが，特に石基部との境界部でそのような集合状態が明瞭である (第11図)．斑晶リム部のこれらの斜長石短冊片にも個々累帯構造が観察される．その組成範囲は$Ab_{53}An_{46}Or_{1.0}$–$Ab_{77}An_{21}Or_{2.0}$とAn成分に富み，既に述べたMME石基を構成する斜長石と類似の特徴を示している．

7.2アルカリ長石

まず，田上花崗岩体を構成する各岩相中のアルカリ長石について言及する．それらのアルカリ長石のバルク組成 (平均組成) は，中–粗粒斑状黒雲母花崗岩では$Or_{81}Ab_{18}An_{0.9}$，中–粗粒黒雲母花崗岩では$Or_{84}Ab_{16}An_{0.5}$である．中–粗粒斑状黒雲母花崗岩，中–粗粒黒雲母花崗岩のどちらのアルカリ長石もパーサイト組織が発達しており，パッチパーサイトやひも状パーサイト，ラメラ状パーサイトを有している．パーサイト組織の化学組成は，中–粗粒斑状黒雲母花崗岩では，Or_{85-99} (ホスト) –Ab_{82-99} (ゲスト)，中–粗粒黒雲母花崗岩ではOr_{94-97} (ホスト) –Ab_{92-98} (ゲスト) という結果が得られた．また，中–粗粒斑状黒雲母花崗岩，中–粗粒黒雲母花崗岩の両岩相中アルカリ長石にはBaゾーニングを示すものがある (Aoki，1995)．なお，アプライト中アルカリ長石の化学組成は$Or_{87}Ab_{14}An_{0.0}$–$Or_{98}Ab_3An_{0.0}$ (MMENS05地点=KTF04 (中 野，2013))，$Or_{80}Ab_{20}An_{0.1}$–$Or_{98}Ab_2An_{0.0}$ (KTF03 (中野，2013)) である．

次に，MME中のアルカリ長石について述べる．アルカリ長石は，MMEの石基部結晶・斑晶ともに，斜長石のコア部を他鉱物とともに置換する産状で，顕微鏡モード測定ではほとんどカウントできない状態で散在している (第12図)．各サンプルのMME中アルカリ長石の化学組成は，$Or_{88}Ab_{11}An_{0.8}$–$Or_{97}Ab_3An_{0.0}$ (MMENS01)，$Or_{89}Ab_{11}An_{0.0}$–$Or_{96}Ab_4An_{0.2}$ (MMENS02)，$Or_{88}Ab_{12}An_{0.5}$–$Or_{98}Ab_2An_{0.0}$ (st.362)，$Or_{95}Ab_5An_{0.2}$–$Or_{98}Ab_2An_{0.0}$ (MMENS03)，$Or_{86}Ab_{14}An_{0.4}$–$Or_{92}Ab_8An_{0.1}$ (st.368)，$Or_{85}Ab_{13}An_{0.2}$–$Or_{91}Ab_7An_{0.0}$ (MMENS04)，$Or_{89}Ab_{11}An_{0.0}$–$Or_{97}Ab_4An_{0.0}$ (MMENS04t)，$Or_{73}Ab_{24}An_{3.1}$–$Or_{94}Ab_5An_{1.1}$ (MMENS04tl)，$Or_{89}Ab_{10}An_{1.3}$–$Or_{97}Ab_3An_{0.1}$ (MMENS05) である．MME中のアルカリ長石 (岩石記載においてカリ長石が使用されているが，それらのほとんどの場合アルカリ長石とすべきである：カリ長石と呼べるのは狭義ではOr_{95} mol %以上広義でもOr_{90} %以上であろう) にはパーサ
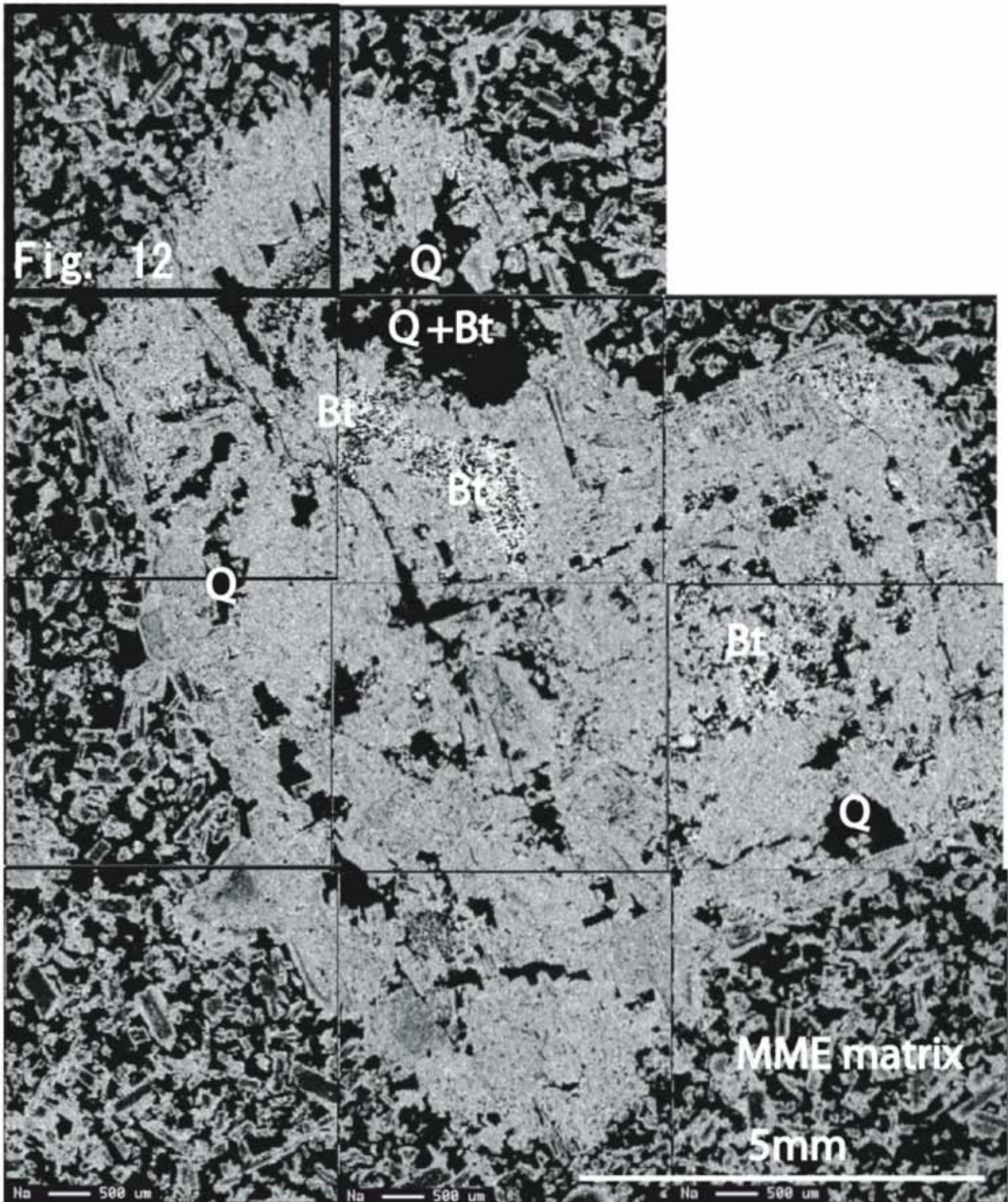
第11図　MMENS03試料中の大きな斜長石斑晶についてのEMPA・Na分布マップ．短冊状の小結晶がほぼ定方位で集合してい
　　　るように見える．内部には虫食い状に石基 (matrix) 部分が入り込んでいる．したがって，その部分は黒雲母 (Bt)・石
　　　英 (Q)・アルカリ長石小片等の集合になっている．本図中の黒色部分はほとんどが石英であり，斜長石斑晶内部に他
　　　鉱物に比べて相対的に大きい石英部分が間隙充填状に点在していることがわかる．

Fig. 11　EMPA collage map of a large plagioclase phenocryst showing Na-distribution. The phenocryst appears to consist of lath-like small
　　　subgrains that are elongated along the nearly the same orientation. Matrix part outside the phenocrysts penetrate into the interior
　　　showing a worm-eaten texture, which consists of small grains of biotite (Bt), quartz (Q), alkali feldspar and so on. In this figure,
　　　black grains are almost quartz so that larger quartz grains or aggregates are scattered in the interior of the plagioclase phenocryst.
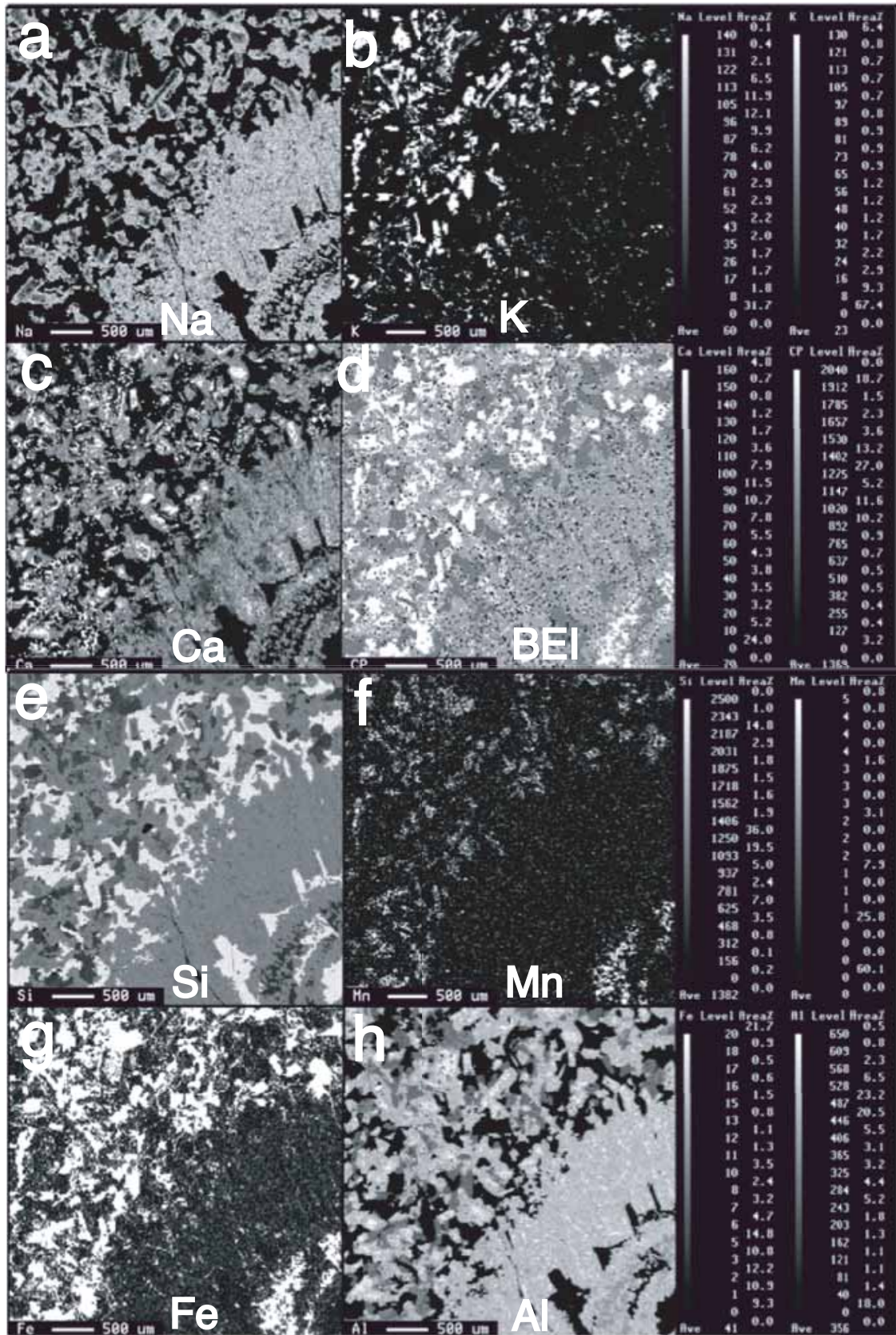
第12図　第11図に示されているMME中斜長石斑晶の左上端部分（石基部分との境界部）についてのEMPA元素マップ.
Fig. 12　Element distribution maps in the part of a large plagioclase phenocryst shown in Fig. 11.

第4表　MME中黒雲母の化学組成.
Table 4 Chemical compositions of biotite in the Tanakami MME.

Rock facies	MME											
Samples	MMENS01			MMENS02			MMENS03			MMENS04		
SiO₂ (wt. %)	35.60	35.60	35.60	36.20	35.90	36.10	35.70	35.40	35.20	36.20	36.00	36.00
TiO₂	2.85	3.31	3.75	2.22	2.62	2.22	3.45	3.31	3.42	3.63	3.64	3.74
Al₂O₃	14.10	14.30	13.90	15.10	15.20	14.70	13.50	13.40	13.40	13.30	13.50	13.20
FeO	29.80	29.30	28.80	29.50	29.90	29.30	28.90	28.90	29.20	28.20	27.90	27.80
MgO	3.79	4.06	4.09	4.14	3.98	4.38	5.30	5.33	5.23	5.99	6.00	5.97
MnO	0.85	1.01	0.91	1.06	1.06	1.01	0.87	0.82	0.83	0.60	0.70	0.58
CaO	n.d.	n.d.	n.d.	n.d.	n.d.	n.d.	n.d.	n.d.	n.d.	n.d.	0.04	n.d.
Na₂O	n.d.	0.04	0.01	0.12	0.10	0.11	0.07	0.10	0.12	0.05	0.05	0.06
K₂O	n.d.	9.65	9.67	10.02	9.60	9.70	9.48	9.74	9.81	9.84	9.63	10.03
Total	n.d.	97.30	96.70	98.40	98.30	97.50	97.30	97.00	97.30	97.80	97.40	97.40
	Atomic proportion (O=8)											
Si	5.677	5.630	5.652	5.663	5.621	5.681	5.635	5.620	5.583	5.659	5.642	5.650
Ti	0.341	0.394	0.448	0.260	0.308	0.264	0.409	0.395	0.408	0.427	0.429	0.443
Al	2.649	2.670	2.604	2.785	2.796	2.728	2.512	2.507	2.515	2.455	2.492	2.445
Fe	3.974	3.876	3.820	3.853	3.908	3.866	3.814	3.837	3.882	3.983	3.651	3.655
Mg	0.902	0.957	0.968	0.964	0.927	1.029	1.247	1.261	1.239	1.395	1.402	1.399
Mn	0.115	0.135	0.123	0.141	0.140	0.134	0.117	0.110	0.112	0.079	0.093	0.078
Ca	n.d.	n.d.	n.d.	n.d.	n.d.	n.d.	n.d.	n.d.	n.d.	n.d.	0.006	n.d.
Na	0.016	0.013	0.004	0.038	0.031	0.033	0.021	0.031	0.037	0.014	0.014	0.019
K	1.979	1.947	1.961	1.998	1.915	1.949	1.908	1.972	1.987	1.962	1.924	2.012
Total	15.655	15.621	15.580	15.702	15.646	15.683	15.654	15.733	15.763	15.974	15.652	15.700
Mg/Fe	0.23	0.25	0.25	0.25	0.24	0.27	0.33	0.33	0.32	0.35	0.38	0.38
Mg/Mg+Fe+Mn	0.18	0.19	0.20	0.19	0.19	0.21	0.24	0.24	0.24	0.26	0.27	0.27
log((Mn/Mg)*100)	1.11	1.15	1.10	1.16	1.18	1.12	0.97	0.94	0.96	0.75	0.82	0.74

イト組織は存在せず，いずれの試料においてもOr_{90}前後のOr成分にやや乏しいアルカリ長石とOr_{95}前後のOr端成分に近いアルカリ長石の二つの部分に分かれている．このようなアルカリ長石ホストの組織と化学組成変化は，基本的に母岩である中−粗粒斑状黒雲母花崗岩のアルカリ長石ホストのそれらと同じであり，琵琶湖周辺の優白質花崗岩体アルカリ長石のパーサイト組織ホストカリ長石部分に見られる組成変化パターンとも同じである (橋本ほか，2005a，b).

7.3 黒雲母

MME中の黒雲母の化学組成を第4表に示す．これに，中野 (2013) のデータと本研究でのさらなるデータを加えて，田上花崗岩体中の黒雲母全体の組成変化を示したのが第13図である．今回分析した田上花崗岩体の中−粗粒黒雲母花崗岩中の黒雲母は，これまで報告されていた田上花崗岩の黒雲母組成 (Hiraoka, 1997, 1998) よりもMg値に富む．この違いは，中野 (2013) が指摘しているように，試料の風化度の違いに起因する可能性が大きい．MME中の黒雲母は，最もMgOに富み (3.08−6.00 wt%)，FeOに乏しい (27.3−31.2 wt%)．MME黒雲母では，MMENS03が最もMg (wt%) に富む組成を示し，MMENS01サンプルのMgO値が低い．一方，アプライト中の黒雲母が，最もMgOに乏しく (0.52−1.17 wt%)，FeO (wt%) に富む (30.5−33.7 wt%)．第13図全体の組成変化と

して，MME，中−粗粒黒雲母花崗岩，中−粗粒斑状黒雲母花崗岩，アプライトの順に，MgOが減少しFeOが増加していく．中−粗粒黒雲母花崗岩中黒雲母は，MME黒雲母と組成範囲が重なる部分も含めて，概略中−粗粒斑状黒雲母花崗岩及びMME黒雲母との中間の組成を示している．

7.4 イルメナイト

今回分析した試料 (MME・中−粗粒斑状黒雲母花崗岩 (Gt2)・中−粗粒黒雲母花崗岩 (Gt3)) は，副成分鉱物としてイルメナイトを含む．イルメナイトの化学組成を第5表に示す．田上花崗岩体中のMMEを含む各岩相において，いずれもイルメナイトはMnOに富む (8.3−13.2 wt%)(田上花崗岩体を含む近畿〜中国地方の花崗岩体中のイルメナイトの化学組成については，Tsusue，1973；Tsusue and Ishihara，1974；Czamanske et al., 1981；Takagi，1992；中野ほか，2003；等を参照).

8.　議論

MMEの形成過程 (成因) については，これまで大きく四つの成因が考えられてきている：(1) レスタイト説，(2) 捕獲岩説，(3) マグマ混合説，(4) 早期晶出相説 (Fershtater and Borodina，1977；Best and Christiansen，2001；Esna−Ashari et al., 2011)．レスタイト説は，花崗岩マグマを生

第5表　イルメナイトの化学組成.

Table 5　Chemical compositions of ilmenite of MME and each constituent rock facies of the Tanakami Granite pluton.

Sample	Gt2		Gt3		In matrix of MMENS03		In plagioclase phenocryst of MMENS03			
SiO_2 (wt%)	n.d.	0.06	n.d.	0.07	0.02	0.02	0.28	0.24	0.08	0.04
TiO_2	53.70	53.90	54.00	54.60	52.30	50.20	53.10	54.50	53.40	54.00
Al_2O_3	0.01	0.02	0.02	n.d.	n.d.	n.d.	0.04	n.d.	0.02	0.01
FeO	36.20	35.20	35.80	35.70	41.60	42.40	36.90	38.40	40.20	38.30
MgO	n.d.	0.02	0.01	n.d.	0.03	0.04	n.d.	0.02	n.d.	0.01
MnO	12.50	12.80	13.20	13.20	8.30	8.70	11.30	10.40	9.00	10.60
CaO	n.d.	n.d.	n.d.	n.d.	n.d.	0.03	0.20	0.20	0.01	n.d.
Na_2O	n.d.	n.d.	0.01	0.01	n.d.	n.d.	n.d.	0.01	n.d.	0.01
K_2O	0.01	0.02	0.02	n.d.	0.01	n.d.	n.d.	0.01	0.01	0.01
Total	102.40	101.90	103.00	103.50	102.10	101.30	101.30	103.30	102.60	102.90
Atomic proportion (O=8)										
Si	n.d.	0.00	n.d.	0.00	0.00	0.00	0.01	0.01	0.00	0.00
Ti	1.00	1.00	1.00	1.00	0.98	0.96	0.99	1.00	0.98	0.96
Al	0.00	0.00	0.00	n.d.	n.d.	n.d.	0.00	n.d.	0.00	0.00
Fe	0.75	0.73	0.73	0.73	0.87	0.90	0.79	0.82	0.85	0.83
Mg	n.d.	0.00	0.00	n.d.	0.00	0.00	n.d.	0.00	n.d.	0.00
Mn	0.26	0.27	0.27	0.27	0.17	0.19	0.24	0.22	0.20	0.22
Ca	n.d.	n.d.	n.d.	n.d.	n.d.	0.00	0.00	0.00	0.00	n.d.
Na	n.d.	n.d.	0.00	0.00	n.d.	n.d.	n.d.	0.00	n.d.	0.00
K	0.00	0.00	0.00	n.d.	0.00	n.d.	n.d.	0.00	0.00	0.00
Total	2.00	2.00	2.00	2.00	2.02	2.04	2.02	2.04	2.02	2.01
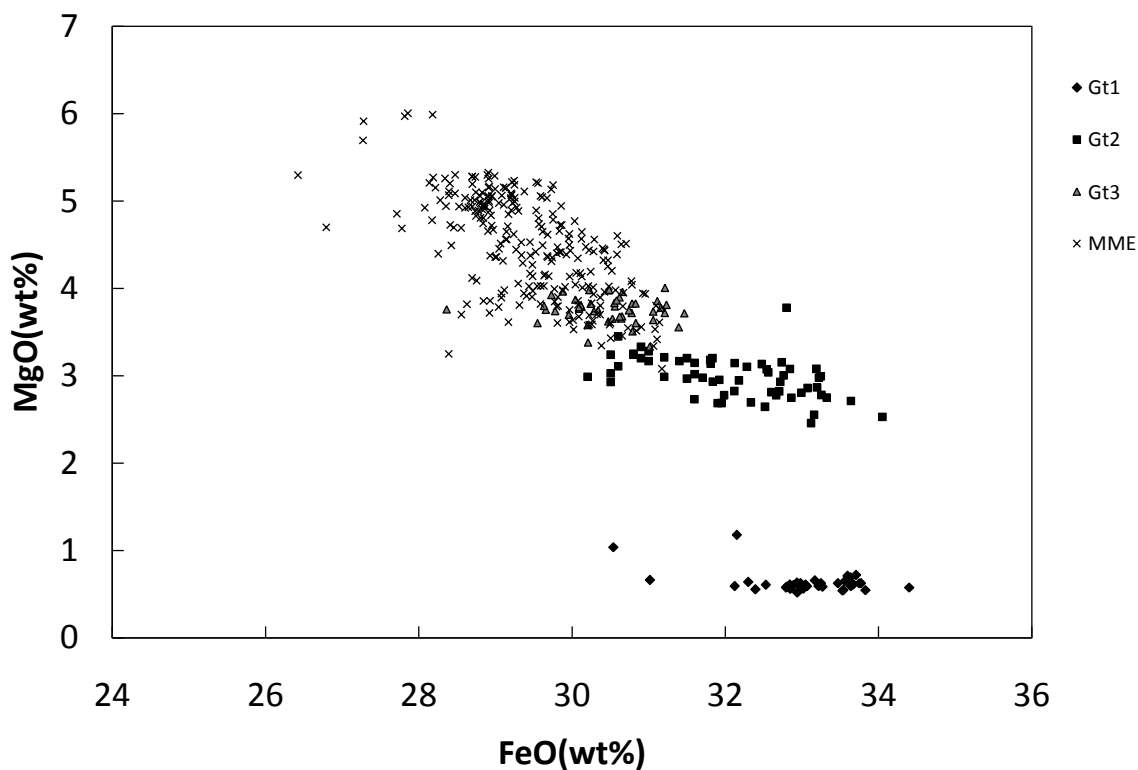
第13図　田上花崗岩体 (Gt1，Gt2，Gt3は中野 (2013) による岩相区分) 及びMME中黒雲母化学組成についての FeO−MgO変化図.

Fig. 13　FeO-MgO variation diagram for biotites in the Tanakami Granites (Gt1, Gt2 and Gt3 show their facies variation according Nakano (2013)) and the MME.

み出した源物質の溶け残りがMMEであるとする (White and Chappell, 1977；Chappell, 1978, 1996；Chappell *et al.*, 1987). しかし，Barbarin and Didier (1992)やVernon (1990)は，レスタイトはMMEとは異なるものであることを指摘している. レスタイトは，一般にSタイプ花崗岩において認められてきており，Iタイプ花崗岩ではそもそもその認定が難しいとされる (Esna-Ashari *et al.*, 2011) うえ，Iタイプ花崗岩中の本MMEの示す鉱物組織はマグマ中で形成された火成組織として考えるのが合理的でありレスタイト説になじまない.

捕獲岩説は，昔からよく知られているように，花崗岩マグマに取り込まれた外来岩片 (例えば堆積岩：天井岩や壁岩の母岩を含む) の再結晶したものがMMEであるとする. この説については更なる実証的検討が必要と考えられるが，本MMEについては，現在まで得られたデータの範囲内でその産状・形状や組織等が直接捕獲岩説を示しているようには思われず，現時点ではこれ以上の議論ができない.

したがって，本稿では，本MMEの成因について，現在までに得られているデータがマグマ混合説と早期晶出相説の二つのうちのどちらになじむのかという観点から，以下の議論を行いたい. マグマ混合 (混交) は，現在最も広く適用されている説 (モデル) である. この説は，MMEの成因を産状や母岩との組成的対比から珪長質マグマとそのマグマ溜まりに貫入する苦鉄質マグマとの混合・混交現象の産物であるとする (Vernon, 1984, 1990；Wiebe *et al.*, 1997；Perugini *et al.*, 2003；Barbarin, 2005；ほか). 同一マグマからの早期晶出相がMMEであるとの説は，cognateモデルとして知られているものである. この説は，Esna-Ashari *et al.* (2011)によると，さらに集積クロット説 (cumulate clot (Dodge and Kistler, 1990；Dahlquist, 2002))，急冷周辺相分離説(disrupted chilled margin (Donaire *et al.*, 2005))，集積相分離説(disrupted cumulate assemblage (Platevoet and Bonin, 1991))に細分される.

近年のマグマ混合説は，珪長質マグマに遅れて塩基性マグマが注入されていく過程を想定しており，その逆は想定されていない. 完全に二つのマグマの混合が起これば (マグマ混合＝magma mixing) その後は融合した一つのマグマの挙動の問題になる. 完全な混合が行われなかった場合，異なる両マグマからの結晶作用の記録が岩体中そして構成鉱物中に保存される. その一つの例がMMEであると考えられている (マグマ混交＝magma mingling). したがって，一般的にはマグマ混合という用語は適切ではなく，実際にはマグマ混交の用語が該当する. 今回の場合も，正確にはマグマ混交とすべきであるが，マグマ混交を含む広義の用語として一般的なマグマ混合を使用する.

8.1 産状から推定される田上MMEの成因

MMEの成因を考える場合，基本的な議論の立地点はやはりその産状であろう. 野外での産状に即した成因論が重要と考えられる. マグマ混合を考える場合，珪長質マグマ溜まりに下部から貫入してきた塩基性マグマの認定が重要な問題である (Wada *et al.*, 2004；薬師寺ほか，2012). 田上花崗岩体では，塩基性マグマの貫入や存在を示す野外での証拠が今のところ得られていない. 深部までの露出がない岩体全体における表層部分での観察データと考えればその存在を否定はできないが，逆にそれを前提にするには根拠がない.

田上花崗岩体においては，中-粗粒斑状黒雲母花崗岩中と中-粗粒黒雲母花崗岩中のMMEは，ともにほぼ共通の肉眼的特徴を有している. そのうち後者のMMEは，岩体天井部の田上花崗岩体西縁部のペグマタイト地帯に産している. この主岩相でのMMEの産出は，岩体天井部での相対的急冷条件に対応していると考えることができる. 一方，前者のMMEについては次のような整理が可能である. すなわち，中-粗粒斑状黒雲母花崗岩相と中-粗粒黒雲母花崗岩相に年代値的な相違は検出されていない (沢田・板谷，1993；松本ほか，2012) が，中-粗粒斑状黒雲母花崗岩が主岩相の中-粗粒黒雲母花崗岩にたいして一部では貫入しているように見える場合がある (周琵琶湖花崗岩団体研究グループ，2000；中野，2013). また，両岩相の境界部分で中-粗粒斑状黒雲母花崗岩の斑状組織が顕著になり一見斑岩的な岩相になる (中野，2013). 岩相分布の形状も，岩体下部の中心相と考えられる中-粗粒斑状黒雲母花崗岩相 (周琵琶湖花崗岩団体研究グループ，2000) が主岩相である上部の中-粗粒黒雲母花崗岩へ岩脈状 (斑岩的) に貫入しているようにみえる. このような産状は，上記の主岩相における天井部の相対的急冷条件を示す産状と共通的に，固結時に相対的な急冷状態が起こったことを示唆しているように思える. そのような場合，最近では天井部での急冷条件として揮発成分の挙動による過冷却現象がその要因として考えられている (細野・牧野，2002；周琵琶湖花崗岩団体研究グループ，2008；河野ほか，2008) ように，同じく揮発性成分の挙動がMMEの形成に何らかのトリガーの役割を果たした可能性が浮上してくる.

田上岩体中-粗粒斑状黒雲母花崗岩相中でのMMEは，既に述べたように同じ露頭でアプライト及びペグマタイトあるいは黒雲母レイアリング (シュリーレン) と共存している場合が多い. 一方，中-粗粒黒雲母花崗岩中MMEは，アプライト及びペグマタイト，あるいは黒雲母レイアリング (シュリーレン)，また球状花崗岩 (稲垣，1966：竹本ほか，1977；中野，2013) が産出している岩体天井部に産することは既述の通りである. これらの共存は，上記で言及した相対的急冷条件と整合的である. すなわち，アプライト・ペグマタイトの成因に関し

ては最近では揮発性成分が触媒として働いてもたらされた急冷条件下での急速成長を考えるのが支配的である (London, 2005；細野・牧野，2002；河野ほか，2008). ただし，アプライト・ペグマタイトはマグマ固結時の最末期での形成がこれまでの一般的な常識なので，両者の形成時期の関係が今後の問題となる．この観点からは，黒雲母シュリーレンについてもこれまでの成因 (例えば，Kubo, 1976；久保，2000；Pupier et al., 2008) だけでなく，MMEの形成やアプライト・ペグマタイトの形成の問題と関連させて検討する必要があろう．

　マグマからの早期晶出によるMMEの形成が考えられているイランのAligoodarz岩体の場合，浅所マグマ溜まりの境界部の急冷とその後のマグマ中でのそれらの破砕と分散がその具体的モデルとして考えられている (Esna-Ashari et al., 2011)．一方，最近では，それほど組成の違いのない珪長質マグマ同士のマグマ混合過程が"self-mixing"説として提起されている．すなわち，Alves et al. (2009)は，進化したマグマ (珪長質包有岩の母岩) とその下にある初生的なマグマとのマグマ混合を考えて珪長質包有岩の成因を与えた．また，Self-mixing現象の一例として，天井層 (壁層) マグマの剥がれ落ちによる中心相マグマとの相互作用が可能性として考えられている (Dodge and Kistler, 1990；Donaire et al., 2005)．田上花崗岩体でも天井相の細粒−細粒斑状花崗岩と主岩相の中−粗粒花崗岩の野外での複雑な関係が確認されている (周琵琶湖花崗岩団体研究グループ，2000；河野ほか，2008；中野，2013) ので，本MMEの形成過程において上記で議論したような急冷条件を想定する場合，このようなマグマダイナミクスの観点からもMMEの生成を検討する必要がある．

8.2 全岩化学組成からのMMEの成因の検討

　ハーカー図 (第7図) において，本研究でのMMEを含む田上花崗岩体中の岩相変化を通しての一連の組成変化が認められる一方，石原・村上 (2006) の苦鉄質包有岩 (MME) がこれらの変化パターンに合わない異質な存在であることがわかる．マグマ混交では，珪長質マグマと (もとの) 苦鉄質マグマの組成変化は基本的には直線状の経路になるはずであるが，今回の場合直線状の変化経路ではない変化トレンドがいくつかの元素で認められる．これらの変化パターンを，田上岩体全体の岩相変化 (MME⇒中−粗粒斑状黒雲母花崗岩⇒中−粗粒黒雲母花崗岩⇒細粒−細粒斑状花崗岩 (アプライト等を含む)) を通しての花崗岩マグマの分化に対応した結果として考えることが可能であろう．これらの変化パターンは，既に言及した本田上MMEが母岩である中粒斑状黒雲母花崗岩マグマからより早期に形成されたものとの考えとより整合的に思われる．

　田上花崗岩体各岩相のコンドライト規格化REEパターン (第8図) は，やや右上がりのパターンである細粒−細

粒斑状黒雲母花崗岩も含めて，各岩相のREEパターンが全体としてはフラットなパターンに近い特徴を有する点で類似していることを示している．田上花崗岩体中のMMEを含む各岩相のREEパターンが類似していることは，MMEを含めた各岩相の形成を同一マグマからの分化による結晶作用の産物と考えることと矛盾しない．ただし，石原・村上 (2006) のMMEは現時点では例外的な存在である．

8.3 鉱物学的観点からのMMEの形成過程検討

斜長石斑晶の成因

　マグマ混合が起こった場合，珪長質マグマと苦鉄質マグマの遭遇以降は通常の花崗岩マグマと比べると相対的に著しい非平衡条件下での結晶作用が進行する．その結果，珪長質マグマの固結産物と苦鉄質マグマの固結産物の双方で，非平衡結晶作用の記録が長石組織等に記録される (例えば，Baxter and Feely, 2002)．そのような解析の場合，斜長石斑晶が詳しく解析される場合 (例えば，Alves et al., 2009) とアルカリ長石斑晶が詳しく解析される場合 (例えば，Slaby and Gotze, 2004；Slaby et al., 2008) がある．

　田上花崗岩体中の各岩相の斜長石コアのAn含有量は，MMEが最大値を示し，中−粗粒斑状黒雲母花崗岩→中−粗粒黒雲母花崗岩→細粒−細粒斑状花崗岩 (アプライト等を含む) の順で低くなる (第10図)．この変化はマグマの分化に伴って起こったと考えることが可能であり，この考えは既に述べた全岩化学組成やREEパターンにおける議論と整合的である．一方，各MMEに散在する斑晶斜長石の化学組成は，斑晶でない普通のMME構成粒子としての斜長石の組成より，An成分に乏しくAb成分に富んでいる．斑晶斜長石の成因が上記斜長石と同じく早期晶出の結果であるとすると，この化学組成の特徴は一見それとは矛盾する．しかし，斑晶斜長石の組織は，既に述べたように一部ではあるが非常に特徴的なものが認められる．すなわち，大きな斑晶斜長石はブロック状−短冊状斜長石の集合体のように見え，その特徴は特に斑晶周辺部で明瞭である (第11図)．また，内部組織も細かいまだら状 (パッチ状) である．したがって，斑晶斜長石は，次に述べるアルカリ長石の存在とも整合的であるが，短冊状斜長石がマグマ晶出後期段階 (熱水段階) での変質作用 (置換) を受けるのに伴って集合してできた一種の斑状変晶と考えられる．

アルカリ長石の産状と化学組成

　MME中のアルカリ長石はいずれもOr成分に富む端成分に近い組成を示しており，これまで報告のある琵琶湖周辺の花崗岩体中のアルカリ長石の化学組成 (青木，1998；Nakano et al., 2001；周琵琶湖花崗岩団体研究グループ，2005；橋本ほか，2005a, b；河野ほか，2008；Nakano and Makino, 2010) と比較検討して考えると，(マ
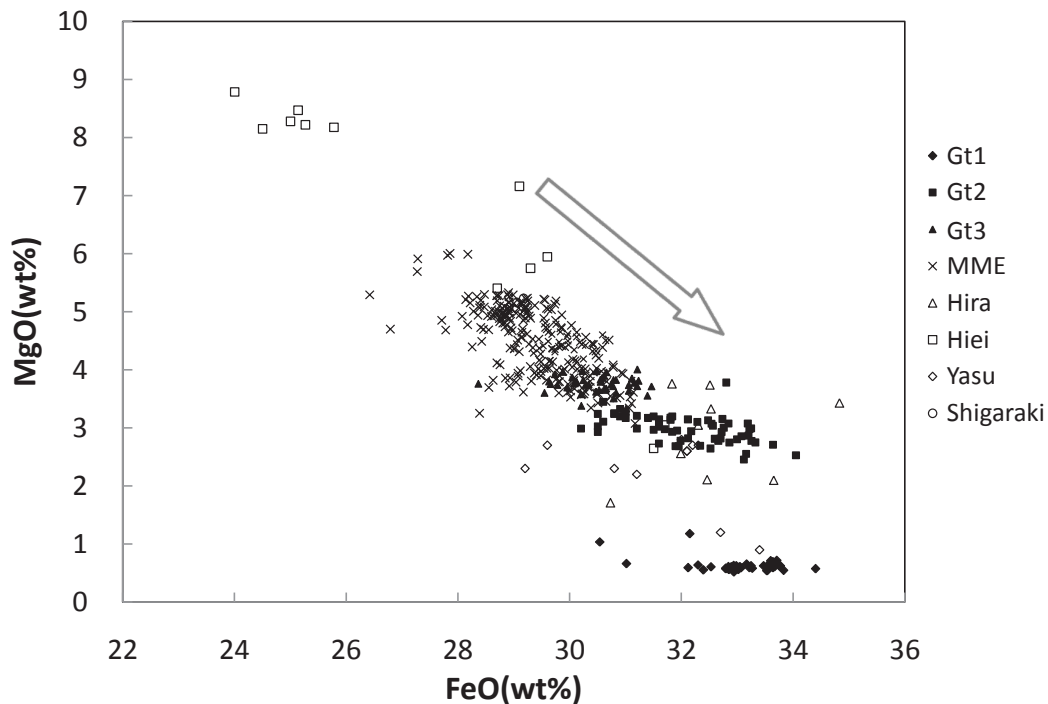
第14図　琵琶湖南半部周辺に分布する花崗岩体中及び田上MME中黒雲母についてのFeO–MgO変化図. 第13図中の黒雲母データに近隣花崗岩体中黒雲母のデータが加えられている. 矢印はマグマ分化に伴って起こると考えられる変化経路を示す.

Fig. 14　FeO-MgO variation diagram for biotites in the granites around the southern half of Lake Biwa. The plotted data consist of the data shown in Fig. 13 and the data of the other nearby granite plutons of Hira, Hiei, Yasu and Shigaraki. An arrow shows a variation trend that is considered to be plausible due to magma differentiation.

グマ後期–) 熱水段階の低温条件での産物とすることができる. MMEアルカリ長石は, 斑晶斜長石を他の石基鉱物とともに特にコア部を置換する産状で出現している. MME中のアルカリ長石は, 斜長石コアを置き換えて (マグマ後期–) 熱水段階で生成したものであり, MME形成とは無関係であろう. なお, 隣接している斜長石とアルカリ長石の組成ペアを使用し, 三成分系2長石温度計 (Fuhrman and Lindsley, 1988；Wen and Nekvasil, 1994) に基づいて2長石の共存温度を見積もると (中–粗粒斑状黒雲母花崗岩と中–粗粒黒雲母花崗岩のアルカリ長石の化学組成はバルク組成を使用), MME, 中–粗粒斑状黒雲母花崗岩, 中–粗粒黒雲母花崗岩の2長石共存温度線 (isotherm) はいずれも約600℃である.

苦鉄質鉱物 (黒雲母) の組成変化

　今回のMME中の主要苦鉄質鉱物として, 角閃石が含まれず基本的には黒雲母のみである点が重要であろう. もし, MME母岩が今回得られたSiO$_2$量 (65 %程度かそれ以下) であれば, 琵琶湖周辺のトーナル岩–花崗閃緑岩に見られるごとく, 角閃石が早期晶出苦鉄質鉱物となるはずと考えられる. 角閃石が皆無である事実は, 本MMEが苦鉄質なマグマからの結晶作用の産物ではなく, 珪長質なマグマからの早期晶出物との考えと整合的にみえる.

　なお, 花崗岩体中の黒雲母の化学組成の特徴として, よりフェルシックな火成岩ほど黒雲母中のMg/Fe比は減少する (周琵琶湖花崗岩団体研究グループ, 2008). 今回の黒雲母組成データ (第13図) に琵琶湖周辺の花崗岩体中の黒雲母の化学組成を加えた変化トレンドを第14図の矢印のように示すことができる. 黒雲母組成から推定されるこの一連の変化トレンドは, 全岩化学組成やREEパターン, 斜長石化学組成からの推定される変化トレンドと整合的であり, 本MMEの成因としての早期晶出説と矛盾しないと考えられる.

9.　要約

　田上花崗岩体を構成する中–粗粒斑状黒雲母花崗岩中のMMEの現在までの産状や岩石学的・鉱物学的データは, 主岩相の中–粗粒黒雲母花崗岩の天井部での同様な産状を考慮した場合, その成因として, 中–粗粒斑状黒雲母花崗岩マグマからの早期晶出相であるとの解釈と現時点でもっとも整合的のようにみえる.

中で進められたものである．第二著者（大橋）は，滋賀大学教育学部卒業研究と教育学研究科修士論文として，主としてEMPAによる解析作業を行った．産業技術総合研究所の竹内圭史氏には，カナダAct Lab社での全岩分析依頼作業をはじめ，図幅関連作業として種々のご助力ご協力をいただいた．主たる薄片製作作業は，産業技術総合研究所・地質標本館・地質試料調製グループの大和田朗・佐藤卓見・福田和幸の各氏におこなっていただいた．この間，周琵琶湖花崗岩団体研究グループの方々及びペグマタイト研究会の方々には，田上花崗岩体とMMEについて種々ご討論をいただき本稿に資する貴重なご教示をいただいた．財津千穂氏（滋賀大学教育学部学生）には，原図の作成及び図表改訂作業に協力をしていただいた．なお，産業技術総合研究所の西岡芳晴氏による大変丁寧な査読の結果多くの貴重なご指摘をいただき原稿が大きく改善された．その際，ノルム計算値の算出に当たり同氏作成のプログラムを使用させていただいた．また，同じく産業技術総合研究所の中野　俊氏と百目鬼洋平氏には，原稿の不備のご指摘をはじめ編集作業全体に渡り大変丁寧なお世話をいただいた．以上の方々に厚く感謝いたします．

文　献

Alves, A., Janasi, V.A., Simonetti, A. and Heaman, L. (2009) Microgranular enclaves as products of self−mixing events：a study of open−system processes in the Maua Granite, Sao Paulo, Brasil, based on in situ isotopic and trace elements in plagioclase. *Jour. Petrol.*, **50**, 2221−2247.

青木映里香 (1998)　Cooling histories of feldspars in the Tanakami and Shigaraki granites from the southeast to Lake Biwa, southwest Japan. 滋賀大学大学院教育学研究科論文集，**1**，62−63.

Barbarin, B. (2005) Mafic magmatic enclaves and mafic rocks associated with some granitoids of the central Sierra Nevada batholith, California：nature, origin, and relations with the hosts. *Lithos*, **80**, 155−177.

Barbarin, B. and Didier, J. (1992) Genesis and evolution of mafic microgranular enclaves through various types of interaction between coexisting felsic and mafic magmas. *Trans. Royal Soc. Edinburgh*：*Earth Sci.*, **83**, 145−153.

琵琶湖基盤地質研究会編 (2001)　琵琶湖のカルデラ形成史の研究．琵琶湖博物館研究調査報告，no.15，120 p.

Baxter, S. and Feely, M. (2002) Magma mixing and mingling textures in granitoids: examples from the Galway Granite, Connemara, Ireland. *Mineral. Petrol.*, **76**, 63−74.

Best, M.G. and Christiansen, E.H. (2001) *Igneous petrology.* Blackwell Sci., 458 p.

Chappell, B.W. (1978) Granitoids from the Moonbi district, New England Batholith, eastern Australia. *Jour. Geol. Soc. Australia*, **25**, 267−283.

Chappell, B.W. (1996) Magma mixing and the production of compositional variations within granite suites：Evidence from the granite of southeastern Australia. *Jour. Petrol.*, **37**, 449−470.

Chappell, B.W., White, A.J.R. and Wyborn, D. (1987) The importance of residual source material (restite) in granite petrogenesis. *Jour. Petrol.*, **28**, 1111−1138.

Czamanske, G.K., Ishihara, S. and Atkin, S.A. (1981) Chemistry of Rock−Forming Minerals of the Cretaceous−Paleocene Batholith in Southwestern Japan and Implications for Magma Genesis. *Jour. Geophys. Res.*, **86**, 10431−10469.

Dahlquist, J.A. (2002) Mafic microgranular enclaves：early crystallization frommetaaluminous magma (Sierra de Chepes), Pampean Ranges, NW Argentina. *Jour. South Amer. Earth Sci.*, **15**, 643−655.

Dodge, F.C.W and Kistler, R.W. (1990) Some additional observations on inclusions in the granitic rocks of the Sierra Nevada. *Jour. Geophys. Res.*, **17**, 841−848.

Donaire, T., Pascual, E., Pin, C. and Duthou, j.-L. (2005) Microgranular enclaves as evidence of rapid cooling in granitoid rocks：the case of the Los Pedroches granodiorite, Iberian Massif, Spain. Contrib. *Mineral. Petrol.*, **149**, 247−265.

Esna−Ashari, A., Hassanzadhe, J. and Valizadeh, M.-V. (2011) Geochemistry of microgranular enclaves in Aligoodarz Jurassic arc pluton, western Iran：implications for enclave generatio by rapd crystallization of cogenetic granitoid magma. *Mineral. Petrol.*, **101**, 195−216.

Fershtater, G.B. and Borodina, N.S. (1977) Petrology of autoliths in granitic rocks. *Inter. Geol. Review*, **19**, 458−468.

Fuhrman, M.L. and Lindsley, D.H. (1988) Ternary feldspar modeling and thermometry. *American Mineralogist*, **73**, 201−215.

橋本　勘・周琵琶湖花崗岩団体研究グループ (2000)　雄琴ボーリングコア花崗岩の記載岩石学．日本地質学会第107年学術大会講演要旨集，163 p.

橋本　勘・赤井純治・中野聰志 (2005a)　田上花こう岩中のアルカリ長石の微細組織とその形成史．岩石鉱物科学，**34**，1−14.

橋本　勘・赤井純治・中野聰志 (2005b)　観音寺花崗閃緑岩中のアルカリ長石の微細組織．地球科学，**59**，117−124.

Hiraoka, Y. (1997) Presumption method for the provenance of weathered products from granites around southern

Lake Biwa, central Japan, based on chemical analysis of biotite. 地質雑, **103**, 1-8.

Hiraoka, Y. (1998) Estimation of the sedimentary source of biotite in the Plio-Pleistocene Osaka Group,Southern Kyoto Prefecture,Japan. Journal of Geosciences,Osaka City University, **41**,1-17.

細野高啓・牧野州明 (2002)　琵琶湖南部，後期白亜紀野洲花崗岩体の岩相変化. 地質雑, **108**, 1-15.

稲垣紘武 (1966)　田ノ上山産花崗岩質球顆岩に就いて. 地学研究，益富記念号，212 p.

石原舜三・村上浩康 (2006)　西南日本花崗岩類のレアアース特性：足摺岬の新第三紀深成岩類と山陽帯の後期白亜紀花崗岩類. 地質調査研究報告, **57**, 89-103.

石原舜三・中野聰志・寺島滋 (2005)　近畿地方田上花崗岩の化学的特性−特に放射性元素と希土類元素の役割−.地質調査研究報告, **56**, 93-98.

角谷安華・河野俊夫・中野聰志・西村彰子・星野美保子 (2012) 滋賀県田上花崗岩体ペグマタイト中のジルコン：産状・形態・組成・化学組成. 地質調査研究報告, **63**, 203-226.

Kocak, K., Zedef, V. and Kansun, G. (2011) Magma mixing/mingling in the Eocene Horoz (Nigde) granitoids, Central southern Turkey：evidence from mafic microgranular enclaves. *Mineral. Petrol.*, **103**, 149-167.

河野俊夫・中野聰志・下村典正 (2008)　滋賀県・田上花崗岩体小ペグマタイト産のマントル長石の形成過程. 地質雑, **114**, 435-446.

Kubo, K. (1976) Layered structure in the basic intrusive mass in the aji islet, Miyagi prefecture, northeast Japan. *Journal of the geological society of Japan*, **82**, 423-440.

久保和也 (2000)　累帯深成岩体の貫入固結過程. 月刊 地球／号外，no.30，153-160.

Le Maitre, R. W. (ed.)(2002) Igneous rocks：A classification and glossary of terms, 2nd edition. Recommendations of the International Union of Geological Sciences, Subcommission of the Systematics of Igneous Rocks, Cambridge University Press, 236 p.

London, D. (2005) Granitic pegmatites：an assessment of current concepts and directions for the future. *Lithos*, **80**, 281-303.

松本哲一・中村仁美・廣田明成・星住英夫・高橋　浩・中野　俊・中野聰志 (2012)　日本列島における年代未詳岩石のK-Ar年代測定 −地質図幅作成地域の火山岩・深成岩 (平成23年度版)−. 地質調査研究報告, **63**, 291-300.

中野聰志 (2013)　京都東南部地域の地質，第4章　白亜紀火成岩類，地域地質研究報告 (5万分の1地質図幅). 産総研地質調査総合センター.

Nakano, S. and Makino, K. (2010) Amazonitic alkali feldspar

from the Tanakami Granitic pegmatites, southwest Japan. Jour. Mineral. Petrol. Sci., 105, 45-56.

Nakano, S., Makino, K. and Eriguchi, T. (2001) Microtexture and water content of alkali feldspar by Fourier−transform infrared microspectrometry. Mineral. Mag., 65, 675-683.

中野聰志・吉見典浩・冨田克敏 (2006)　田上花崗岩体中の熱水変質. 滋賀大教育紀要 (自然), 56, 35-49.

中野聰志・川辺孝幸・原山智・水野清秀・高木哲一・小村良二・木村克己 (2003)　水口地域の地質.地質調査総合センター，83 p.

西堀　剛・西川一雄・小早川　隆・但馬達夫・岨中貴洋 (1991)　湖東流紋岩類. 滋賀県自然誌編集委員会編，滋賀県自然誌，滋賀県自然保護財団，387-422.

西川一雄・西堀　剛・小早川　隆・但馬達夫・辻　一信・佐藤義成 (1979)　湖東流紋岩類. 滋賀自然環境研究会編，滋賀県の自然　総合学術調査研究報告，滋賀県自然保護財団，387-422.

西川一雄・西堀　剛・小早川　隆・但馬達夫・上嶋正人・三村弘二・片山正人 (1983)　湖東流紋岩およびその活動について. 岩鉱, **77**, 51-64.

大林達生 (2002)　田上地方のペグマタイト鉱物−日本のペグマタイト産地　その1−. 中津川市鉱物博物館，20 p.

Perugini, D., Poli, G., Christofides, G. and Eleftheriadis, G. (2003) Magma mixing in the Sithonia Plutonic Complex, Greece：evidence from mafic microgranular enclaves. *Mineral. Petrol.*, **78**, 173-200.

Platevoet, B. and Bonin, B. (1991) Enclaves and mafic−felsic associations in the Permian alkaline province of Corsica, France：physical and chemical interactions between coeval magmas. In Didier, J., Barbarin, B. (eds.) Enclaves and granite petrology, developments in petrology 13. Elsevier, Amsterdam, 191-204.

Pupier, E., Barney, P., Toplis, M.J. and Bussy, F. (2008) Igneous layering, fractional crystallization and growth of granitic plutons：the Dolbel Batholith in SW Niger. *Jour. Petrol.*, **49**, 1043-1068.

Rakovan, J., Ono, M. and Francis, C.A. (2009) Tanakamiyama. *Rocks & minerals*, **84**, 520-527.

沢田順弘・板谷徹丸(1993)　琵琶湖南部後期白亜紀環状花崗岩質岩体のK-Ar年代−巨大コールドロンにおける冷却史−. 地質雑, **99**, 975-990.

沢田順弘・加々美寛雄・松本一郎・杉井完治・中野聰志・周琵琶湖花崗岩団体研究グループ (1994)　琵琶湖南部白亜紀環状花崗岩質岩体と湖東コールドロン. 地質雑, **100**, 217-233.

Sergi, A. (1997) Mafic microgranular enclaves from the Xanthi plton(Northern Greece)：an example of mafic−felsic magma interaction. *Mineral. Petrol.*, **61**, 97-117.

Shin, Ki−C., Kurosawa, M., Anma, R. and Nakano, T. (2009) genesis and mixing/mingling of mafic and felsic magmas of bacK-Arc granite：Miocene Tsushima Pluton, southwest Japan. *Resour. Geol*., **59**, 25−50.

Slaby, E. and Gotze, J. (2004) Feldspar crystallization under magma−mixing conditions shown by cathode luminescence and geochemical modeling−a case study from the Karkonosze pluton (SW Poland). *Mineral. Mag*., **68**, 561−577.

Slaby, E., Gotze, J., Gerhard Worner, Klaus Simon, Roman Wrzalik, Michal Smigielski (2008) K−feldspar phenocrysts in microgranular magmatic enclaves：A cathode luminescence and geochemical study of crystal growth as a marker of magma mingling dynamics. *Lithos*, **105**, 85−97.

周琵琶湖花崗岩団体研究グループ (1982)　琵琶湖周辺の花崗岩質岩体-甲賀地方の花崗岩類-. 地質雑, **88**, 289−298.

周琵琶湖花崗岩団体研究グループ (1997)　琵琶湖周辺の花こう岩質岩体−その4. 比良山地の花こう岩類. 地球科学, **51**, 188−198.

周琵琶湖花崗岩団体研究グループ (2000)　琵琶湖周辺の花こう岩質岩体−その5. 田上地域の花こう岩類. 地球科学, **59**, 380−392.

周琵琶湖花崗岩団体研究グループ (2005)　琵琶湖周辺の花こう岩質岩体-その6. 野洲花こう岩. 地球科学, **59**, 89−102.

周琵琶湖花崗岩団体研究グループ (2008)　比叡花崗岩体の形成史と白亜紀化成活動史における位置づけ. 地質雑, **114**, 53−69.

Sun, S.−s. and McDonough, W.F. (1989) Chemical and isotopic systematics of oceanic basalts: implications for mantle composition and processes. *In* Saunders, A.D. and Norry, M.J., eds., *Magmatism in the ocean basins* (Spec. Publ. Vol. Geol. Soc. Lond., no.42), 313−345.

杉井完治・沢田順弘 (1999)　琵琶湖北東部，後期白亜紀貝月山花崗岩体. 島根大学地球資源環境学研報, **18**, 69−84.

Takagi, T. (1992) Mineral equilibria and crystallization conditions of Ukan Granodiorite (ilmenite−series) and Kayo Granite (magnetite−series), San'yo Belt, Southwest Japan. *Jour. Geol. Soc. Japan*, **98**, 101−124.

竹本健一・吉田源市・中野聰志 (1977)　滋賀県大津市田上山における球顆花崗岩の新露頭の発見. 地球科学, **31**, 130−131.

Tsusue, A. (1973) The distribution of manganese and iron between ilmenite and granitic magma in the Osumi Peninsula, Japan. Contrib. *Mineral. Petrol*., **40**, 305−314.

Tsusue, A. and Ishihara, S. (1974) The iron−titanium oxides in the granitic rocks of Southwest Japan. *Mining Geol*., **24**, 13−30. (in Japanese with English abstract)

Vernon, R.H. (1984) Microgranitoid enclaves：Globules of hybrid magma quenched in a plutonic environment. *Nature*, **304**, 438−439.

Vernon, R.H. (1990) Crystallization and hybridism in microgranitoid enclave magmas：microstructural evidence. Jour. *Geophsy. Res*., **95**, 849−859.

Wada, H., Harayama, S. and Yamaguchi, Y. (2004) Mafuc enclaves densely concentrated in the upper part of a vertically zoned felsic magma chamber：The Kurobegawa granitic pluton, Hida Mountain Range, central Japan. *Geol. Soc. Amer. Bull*., **116**, 788−801.

Wen, S. and Nekvasil, H. (1994) Solvcalc：an interactive graphics program package for calculating the ternary feldspar solvus and for two−feldspar geothermometry. *Computer & Geosciences*, **20**, 1025−1040.

White, A.J.R. and Chappell, B.W. (1977) Ultrametamorphism and granitoid genesis. *Tectnophys*., **43**, 7−22.

Wiebe, R.A., Smith, D., Strum, M., King, E.M. and Seckler, M.S. (1997) Enclaves in the Cadillac Mountain Granite (Coastal Maine)：samples of hybrid magma from the Base of the Chamber. *Jour. Petrol*., **38**, 393−423.

薬師寺亜衣・亀井淳志・柴田知之 (2012)　山陰帯島根県尾原に分布する混成岩および優白質花崗岩の火成活動. 地質雑, **118**, 20−38.

Article

Distribution of some ore metals around
the Mau Due stibnite deposits, northernmost Vietnam

Shunso Ishihara[1, *] and Pham Tich Xuan[2]

Shunso Ishihara and Pham Tich Xuan (2013) Distribution of some ore metals around the Mau Due stibnite deposits, northernmost Vietnam. *Bull. Geol. Surv. Japan*, vol. 64 (1/2), p. 51-57, 4 figures, 3 tables.

Abstract: Soil and stream sediments were studied geochemically around the Mau Due ore deposits of the northernmost Vietnam. The ore deposits are fracture-filling type occurring in Devonian sediments composed mainly of impure calcareous sediments. The chemical elements brought up by the mineralizations are mainly S and Sb, and small amount of As and base metal. The analyzed surface samples were collected in the wet season (May to September) and the dry season (October to April).

Sb contents of surface materials are sporadically high in the soil samples, and have smaller variation in the stream sediments than in the soil samples. Sb contents of the soil of the wet season, 932 ppm Sb in the average, are higher than the average of 342 ppm Sb of the dry season. The Sb contents are much higher in the stream sediments, averaged as 2,536 ppm in the wet season and 2,504 ppm in the dry season.

Generally speaking, As contents of the soil are positively correlated with Sb contents, but the amounts are much lower than the Sb contents, averaged as 29 and 26 ppm in soil of the wet and dry seasons, respectively, but higher as 68 and 67 ppm in the stream sediments. These abundance data of Sb and As are best explained by both elements are present finest grained sulfides in the soil and river sediments. The Devonian host rocks may be originally high in the Sb contents, as compared with the Japanese eugeosynclinal sediments.

Keywords: Mau Due mine, stibnite, heavy metals, pollution, Vietnam

1. Introduction

Antimony is concentrated in many hydrothermal ore deposits of simple stibnite type and complex sulfide-sulphosalts type, and its production is heavily dependent upon the stibnite type in sedimentary terrain in the Xikuangshan area, Hunan province of China, which produces 83-90 % of the world production in the past five years (Ishihara and Ohno, 2011). The element is considered as a good geochemical marker for antimony ore deposits, particularly of the sulfide-sulphosalt type (Boyle and Jonasson, 1984).

Soils and stream sediments around given antimony ore deposit have been polluted by the ore metals, especially of antimony and arsenic (Flynn *et al.*, 2003; Murciego *et al.*, 2007).

In one case of mesothermal antimony deposits, the stibnite can contain up to 5,000 ppm As. Together with common occurrence of arsenopyrite and arsenian pyrite, dissolution of these minerals causes strong contamination of antimony and arsenic into the soil, stream sediments and plants of the antimony mining area (Ashley *et al.*, 2003; Murciego *et al.*, 2007).

In the largest mineralized area of the Hunan province, Wang *et al.* (2010) examined 10 heavy metals (Sb, As, Cd, Cr, Cu, Hg, Mn, Ni, Pb and Zn) of the surrounding agriculture soils in the mining region, and found that the strongest contamination on Sb (236 times), Cd (52 times), Hg (14 times), and As (3.1 times), Zn (2.9 times) and Pb (2.5 times), in which cadmium concentration is rather unusual.

In this paper, reconnaissance geochemical work has been done around the Mau Due stibnite mine area. This mine is located at a part of mountainous region, 300 to 1,000 m above sea level, in the northernmost part of Vietnam (N23°04′24″, E105°15′10″, Fig. 1), and are very close to the In-bearing Sn-Pb-Zn deposits of Du Long mine, China (Ishihara *et al.*, 2011). The Mae Due mine area is composed of two distinct seasons; wet and hot summer, and dry and cool winter. Average rainfall is 1200 to 1800 mm in a year, in which majority (73-81%) falls in the rainy season of May to September.

[1]AIST, Geological Survey of Japan

[2]Institute of Geological Sciences, Vietnamese Academy of Science and Technology, Hanoi, Vietnam.

*Corresponding author: S. ISHIHARA, Central 7, 1-1-1 Higashi, Tsukuba, Ibaraki 305-8567, Japan. Email: s-ishihara@aist.go.jp
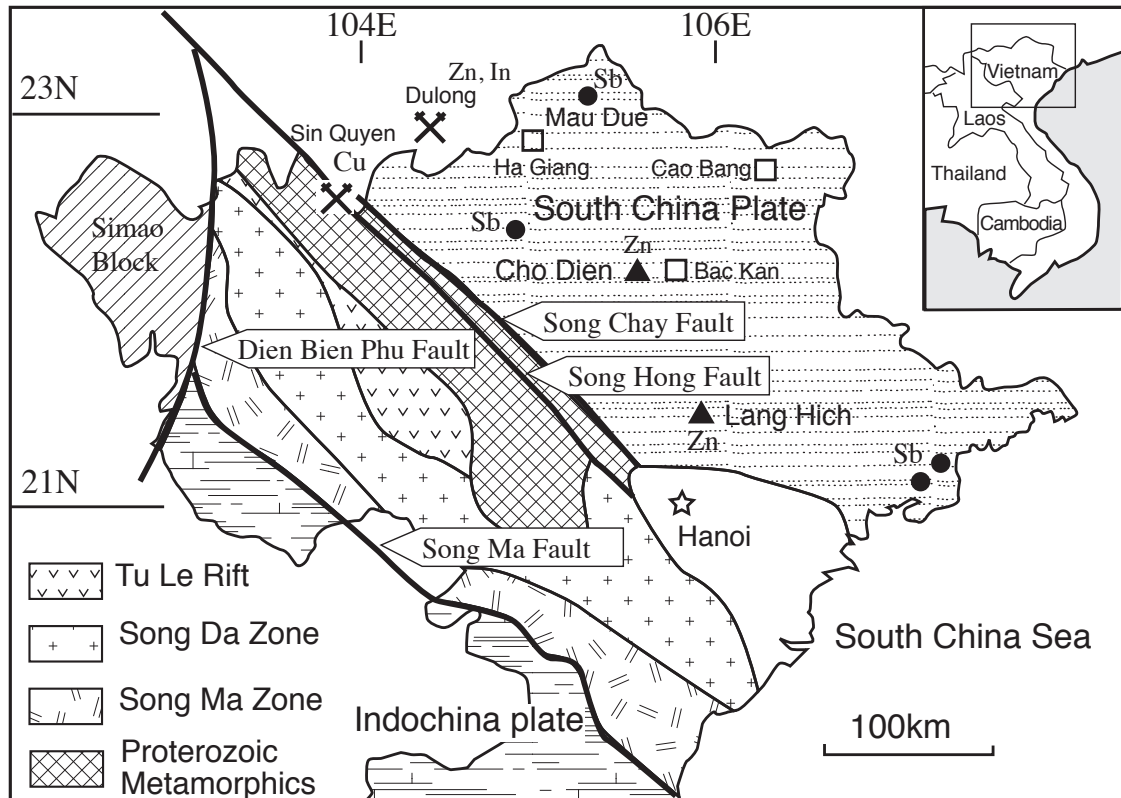
Fig. 1 Index map for the Mau Due mine occurring in the sedimentary terrain of the South China plate.

2. Geological background

Northeastern side of the Red River Fault in the northern Vietnam is essentially Paleozoic-Mesozoic sedimentary terrain intruded by Mesozoic granitoids. Small fracture filling-type antimony deposits are known at Lang Vai mine of the central part (500 tons Sb metal, 1986-1992), and Khe Chim, Duong Huy, and Dong Mo localities. In the northernmost part of Ha Giang province, an open pit mining was initiated in 1993 and is called Mau Due mine. A refinery was set up in 2002, and the mine produces annually 100 tons Sb metal since then.

This mine area is underlain by the Devonian Na Quan Formation (D1-2nq) of about 500 m thick, consisting of limestone alternated with carbonaceous shale and black shales (Tran Xuyen, 2001). The limestone is usually dolomitized. Other Devonian strata of the Toc Tat Formation (D3tt) comprise fine-layered silicic limestone alternated with silicic shale, shale, and carbonaceous shale. The thickness is about 300 m.

The Song Hien Formation (T1sh) is most widely distributed in the mine area. It is composed of sandstone, black shale and sericitic shale. The thickness is about 300 m. Quaternary sediments (Q) are distributed along the Nam Tam river, and are composed of pebbles, sand and clay.

3. Mineralization at Mae Due mine

Devonian sediments of the Na Quan Formation (D1-2nq) which have been folded with NNE-SSW axes and cut by the same NNE-SSW faults, host the stibnite deposits. The stibnite mineralizations are seen along the NNE-SSW structures, and are divided into three orebodies as I, II and III from the west to east.

The orebody I is 350 m long with the width of 3.7 m and dip of 70°W, and average grade of 10.3 % Sb. The orebody II is 410 m long, 10.1 m wide dipping 40-70° west. The average grade is 11.2 % Sb. The orebody III is 200 m long, 4.1 m wide, dipping 70° east. The average grade is 13.6 % Sb. These orebodies are mostly composed of quartz (20-70 %) and small amounts of calcite. The ore minerals are stibnite, and very small amounts of pyrite, arsenopyrite, sphalerite and berthierite. At the top of the orebodies, such secondary minerals as valetinite and lewisite may occur together with limonite.

Some ore components are analyzed for total carbon and sulfur by infrared method, and Fe, Sb, As, Se, Mo, Cu, Pb, Zn, Cd, Bi, Mn, Co, and Ni by ICP-MS methods on the ores and wastes of the Mau Due mine, and the results are listed in Table 1. The antimony ores only dominant in Sb, S, and Se, while other ore elements such As, Cu, Pb, Zn, Ni, Co, and Mo are rich in the wastes, implying that these elements are marginal

Table 1　Selected ore components of the ores and wastes of the Mau Due mine.

No.	Sample no. & samples	Al	Fe	Total S	Total C	Sb	As	Se	Mo	Cu	Pb	Zn	Cd	Bi	Co	Ni	Mn
	Detection limit	0.01%	0.01%	0.01%	0.01%	0.1	0.1	0.1	0.2	0.2	0.5	0.2	0.1	0.02	0.1	0.5	1
102	MD2-Q1, Sb ore, dry	0.44	0.02	28.00	0.65	176,000	17.5	153	1.5	3.9	< 0.5	4.2	0.7	0.09	< 0.1	0.8	3
103	MD2-Q2. Sb ore, dry	1.11	0.05	23,70	0.25	154,000	16.8	115	< 0.1	2.8	< 0.5	4.1	0.8	0.1	< 0.1	0.5	5
	Average(n=2)	0.78	0.04	25.85	0.45	165,000	17.2	134	0.8	3.4	<0.5	4.2	0.8	0.1	<0.1	0.7	4
104	MD2-BT1, waste, dry	>10	5.45	2.03	2.44	232	73.3	9.2	9.7	96.1	40.4	321	2.2	0.75	21.1	99.4	873
105	MD2-BT2, waste, dry	6.03	2.86	0.04	0.08	47.2	20.1	1.9	1.7	54.9	35.3	77.5	0.5	0.41	24.9	41.9	992
106	MD2-BT3, waste, dry	8.16	9.17	1.32	19.6	1200	18.8	4.7	24.4	118.0	7.3	33.4	< 0.1	0.07	45	123	421
107	MD2-BT4, waste, dry	6.09	10.6	1.37	12.9	13500	4.7	4.8	2.4	123.0	11.2	54.7	0.2	0.2	59.4	185	317
99	MD-BT6, waste, wet	7.44	3.68	0.04	2.58	43.7	22.1	2.5	4.0	60.1	28.6	125	0.2	0.52	9.4	35.4	299
101	MD-BT7, waste, wet	6.69	4.21	0.03	1.09	7.1	32.9	3.9	5.4	62.0	26.0	73.1	< 0.1	0.6	3.6	26.8	167
100	MD-BT8, waste, wet	6.19	3.19	0.37	1.39	148	46.5	6.3	6.2	45.6	21.5	80.5	0.3	0.41	4.3	37.7	303
	Average(n=7)	7.23	5.6	0.74	5.73	2,168	31.2	4.8	7.7	80.0	24.3	109	0.5	0.42	24	78.5	482

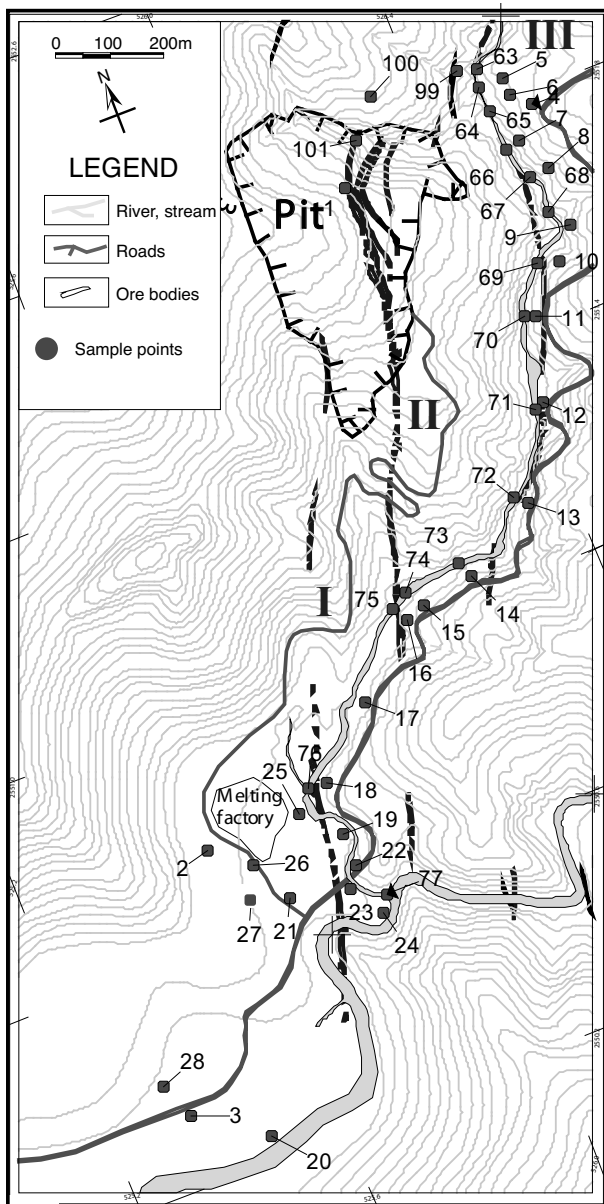* Analytical unit is ppm, unless otherwise noted.

Fig. 2 Locality map of soils and stream sediments in the wet season.
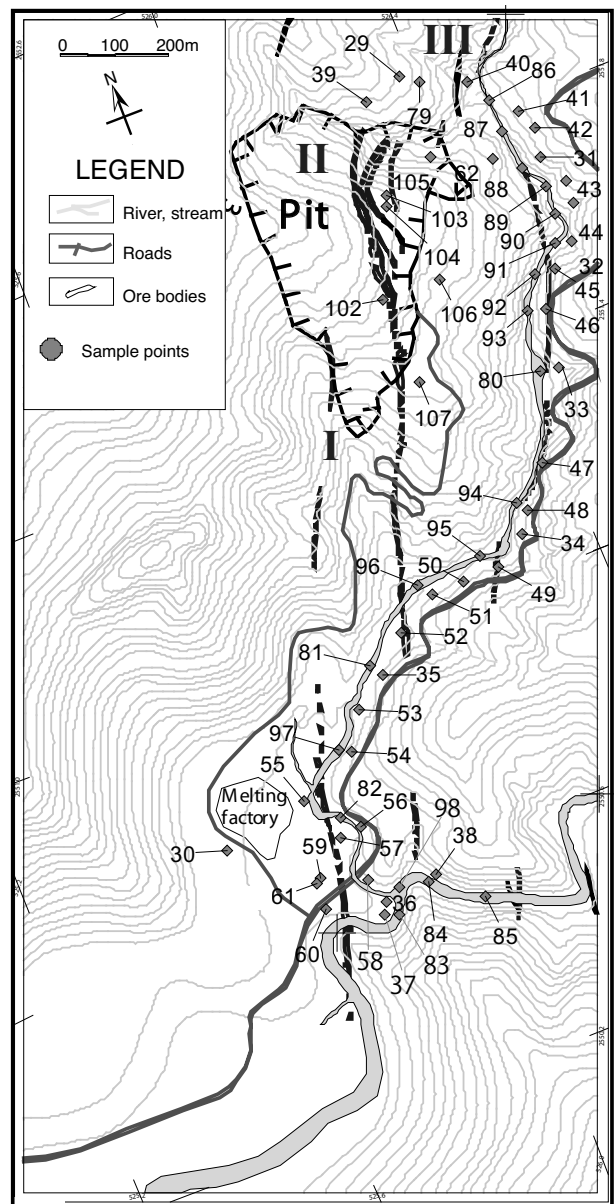

Fig. 3 Locality map of soils and stream sediments in the dry season.

Table 2   Selected ore components of the soil samples of the wet and dry seasons.

Sample no		Ai	Fe	Sb	As	Se	Mo	Cu	Pb	Zn	Cd	Bi	Co	Ni	Mn
1	MD-D1 wet	>10	3.69	2700	31.7	2.3	3.8	42.9	34.6	63.5	0.2	0.6	3.2	24.9	96
2	MD-D4	>10	6.44	49	61.7	2.9	4.1	71.8	94.9	224	0.5	1.0	30.8	77.5	3160
3	MD-D5	6.66	3.37	28	32.1	1.3	4.1	60.6	43.2	225	0.5	0.6	15.7	49.1	2000
4	MD-D6	8.29	3.73	19	24.3	2.6	3.4	53.4	25.4	136	0.1	0.5	3.3	27.5	266
5	MD-D7	2.91	2.60	393	21.5	2.1	3.6	34.2	27.5	67	0.2	0.4	4.0	21.8	188
6	MD-D8	4.59	3.55	10	17.2	1.9	3.5	48.9	27.1	84.8	0.1	0.4	12.0	30.7	488
7	MD-D9	9.40	4.71	13	17.8	2.9	5.2	75.2	35.0	123	0.2	0.6	20.9	38.1	936
8	MD-D10	>10	4.92	100	24.1	3.6	6.3	104	34.6	201	0.2	0.7	26.7	55.5	2560
9	MD-D11	8.23	4.22	7300	13.8	3.4	1.2	72.1	37.2	148	0.5	0.6	20.9	44.1	1590
10	MD-D12	7.50	3.79	1100	22.0	3.5	3.6	58.8	37.3	113	0.4	0.5	28.3	44.6	1340
11	MD-D13	7.18	3.47	5500	23.0	4.1	1.8	89.5	34.9	159	1.2	0.5	26.9	70.5	1350
12	MD-D14	0.07	4.57	90	21.0	2.9	6.0	101	33.1	147	0.2	0.6	23.3	48.6	2060
13	MD-D15	8.38	4.10	7600	11.7	2.2	1.0	71	33.2	105	0.3	0.5	24.2	44.7	1130
14	MD-D16	3.15	2.52	50	11.1	3.6	5.5	87.3	31.9	115	0.4	0.4	26.4	54.0	1360
15	MD-D17	6.90	4.48	261	30.5	9.0	9.1	103	31.2	114	0.3	0.5	33.2	44.3	1130
16	MD-D18	7.51	3.51	41	47.3	2.3	21.0	74.7	31.2	132	0.3	0.5	13.8	79.7	331
17	MD-D19	>10	3.74	3	9.3	2.8	3.2	74.7	28.6	64.7	0.2	0.6	22.9	55.1	457
18	MD-D20	8.12	3.97	80	29.8	2.8	2.2	54.9	54.6	335	3.0	0.6	45.2	106.0	2240
19	MD-D21	>10	4.26	45	34.7	2.0	2.5	50.9	44.5	123	0.3	0.6	20.0	37.9	921
20	MD-D22	6.54	3.03	1	6.8	1.5	< 0.1	46	28.8	121	0.4	0.4	15.7	43.8	677
21	MD-D23	>10	6.67	33	49.5	1.6	2.1	76.5	69.5	211	0.4	0.9	23.5	65.6	1240
22	MD-D24	>10	7.28	9	80.1	2.4	6.6	73.9	68.7	231	0.9	1.0	30.8	103.0	3670
23	MD-D25	7.70	4.06	6	24.6	2.1	3.2	58	35.2	148	0.3	0.5	22.8	56.2	908
24	MD-D26	2.87	2.76	19	10.2	1.6	2.3	41.3	23.0	105	0.4	0.3	14.1	44.3	790
25	MD-D27	6.67	3.52	26	23.5	2.0	1.7	43.6	47.3	183	1.3	0.6	22.9	67.7	1200
26	MD-D28	8.18	4.20	239	28.6	1.9	1.2	50.1	73.8	175	0.5	0.7	19.9	47.0	1550
27	MD-D29	>10	5.55	81	45.3	1.8	4.4	62.4	87.6	192	0.3	0.9	27.1	60.3	2350
28	MD-D30	> 10	5.26	46	59.9	1.5	6.7	58.5	52.1	216	0.2	0.8	21.2	46.0	2060
	Average	>7.53	4.21	923	29.0	2.7	4.3	65.7	43.1	152	0.5	2.5	21.4	53.3	1359
29	MD2-D1, dry	4.15	4.35	24	32.7	3.8	7.0	68.2	26.2	86.6	< 0.1	0.7	4.0	29.1	187
39	MD2-D2	8.01	3.59	113	47.1	3.4	7.1	52	30.2	60.5	0.1	0.8	2.2	21.8	127
30	MD2-D3	>10	6.02	22	31.9	1.6	1.8	73.9	82.0	201	0.2	0.9	27.3	61.0	2300
40	MD2-D4	7.35	3.17	44	21.8	2.6	4.7	56.1	32.1	99.9	0.3	0.5	3.9	27.3	128
41	MD2-D5	>10	4.07	12	25.1	3.9	7.6	53.7	38.3	86.1	< 0.1	0.6	16.0	34.3	439
42	MD2-D6	>10	5.24	10	23.3	3.0	6.3	76.2	34.0	109	0.3	0.6	39.1	49.4	1080
31	MD2-D7	>10	3.27	15	16.2	2.3	6.7	46.7	49.9	113	0.2	0.6	26.2	38.1	780
43	MD2-D8	2.46	3.58	147	15.5	2.0	4.2	89.9	34.4	166	0.4	0.5	29.1	44.9	2370
44	MD2-D9	6.84	4.49	469	15.3	3.5	3.5	82	37.6	125	0.2	0.6	38.7	37.7	2340
32	MD2-D10	8.18	5.04	3300	24.3	3.3	4.3	84.2	37.2	133	0.3	0.6	20.8	44.1	989
45	MD2-D11	7.79	3.68	4700	17.5	2.8	2.8	66.6	32.1	118	0.5	0.5	18.1	51.5	692
46	MD2-D12	>10	4.34	200	35.8	1.6	4.0	36.3	56.0	139	0.5	0.7	18.4	46.9	1720
33	MD2-D13	7.46	4.59	61	23.9	2.9	1.2	67.6	36.2	190	0.5	0.6	24.9	58.3	1610
47	MD2-D14	8.26	3.70	23	18.5	3.5	6.6	70	33.8	88.4	0.3	0.6	15.1	43.2	1050
48	MD2-D15	>10	4.94	187	18.4	4.4	9.1	136	50.2	269	1.7	0.7	67.9	169.0	4010
34	MD2-D16	8.09	3.29	85	16.4	5.8	5.1	84.4	32.6	140	0.6	0.8	26.2	60.6	1650
49	MD2-D17	9.78	5.61	19	18.7	2.2	3.9	62.6	25.6	86.7	< 0.1	0.6	4.9	36.0	185
50	MD2-D18	5.96	4.12	15	13.6	2.0	4.3	57.9	30.7	58.6	< 0.1	0.5	5.9	37.8	161
51	MD2-D19	4.11	2.78	33	47.8	2.1	7.2	78.1	32.3	145	0.5	0.5	21.3	68.0	1680
52	MD2-D20	6.89	3.19	89	42.8	2.1	15.1	69.5	31.2	141	0.3	0.5	19.3	68.2	867
35	MD2-D21	6.58	3.58	13	48.7	2.2	16.3	93.5	32.4	162	0.5	0.6	18.2	41.8	871
53	MD2-D22	8.19	3.77	96	32.3	3.8	1.7	87.2	41.4	213	2.2	0.8	24.7	76.7	1470
54	MD2-D23	6.36	3.06	29	19.9	1.2	4.7	38.6	33.4	82.8	0.4	0.3	18.4	48.0	1820
55	MD2-D24	>10	3.84	65	18.4	3.9	8.2	66.7	42.5	109	0.2	0.8	24.6	45.7	1580
56	MD2-D25	8.27	4.53	42	22.9	2.2	4.2	54	33.4	123	0.3	0.5	27.0	43.9	1020
57	MD2-D26	7.78	3.59	132	25.7	2.2	1.3	50.9	41.6	139	0.7	0.5	17.8	48.1	1130
58	MD2-D27	7.72	3.77	27	17.2	2.0	5.6	42.1	38.5	115	0.2	0.5	11.4	30.4	452
36	MD2-D28	6.00	2.94	17	13.3	1.7	1.1	40.1	34.6	106	0.5	0.4	15.5	41.7	1290
37	MD2-D29	2.78	3.21	27	13.6	1.3	2.8	51.1	25.7	105	0.4	0.4	18.2	45.8	1560
38	MD2-D30	6.78	3.45	35	23.3	2.1	3.2	54.8	37.6	158	0.5	0.5	19.6	45.6	1340
61	MD3-D8	6.03	20.20	1200	55.0	17.2	10.7	110	25.4	1360	3.0	0.2	30.1	121.0	873
59	MD3-D11	7.10	2.94	22	14.7	1.6	1.7	45.8	69.4	177	0.8	0.6	22.9	58.3	1080
62	MD3-D14	6.60	3.36	4	12.6	1.7	1.7	47.5	75.7	133	0.5	0.5	16.1	42.3	711
	Average	>7.44	4.40	342	25.0	3.1	5.3	66.5	39.2	168	0.5	0.6	21.0	52.0	1199

Table 3   Selected ore components of the stream sediment samples of the wet and dry seasons.

Sample Nos.	Al	Fe	Sb	As	Se	Mo	Cu	Pb	Zn	Cd	Bi	Co	Ni	Mn
63 MD-TT1, wet	9.27	4.52	13	33.9	2.4	4.1	81	28.8	146	0.2	0.5	20.9	55.3	690
64 MD-TT4	>10.0	4.37	344	69.2	7.0	4.9	133	61.3	466	3.2	0.6	33.7	154.0	1740
65 MD-TT5	8.29	4.22	336	77.1	6.3	5.5	102	54.6	340	2.3	0.5	22.0	117.0	1330
66 MD-TT6	9.03	4.53	4000	86.2	7.6	10.7	92.7	44.2	264	2.2	0.5	31.3	129.0	1860
67 MD-TT7	9.20	4.42	4200	88.0	9.9	16.6	101	45.8	252	2.1	0.5	19.8	108.0	1100
68 MD-TT8	6.24	3.87	3400	73.6	6.4	7.2	105	47.9	322	2.3	0.5	28.2	123.0	1500
69 MD-TT9	7.68	4.22	3700	76.3	7.7	11.7	100	38.4	331	2.3	0.4	27.4	126.0	1420
70 MD-TT10	9.86	4.25	3700	76.0	6.5	12.8	98	53.0	274	2.2	0.5	27.6	120.0	1810
71 MD-TT11	8.52	4.22	4100	70.2	6.8	9.5	101	43.1	282	2.3	0.5	27.7	121.0	1520
72 MD-TT12	9.20	4.22	3800	68.8	6.4	7.0	105	50.1	343	2.2	0.5	27.7	126.0	1640
73 MD-TT13	9.40	4.39	3300	76.3	6.2	12.4	114	51.7	411	2.0	0.6	30.9	129.0	1370
74 MD-TT14	9.21	4.39	3200	70.3	7.3	11.7	119	56.0	460	2.7	0.6	35.0	157.0	1640
75 MD-TT15	>10.0	4.53	3400	73.8	6.1	11.8	98.3	47.7	261	1.6	0.6	25.6	107.0	1520
76 MD-TT16	9.37	4.34	215	21.6	5.4	0.3	68.6	78.4	214	1.6	0.7	27.6	78.6	2360
77 MD-TT17	6.29	3.92	337	60.7	6.3	5.3	91.4	35.2	324	2.9	0.5	35.9	138.0	1300
Average	>8.58	4.29	2536	68.1	6.6	8.8	100.7	49.1	313	2.1	0.5	28.1	119.0	1520
78 MD2-TT1, dry	1.90	4.62	456	91.6	7.3	8.6	66.4	33.4	92.1	0.4	0.6	4.0	44.3	250
85 MD2-TT2	7.53	5.71	1800	74.3	4.2	22.4	155	63.2	537	2.2	0.6	38.3	153.0	1960
86 MD2-TT3	7.34	4.25	11900	90.6	10.6	7.6	95.1	48.4	221	2.4	0.7	18.8	97.7	1060
87 MD2-TT4	8.76	6.83	2000	70.0	6.9	19.9	86.5	48.4	232	1.0	0.5	18.3	93.6	1070
88 MD2-TT5	7.86	5.13	2500	71.8	5.5	19.6	91.1	54.7	219	1.4	0.5	22.2	91.9	1350
89 MD2-TT6	8.03	6.30	2600	76.8	6.3	16.8	65.4	46.4	200	1.0	0.6	14.8	74.1	854
90 MD2-TT7	7.78	4.59	3500	78.4	6.7	17.3	86	112.0	208	1.4	0.5	26.1	102.0	1500
91 MD2-TT8	8.41	6.44	2600	72.4	6.8	16.6	78.3	44.7	240	1.3	0.5	19.8	92.5	1180
92 MD2-TT9	6.89	4.15	3300	71.1	6.0	12.7	95.4	50.3	205	1.4	0.5	21.7	101.0	1220
79 MD2-TT10	9.95	4.93	2600	84.0	5.9	22.3	127	76.0	287	1.4	0.7	25.3	128.0	1890
93 MD2-TT11	2.61	3.41	3300	75.6	4.9	19.5	85.4	55.8	217	1.3	0.4	22.2	88.4	792
94 MD2-TT12	4.15	3.92	3500	76.1	5.8	13.0	81	39.2	234	1.9	0.5	28.0	104.0	1320
95 MD2-TT13	9.80	4.99	2800	81.9	5.7	25.6	112	70.1	271	1.1	0.7	22.0	112.0	1800
90 MD2-TT14	8.94	9.56	2300	72.8	7.2	17.5	103	48.8	536	1.5	0.6	41.7	138.0	1050
96 MD2-TT15	7.52	4.26	2600	74.7	5.7	19.8	109	53.2	308	1.8	0.5	33.2	125.0	1700
81 MD2-TT16	7.28	6.23	2300	64.4	5.3	10.7	93.2	47.6	738	3.2	0.5	52.7	142.0	1440
97 MD2-TT17	8.25	7.40	2200	65.3	6.6	12.7	95.2	48.7	979	4.4	0.5	95.6	214.0	2020
82 MD2-TT18	4.16	2.08	16.4	13.5	0.9	0.7	22.1	23.5	64.1	0.2	0.3	9.6	23.9	682
83 MD2-TT19	6.01	2.75	135	21.3	1.7	2.7	35.5	31.1	145	0.7	0.4	16.8	41.7	774
84 MD2-TT20	4.68	2.44	78.9	16.3	1.7	2.1	33.9	24.0	159	0.7	0.3	19.0	47.6	622
98 MD3-B6 (MD3-TT6	2.23	3.60	94.9	59.4	6.4	12.3	88.5	28.2	552	4.3	0.5	24.4	161.0	921
Average	6.67	4.93	2504	66.8	5.6	14.3	85.9	49.9	316	1.7	0.5	27.4	103.6	1212

* Analytical unit and detection limits are the same as those in Table 1.

to the main antimony mineralization. Another characteristic is very low Al contents and high stibnite components, implying all the feldspars of the original rocks were replaced by stibnite. The mineralized fluids must have been strongly enriched in sulfur and antimony.

4. Ore components in soil and stream sediments

Localities of the studied samples are shown in Figs. 2 (wet season) and 3 (dry season). Chemical analyses of the soil and stream sediments were listed in Tables 2 and 3. Stream sediments of Table 3 are listed from the upper stream side to the down stream side. Therefore, the contents increase to the orebody site, then decrease downward.

The stream sediments have smaller variation than the soils in the contents, which is largely due to homogenization in the water relative to the soil samples, as best shown by Sb contents. The samples were also grouped into those taken in the wet season of May to September and the dry season of October to April. Compared with the average values of the two seasons, antimony seems to be predominant in the wet-season soil samples (932 ppm vs. 342 ppm). On the other hand, molybdenum is definitely higher in the stream sediments of the dry season (14.3 ppm vs. 8.8 ppm Mo).

Antimony of the soil is sporadically high due to mixing of high-grade ores, but the high values are lowered in the stream sediments (Fig. 4A), which is considered resulted from mechanical mixing of other rocks during sedimentation. Arsenic has a positive correlation with antimony in general, implying both the elements were essentially derived from the mineralized rocks as sulfides. However, the amounts are higher as 67 ppm As (average) in the stream sediments, than the soil of 27 ppm As (average), thus arsenic is considered concentrated as finest grained arsenopyrite in the stream sediments.

Sporadic high values are found in the soils of the wet season and also the stream sediments of the wet season.
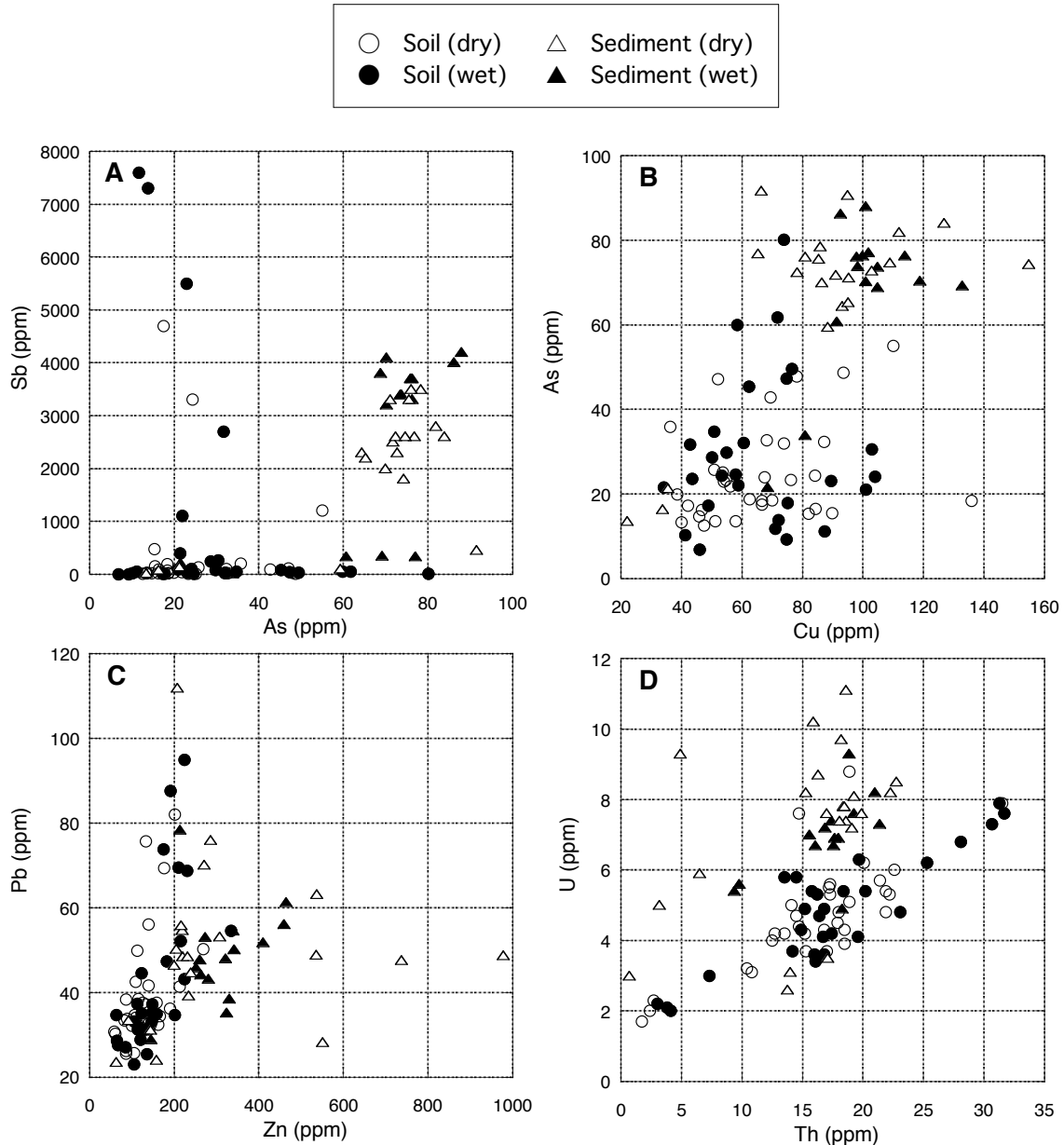
Fig. 4 Variation diagrams of the selected ore components.

A positive correlation of antimony and arsenic of the sediments is unclear on the soil samples (Fig. 4A). Arsenic and copper have broadly positive correlation (Fig. 4B), and stream sediments show higher values in both the elements relative to the soil samples. Lead of the soil samples have a narrow range between 20 and 100 ppm, but zinc contents are scattered especially on those of dry season (Fig. 4C). Thorium and uranium show unique variations. Thorium of wet and dry seasons soils have a good positive variations with uranium. Uranium of sediments is, however, enriched, especially on those of dry season (Fig. 4D), indicating secondary concentration in the element.

5. Geochemical setting of Sb-mineralized terrain in Japan

Antimony deposits in Japan are best concentrated in sedimentary terrains of the Outer Zone of Southwest Japan. They are quartz vein or fracture-filling types with simple ore mineralogy of stibnite with quartz. This kind of ore deposits are best concentrated in western Shikoku, where the famous Ichinokawa deposits are located (Ishihara, 2012). The antimony deposits occur in the Sanbagawa metamorphic belt and southward of the Shimanto sedimentary terrains. Antimony contents of these metamorphic and sedimentary rocks were examined by the same analytical method as of the Mae Due samples, and found to have the following range and

average values of antimony:

Sanbagawa metamorphic rocks (n=3): 0.2~0.9 ppm. Average 0.5 ppm Sb.

Chichibu-Sanbosan, Sandstone (n=4): <0.1~2.9 ppm. Average 0.9 ppm Sb,

Shale (n=6): <0.1~5.4 ppm. Average 1.0 ppm Sb.

Shimanto Belt, North, Sandstone (n=2): <0.1~2.2 ppm. Average 1.1 ppm Sb,

Shale (n=7):<0.1~5.2 ppm. Average 1.2 ppm Sb.

Shimanto Belts, South, Sandstone (n=6): <0.1~1.6 ppm. Average 0.6 ppm Sb,

Shale (n=6): <0.1~2.6. Average 0.9 ppm Sb.

The same set of sedimentary rocks is not available in the Mau Due mine area. But the soils of nos. 4, 6, 7 and 8 are located in un-mineralized area at northeastern side of vein III, and they have the range of 10 to 100 ppm Sb and average of 36 ppm Sb (n=4). Thus, Devonian sediments of north Vietnam, which are supposed to be continental in origin, appear to be one or two order of magnitude higher in trace amounts of antimony than eugeosynclinal sediments of western Shikoku of the Japanese Islands.

6. Conclusions

Soils and stream sediments around the Mau Due stibnite deposits were geochemically studied together with some ores and mineralized wastes. The mineralization brought up largely stibnite components. The host sediments seem to have enriched Sb contents, as compared with eugeosynclinal sediments. Pollution due to As and base metals around the ore deposits is found to be weak.

References

Ashley, P. M., Craw, D., Graham, B. P. and Chappell D. A. (2003) Environmental mobility of antimony around mesothermal stibnite deposits, New South Wales, Australia and southern New Zealand. *Jour. Geochem. Expl.*, **77**, 1-14.

Boyle, R. W. and Jonassan, I. R. (1984) Geochemistry of antimony and its use as an indicator element in geochemical prospecting. *Jour. Geochem. Expl.*, **20**, 223-302.

Flynn, H. C., Meharg, A. A., Bowyer, P. K. and Paton, G. I. (2003) Antimony bioavailability in mine soils. *Environ. Pollution*, **124**, 93-100.

Ishihara, S. (2012) On the main antimony ore deposits in Japan and their genetic problems. *Shigen-Chishitsu*, **62**, 151-161 (in Japanese with English abstract).

Ishihara, S. and Ohno, T. (2011) Present status of antimony mineral resources of this world. *Shigen-Chishitsu*, **62**, 91-97 (in Japanese with English abstract).

Ishihara, S., Murakami, H. and Li, X. (2011) Indium concentration in zinc ores in plutonic and volcanic environments. Examples at the Dulong and Dachang mines, South China. *Bull. Geol. Surv. Japan*, **62**, 259-272.

Murciego, A. M., Sanchez, A. G., Gonzalez, M. A. R., Gil, E. P., Gordillo, C. T., Fernandez, J. C. and Triguero, T. B. (2007) Antimony distribution and mobility in top soils and plants from polluted Sb-mining areas in Extremadura (Spain). *Environ. Pollution*, **145**, 15-21.

Tran Xuyen compiled (2001) Geology and mineral resources of Ma Quan sheet. Scale 1:200,000, Text 42 p., Geol. Surv., Ministry of Industry, Vietnam.

Wang, X., He, M., Xi, J. and Lu, X. (2010) Heavy metal pollution of the world largest antimony mine-affected agricultural soils in Hunan province (China). *Jour. Soils Sediments*, **10**, 827-837.

ベトナム北部の Mau Due アンチモン鉱床周辺の重金属元素分布について

石原舜三・Pham Tich XUAN

要 旨

ベトナム最北部の Mau Due 鉱床はデボン紀の不純なドロマイト質頁岩中の裂罅充填性の輝安鉱鉱床である．その地化学的な研究によると，その鉱化成分は主として S 及び Sb からなり，若干の As・ベースメタル成分を伴う．土壌中の Sb 含有量は変化が激しく，これは鉱石成分の混在によるものと考えられる．雨季 (5–9 月) と乾季 (10–4 月) に分けられた採取試料の分析結果，土壌の Sb 平均含有量は雨季 932 ppm，乾季 342 ppm であって雨季で高く，一方河川堆積物では，雨季 2,563 ppm，乾季 2,504 ppm であり，両者で著しく増加する．As は Sb と同様な挙動をとり，その含有量は雨季／乾季の土壌において 29/26 ppm と，絶対量が少ない．河川堆積物では 68-67 ppm に増加するが，この事実は Sb, As が微細な硫化物として存在することを示唆している．日本の地向斜帯の堆積岩と比べてベトナムの堆積岩類は，微量成分としての Sb に富んでいる可能性がある．

地質調査総合センター研究資料集

地質調査総合センターの最新出版物

200 万分の 1 地質編集図	No. 4	日本地質図第 5 版
20 万分の 1 地質図幅	伊勢・静岡及び御前崎（第2版）・与論島及び那覇・八代及び野母崎の一部・新潟（第2版）	
5 万分の 1 地質図幅	西郷・延岡・野田・加茂・戸賀及び船川（第2版）・熱海・榛名山・阿仁合（第2版）・足助	
海外地球科学図	アジア地質図（1:500 万）	
	中央アジア鉱物資源図（1:300 万）	
海洋地質図	No. 77	日高舟状海盆海底地質図　（1:20 万）
	No. 78	宗谷岬西方海底地質図　（1:20 万）
	No. 79	野間岬沖表層堆積図　（1:20 万）
	No. 80	奥尻島北方表層堆積図　（1:20 万）
構造図	No. 14	全国主要活断層活動確率地図
火山地質図	No.15	樽前火山地質図（1:3 万）
	No.16	十勝岳火山地質図（1:3 万）
鉱物資源図	No. 7	南西諸島（1:50 万）
特殊地質図	No. 39	千葉県清和県民の森周辺の地質図
重力図	No. 27	岡山地域重力図（ブーゲー異常）
	No. 28	高知地域重力図（ブーゲー異常）
	S3	甲府地域重力構造図（ブーゲー異常）
空中磁気図	No. 44	岩手火山地域高分解能空中磁気異常図
	No. 45	福井平野地域高分解能空中磁気異常図
数値地質図	G-16	20 万分の 1　日本シームレス地質図　DVD 版
	G-17	九州地質ガイド
	FR-2	燃料資源地質図「東部南海トラフ」
	GT-4	全国地熱ポテンシャルマップ
	S-1	海陸シームレス地質情報集「能登半島北部沿岸域」　DVD 版
	S-2	海陸シームレス地質情報集「新潟沿岸域」　DVD 版
	V-3	口永良部島火山地質データベース
	P-7	有珠火山地域地球物理総合図」
	G20-1	20 万分の 1 数値地質図幅集「北海道北部」第 2 版
	G20-2	20 万分の 1 数値地質図幅集「北海道南部」第 2 版
	E-5	表層土壌評価基本図　〜富山県地域〜
その他	日本の熱水系アトラス	
	海と陸の地球化学図	

地質調査研究報告 第64巻 第1/2号
平成25年4月22日　発行

独立行政法人 産業技術総合研究所
地質調査総合センター
〒305-8567 茨城県つくば市東1-1-1
つくば中央第7

本誌掲載記事の無断転載を禁じます。

Bulletin of the Geological Survey of Japan
Vol.64 No.1/2 Issue April 22, 2013

National Institute of Advanced Industrial
Science and Technology
Geological Survey of Japan
AIST Tsukuba Central 7, 1-1, Higashi 1-chome,
Tsukuba, Ibaraki 305-8567 Japan

All rights reserved.

BULLETIN
OF THE
GEOLOGICAL SURVEY OF JAPAN

Vol. 64   No. 1/2   2013

CONTENTS